BLTP Bogoliubov Laboratory of Theoretical Physics

Joint Institute for Nuclear Research, Dubna, Russia

Nuclear Reaction Mechanisms in Heavy Ion Collisions (Lecture II)

NASIROV Avazbek*

2013 NUCLEAR PHYSICS SCHOOL, June 24-28

UNIPARK SEOGWIPO, JEJU

27 June 2013

*Institute of Nuclear Physics, Tashkent, Uzbekistan


MAPQUEST.COM
Asia
0 1,000 Miles
0 1,000 Kilometers
60° N
40° N
Bering Sea
Tropic of Cancer
180°
20° N
160° E
0°
20° S
40° E
60° E
80° E
100° E
120° E
flight
7 hours 20 min
Moscow
Tashkent
EUROPE
Russia
Georgia
Armenia
Turkey
Azerbaijan
Kazakhstan
Cyprus
Lebanon
Israel
Syria
Jordan
Iraq
Turkmen.
Kyrgyzstan
Tajikistan
Iran
Afghan.
Kuwait
Bahrain
Qatar
Saudi Arabia
U.A.E.
Yemen
Oman
Pakistan
China
Mongolia
North Korea
South Korea
Japan
Bhutan
Nepal
India
Bangladesh
Myanmar
Laos
Thai.
Vietnam
Cambodia
Macao (China)
Hong Kong (China)
Philippines
Brunei
Malaysia
Singapore
Indonesia
East Timor
Maldives
Sri Lanka
AFRICA
Arabian Sea
Bay of Bengal
Philippine Sea
PACIFIC OCEAN
INDIAN OCEAN
AUSTRALIA

Physical map of Uzbekistan

UZBEKISTAN

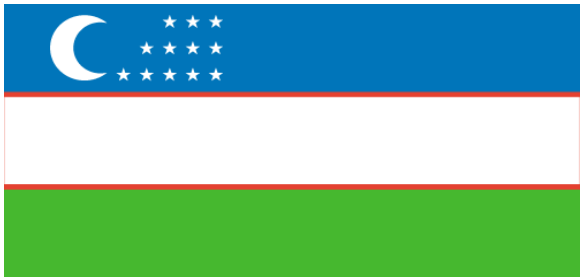

Population: 30 million
Capital: Tashkent (more than 2 million)
Area: 447,400 sq km (172,700 sq miles)
Major language: Uzbek, Russian, Tajik
Major religion: Islam
Life expectancy: 66 years (men), 72 years (women)
Monetary unit: 1 $ = 2000 uzbek som
Main exports: Cotton, gold, natural gas, mineral fertilizers, ferrous metals, textiles, motor vehicles

Introduction

The experimental knowledge about fusion-fission reactions at sub- and near-barrier energies has grown considerably in the last twenty years.

The theoretical models are able to reproduce and predict the main features of such processes, even the cross sections for synthesis of superheavy elements estimated more or less to the experimental data. But properly understanding the fusion dynamics for heavy systems requires many more ingredients. The need for more experimental data to disentangle various concurrent effects, is clearly felt. A full understanding of all steps of the reaction dynamics is very important for the challenging issue of superheavy elements production and new isotopes far from the valley of stability.

The mixing of deep-inelastic collisions and quasifission products, as well as the mixing of the quasifission and fusion-fission products in the experimental data causes the difficulties in the theoretical estimation the hindrance to complete fusion of nuclei.

Topicality of the problem

Experimental data are subject to study and to be interpret. The main problem is to install universal physical laws to describe and to make conclusions about the reaction mechanism on the base of measured mass, charge, energy and angular distribution of products.

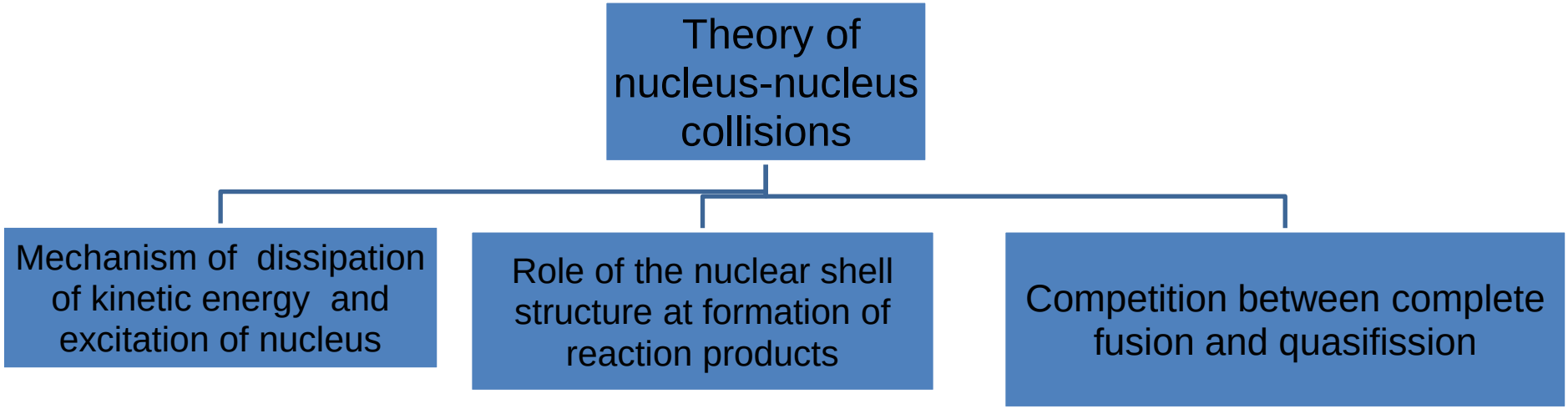

Theory: nucleus-nucleus interaction potential, friction coefficient, deformation parameters of interacting nuclei and coupling of the relevant degrees of freedom leading to dissipation of kinetic energy and angular momentum.

Complete microscopic calculations seem not to be possible if we would like to describe experimental data observed for different characteristics of reaction products. There are strong correlations between collective motion of nuclei and microscopic degrees of freedom of nucleons. Therefore, there is not established nature of friction coefficients and tensors of masses which are universal for the wide energy range of collision and large amplitude of collective motion.

Reaction types in heavy ion collisions

For collisions near the Coulomb barrier, ***R*** is the most important collective variable.

It is used to classify collisions into several types, depending on its time evolution.

If the nuclear surfaces never touch, we have either elastic scattering or Coulomb excitation .

If the surfaces barely touch, we have a grazing collision .

If the nuclei make firm contact with each other, but still separate afterwards, we have a deeply inelastic collision or quasifission .

Finally, if the nuclei become sufficiently attached to each other, they may form a compound nucleus in a fusion reaction .

If the angular momentum and total charge are both very large, this combined nucleus may not live long enough to reach its equilibrium shape before it fissions into two or more large fragments in incomplete fusion .

Of course, in all these collisions except elastic scattering , other collective degrees of freedom also come into play; in the fusion reactions and incomplete fusion processes, ***R*** eventually loses not only its dominant role but even its meaning as the nuclear state evolves in time until the projectile and target nuclei can no longer be distinguished.

Basic quantities for colliding nuclei

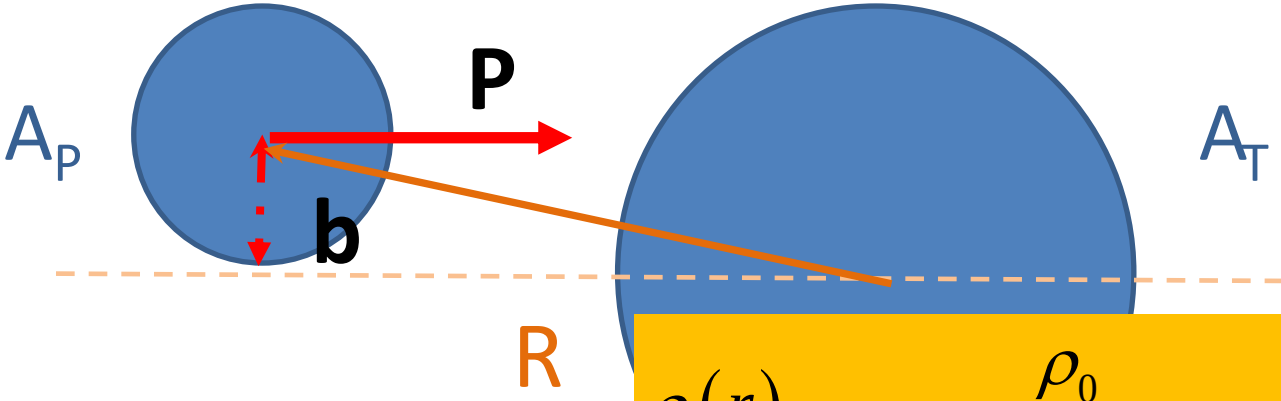

$E_{c.m.}$, A_p, A_T, Z_P, Z_T

L=[b x P]

$$\rho(r) = \frac{\rho_0}{1+\exp\left[\frac{r-R_i}{a}\right]}, \qquad \rho_0 = 0.17\,\mathrm{fm}^{-3}$$

$$a = 0.54\,\mathrm{fm}, \quad R_i = r_0 A_i^{1/3}$$

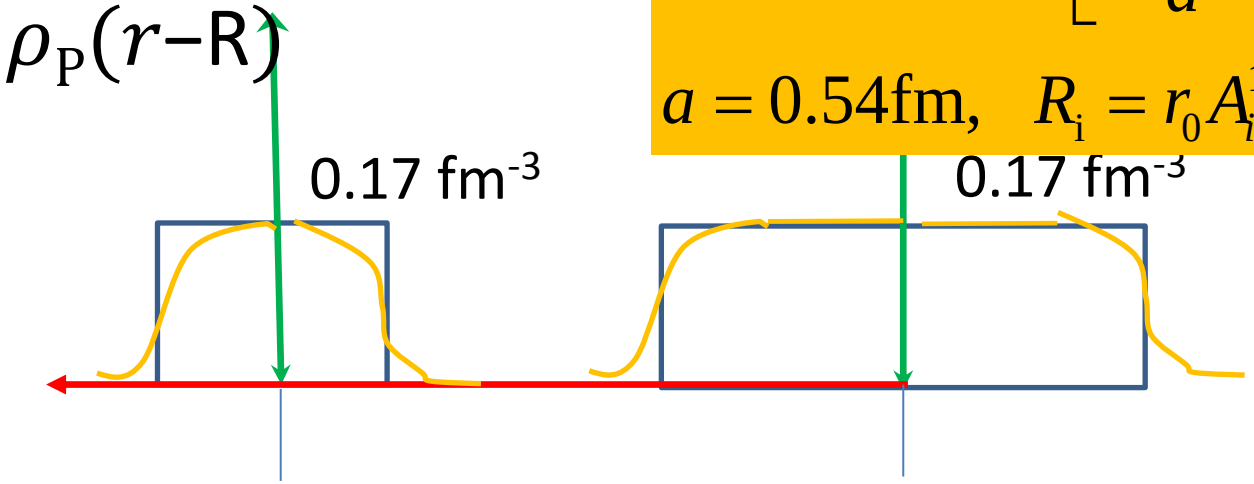

The density distributions of the nuclei $^{16}0$ and ^{208}Pb when their centers are separated by the strong absorption radius appropriate for scattering at energies between about 100 and 200 MeV . some information about its slope [1821. This is the situation pertaining to much of heavy-ion elastic

M.E. Brandan, G.R. Satchler / Physics Reports 285 (1997) 143–243

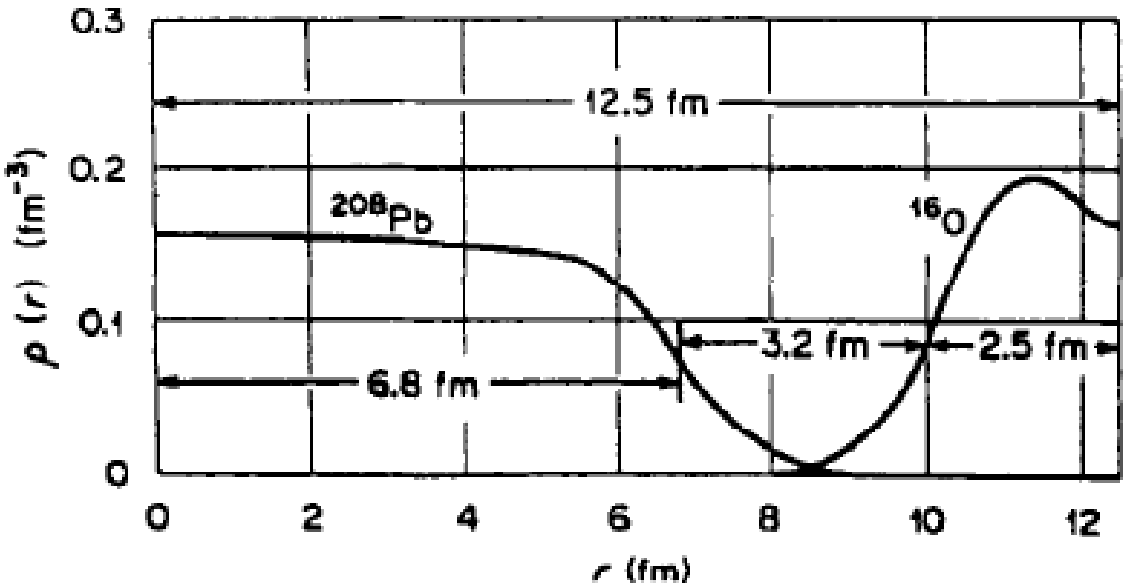

Validity of the mean-field approximation based on the analysis of the experimental data

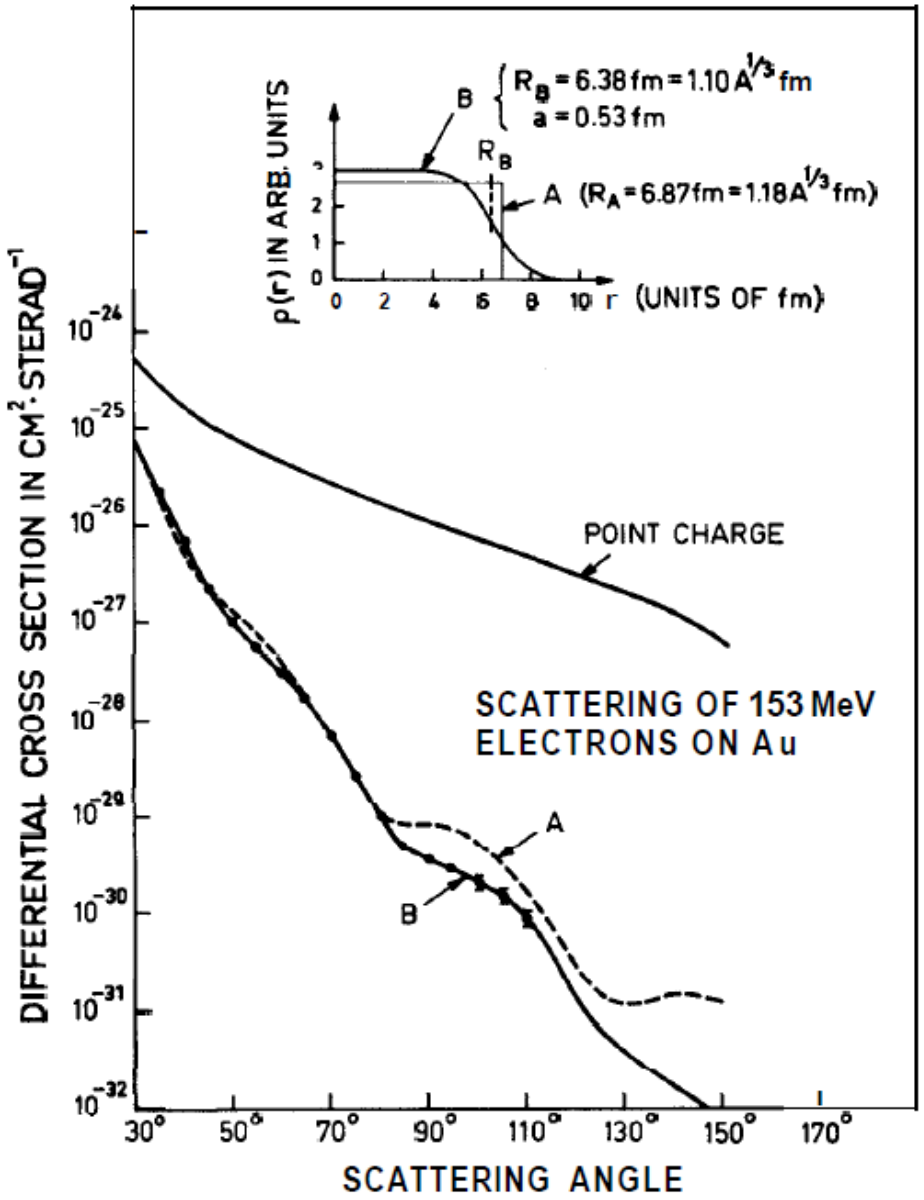

The differential cross section observed for electrons of 153 MeV scattered from a gold target. It is seen that, for the angles studied, the intensity of the scattering is at least an order of magnitude weaker than for a point charge of ***Z*** = 79. The angular distribution exhibits mild oscillations characteristic of scattering by a system with a rather well-defined radius The experimental data and the theoretical analysis are taken from **B.**Hahn, et al. ***Phys. Rev.*** **101, 1131 (1956);** ***D.*** R. Yennie, et al, ***Phys. Rev.*** **95,500 (1954);** R. Herman and R. Hofstadter, ***High Energy Electron Scattering Tables,*** Stanford Univ. Press, Stanford, California, **1960.**

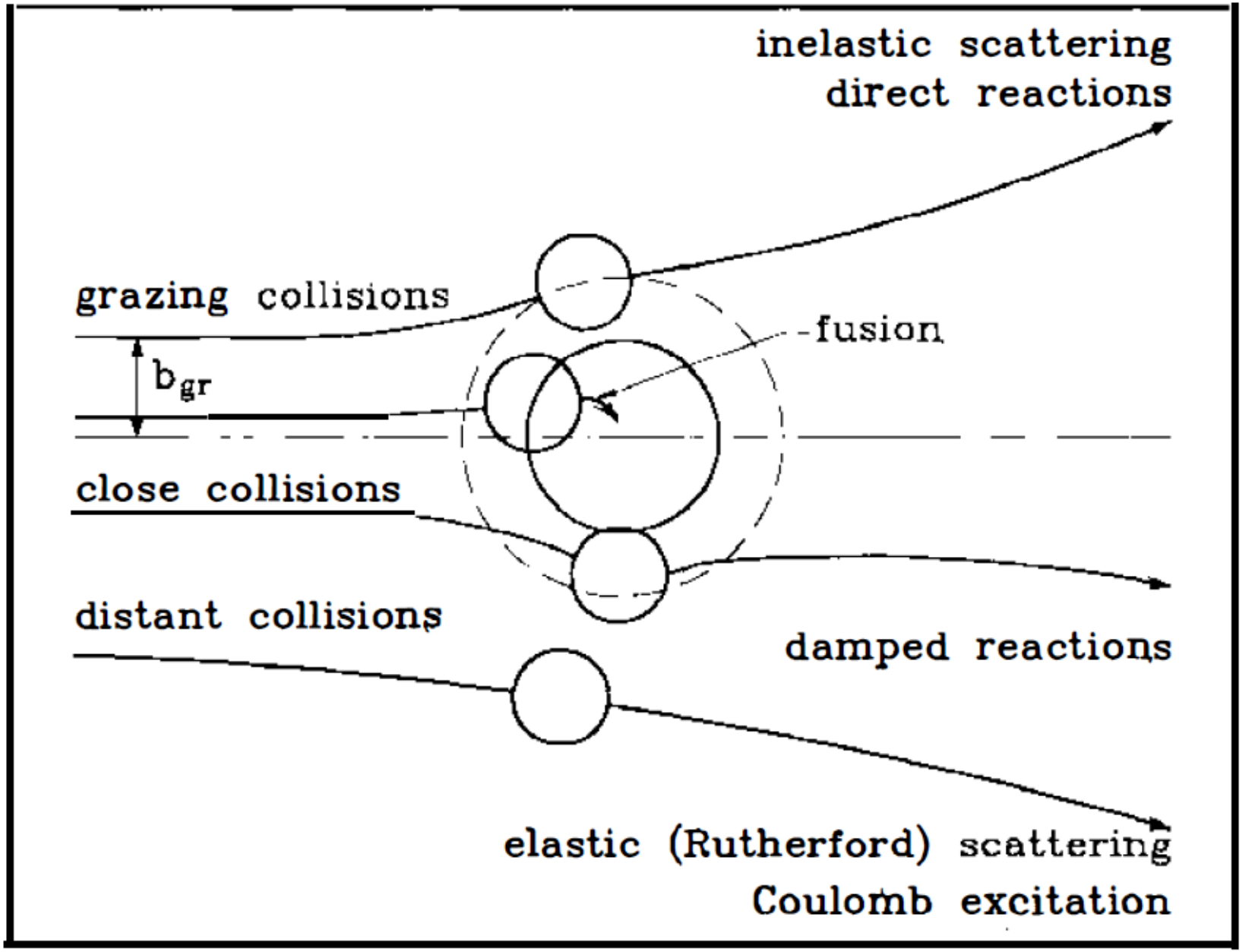

Figure 1 Classes of heavy-ion collisions associated with different values of impact parameters.

Dependence of energy distribution of reaction products on the initial angular momentum at given beam energy

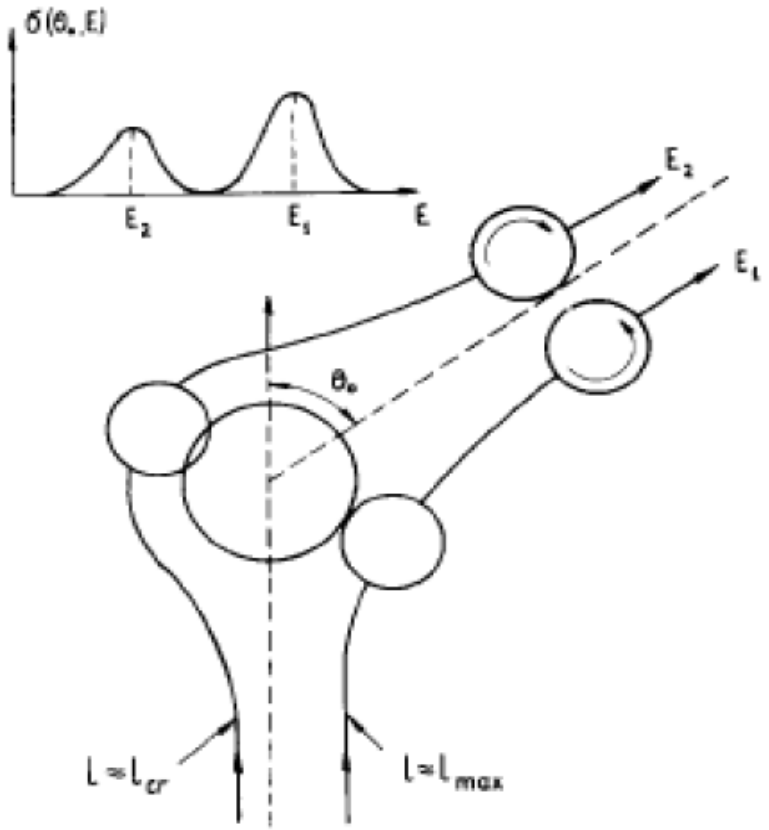

Illustration of the formation of two peaks in the energy spectrum

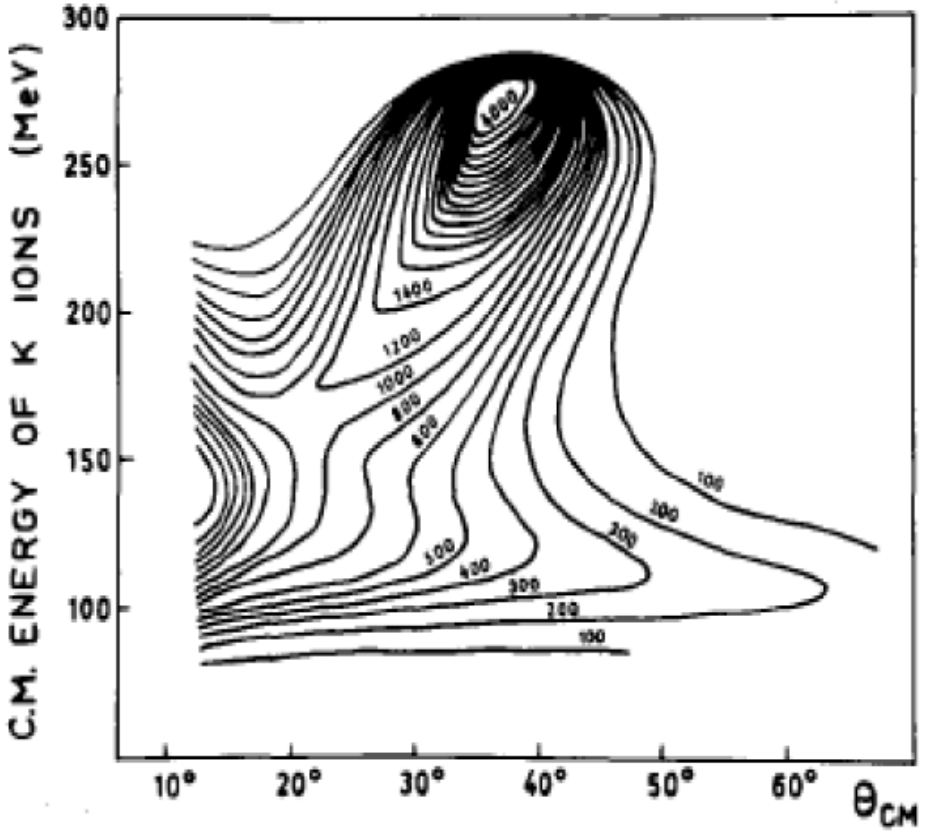

Contour diagram representing the transfer reaction data for ^{232}Th(^{40}Ar,K) at 388 MeV

Elastic scattering and Coulomb excitation .

Elastic scattering is the main reaction channel of heavy-ion collisions at all incident energies and, thus, it is a useful experimental tool for study of nuclear structure and nucleus-nucleus interaction potential.

In the elastic scattering channel both nuclei remain in their ground states because total energy and momentum are conserved.

$$P_1 + P_2 = P_1' + P_2'$$

.

$$E_1 + E_2 = E_1' + E_2'$$

At above barrier incident energies and when distances between colliding nuclei reaches small values a considerable part of incoming flux goes away from the elastic scattering into the other reaction channels. due to strongly coupled to other degrees of freedom.

Elastic scattering and Coulomb excitation

For all nuclear particles, with the exception of neutrons, the Coulomb repulsive interaction dominates at large distances: . When nuclei approach each other, the attractive nuclear forces have an effect. Resulting nucleus-nucleus interaction potential looks as shown in Figure.

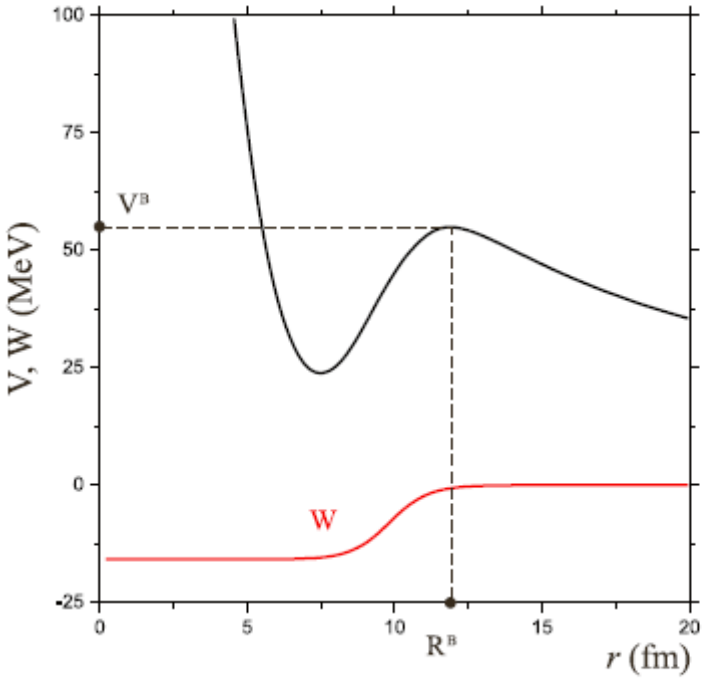

Fig. 1. Interaction potential of ^{12}C with ^{208}Pb calculated within the proximity model (real part) and schematic view of the absorption potential $W(r)$.

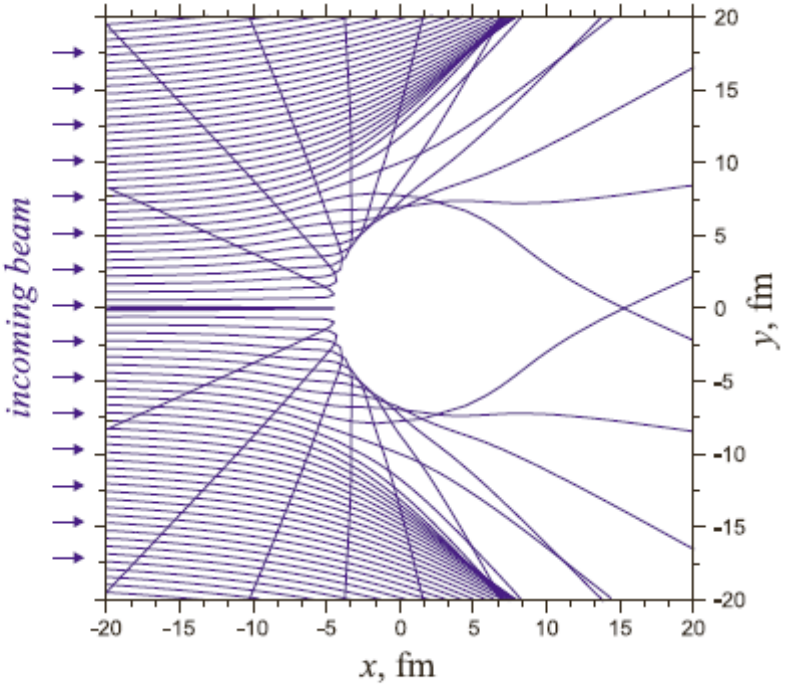

Fig. 2. Classical trajectories, calculated within classical model of nuclear scattering for the ^{12}C + ^{208}Pb elastic scattering at laboratory beam energy of 100 MeV.

Grazing angular momentum ℓ_{gr}

Inelastic processes play a large role if the projectile's energy is large enough to surmount the Coulomb barrier and the angular momentum of the relative motion is small enough for the nuclear surfaces to touch: then the strong-interaction forces come into play.

The distance of closest approach R_L for a Coulomb trajectory of angular momentum $\ell\hbar$ and energy E is given implicitly by

$$E = \frac{\ell(\ell+1)\hbar^2}{2\mu {R_L}^2} + \frac{Z_1 Z_2 e^2}{R_L}.$$

The value of ℓ for which R_L is equal to the sum of the nuclear radii $R_{gr} = r_0\left({A_1}^{1/3} + {A_2}^{1/3}\right)$ is called the grazing angular momentum ℓ_{gr}. It can be find

$$\ell(\ell+1) = 2\mu(E - U_C){r_0}^2\left({A_1}^{1/3} + {A_2}^{1/3}\right)^2/\hbar^2$$

Rutherford's formula describes elastic scattering

$$\frac{d\sigma_{Ruther}}{d\Omega} = \left(\frac{Z_1 Z_2 e^2}{2\mu v^2}\right)^2 \frac{1}{\sin^4 \vartheta/_2}$$

The value of *L* for which the closest distance between nuclei is equal to the sum of the nuclear radii

is called grazing value of the orbital angular momentum.

Grazing collisions

Grazing collisions are board between elastic and inelastic collisions. Geometrical cross section for the reactions dominated by the strong nuclear interaction may be estimated by adding the contributions to the absorptive cross section. The grazing angle is found from the condition between the reaction cross section and Rutherford cross section:

$$\frac{\sigma_R(\theta_{gr})}{\sigma_{Rutherford}(\theta_{gr})}=1/4$$

An effective nuclear interaction radius *R* can be determined based on the total reaction cross section σ and the observed quarter-point angle $\theta_{1/4}$, defined as the angle which satisfies a condition $\sigma_{\text{elastic}} / \sigma_{\text{Rutherford}}=1/4$.

The scattering angle as a function of impact parameter *b*, or angular momentum $(\ell + 1/2)\hbar = P\,\boldsymbol{b}$, is called the ***deflection function Θ(ℓ)*** and is shown on the right figure. Trajectories with positive ***Θ***, in this case the peripheral ones that are dominated by the Coulomb repulsion, constitute nearside scattering, while those drawn to negative ***Θ*** by the attractive nuclear potential represent far side scattering.

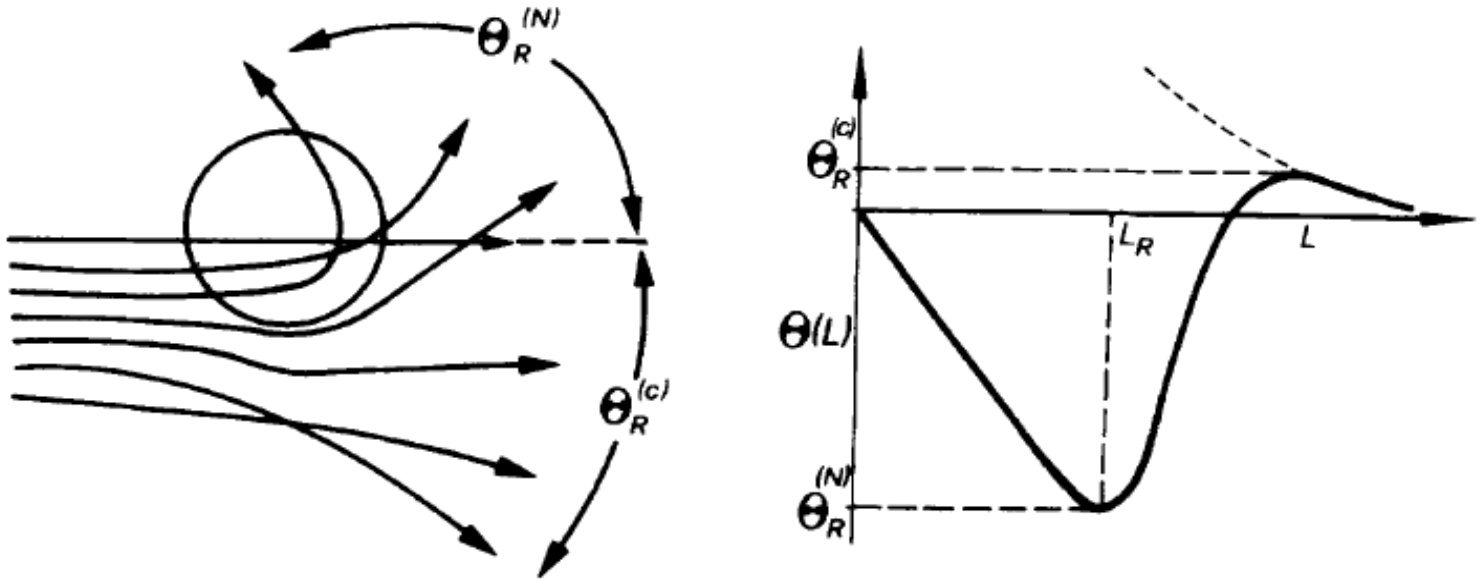

Fig. 3.1. Left: classical trajectories that lead to Coulomb (C) and nuclear (N) rainbows. Right: the corresponding deflection function (from [184]).

Theoretical distinguish of the rainbow from the differential cross section depending on angular momentum

Classical differential cross section becomes infinitive at $\Theta \approx \Theta_r$,

$$\frac{d\sigma}{d\theta}(classical) = \frac{d\sigma}{dL}\frac{dL}{d\theta_{cl}} = \frac{d\sigma}{dL}\left(\frac{d\theta_{cl}}{dL}\right)^{-1}$$

because many classical trajectories lead to the same scattering angle ,

$$\theta_{cl}(L_1) = \theta_{cl}(L_2) = \theta_{cl}(L_3) = \ldots$$

$$\frac{d\theta_{cl}(L)}{dL} = 0$$

Since the flux of incident particles is smoothly distributed in the angular momentum L and $d\sigma/dL$ is finite number.

Classical trajectories, deflection function, and differential cross section of ^{3}He elastic scattering by ^{14}C target at beam energy of 24 MeV/nucleon

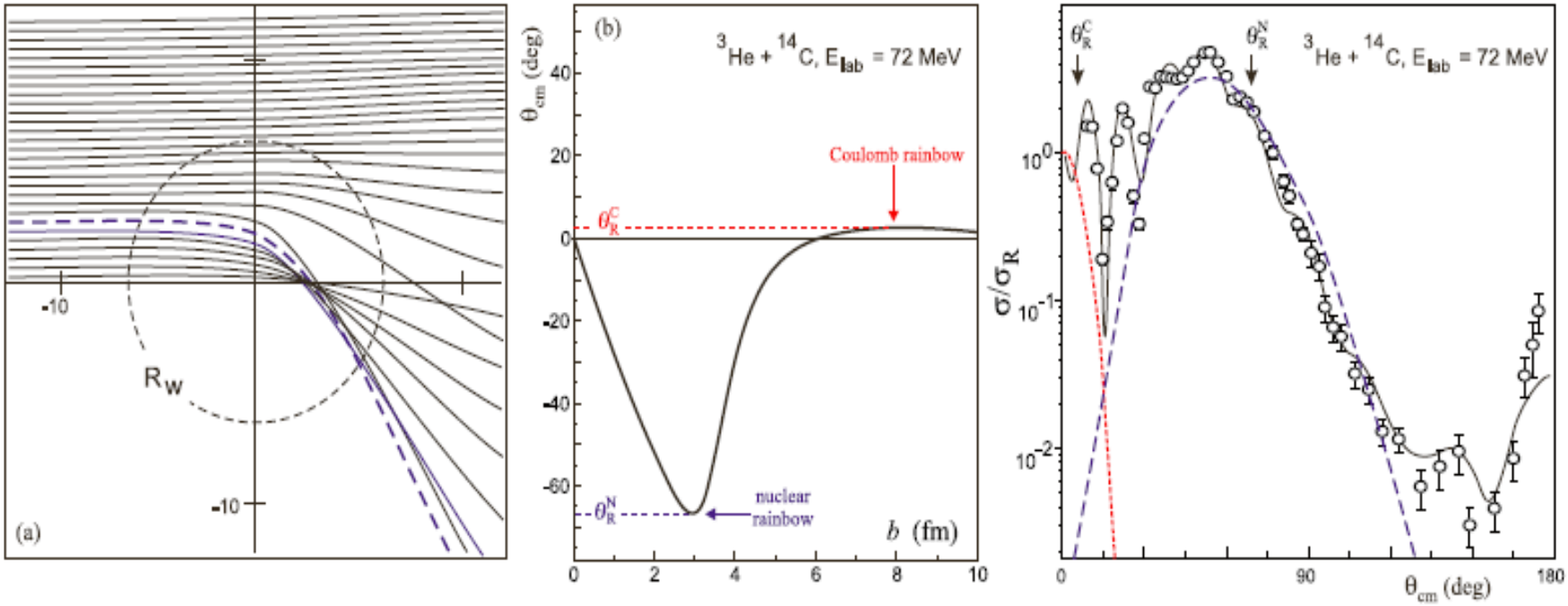

Fig. 3. (a) Classical trajectories of ^{3}He projectile scattered by ^{14}C target at beam energy of 24 MeV/nucleon. Dashed line corresponds to the nuclear rainbow impact parameter. The absorptive region (non-zero values of imaginary part of the optical potential) is shown by dashed circle. (b) Classical deflection function. Coulomb ($\theta_R^C \approx +2^\circ$) and nuclear ($\theta_R^N \approx -67^\circ$) rainbow angles are shown. (c) Differential cross section of ^{3}He elastic scattering by ^{14}C at energy 24 MeV/u. Doted and dashed curves show the contribution of the Coulomb and nuclear rainbow. Solid curve is the result of quantum calculation performed within the optical model.

Appearance of inelastic collisions in the angular distribution of the elastic scattering

For larger ℓ, the deflection angle is smaller because the Coulomb trajectories keep the nuclei farther from each other: $b \gg (R_1 + R_2)$, where R_1 and R_2 are radii of colliding nuclei.

For smaller ℓ, the deflection angle is reduced because the attractive nuclear force pulls the nuclei together, reversing the deflection due to the Coulomb force. θ_r is called the rainbow angle.

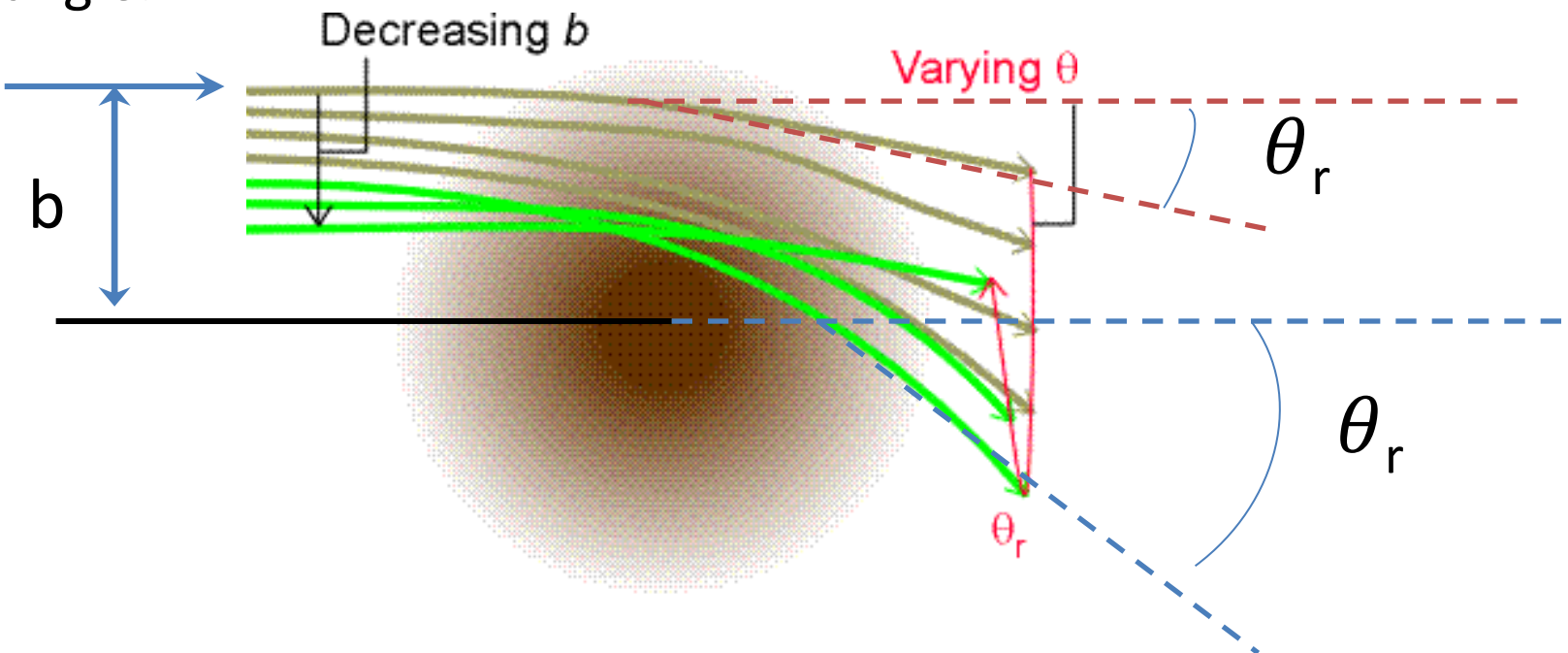

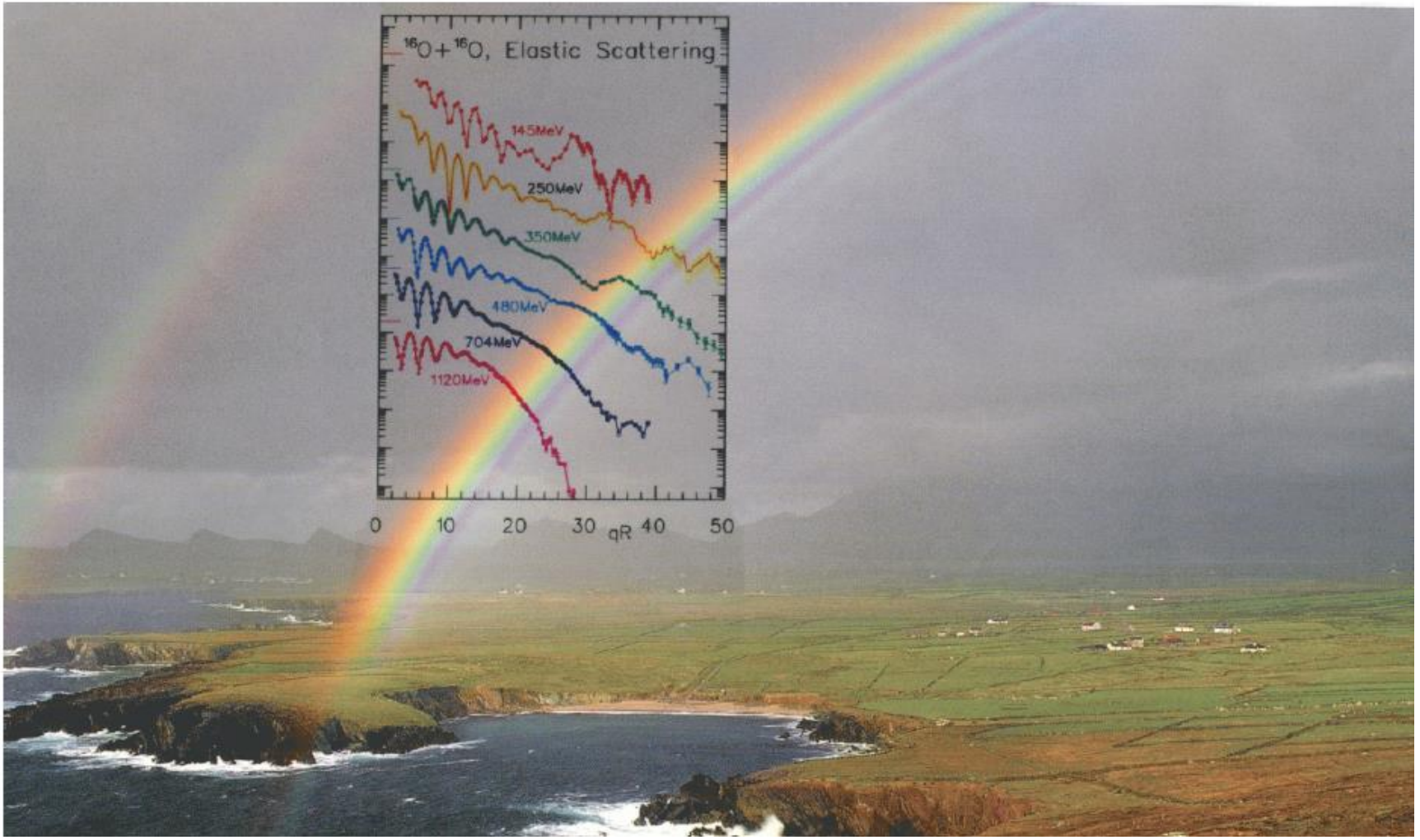

Atmospheric rainbow with both the primary and secondary rainbows and in the insert the elastic $^{16}O+^{16}O$ scattering data as function of momentum transfer measured at different laboratory energies.

W. von Oertzen W, et al. *Europhysicsnews* **31** (2000) p.5; *Acta Physica Polonica B* **33** (2002)93.

Atmospherical Rainbow=Refraction+Reflection+Refraction

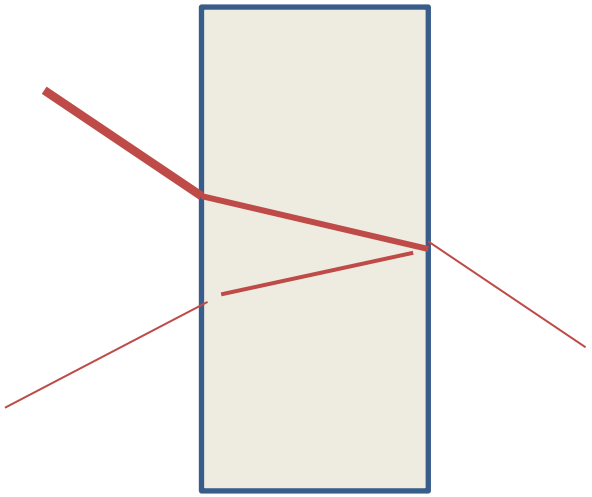

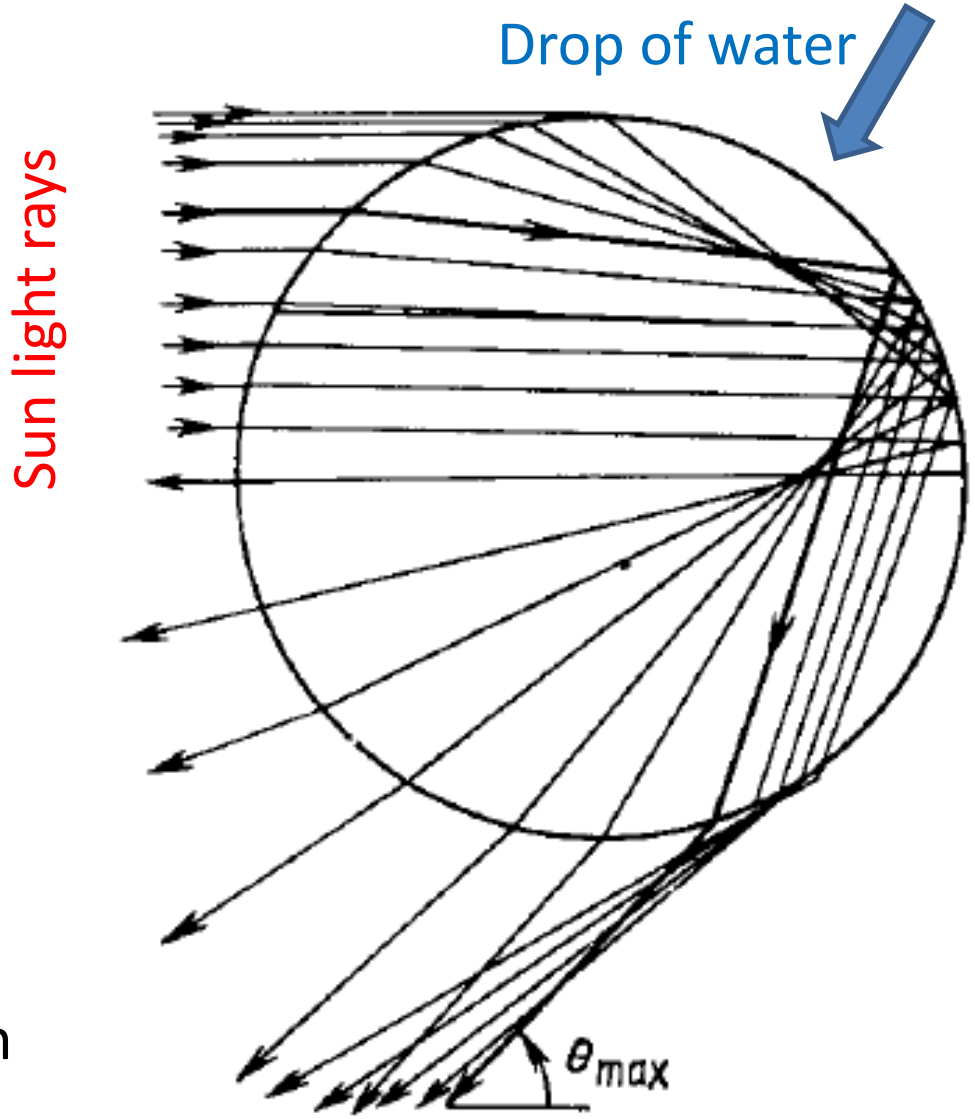

At angle Θ_{max} the intensity of outgoing light rays increase due to thickening after reflection and refraction in the drop of water.

The interference of the refractive nucleus-nucleus scattering gives rise to the nuclear rainbow which is similar to the atmospheric rainbow.

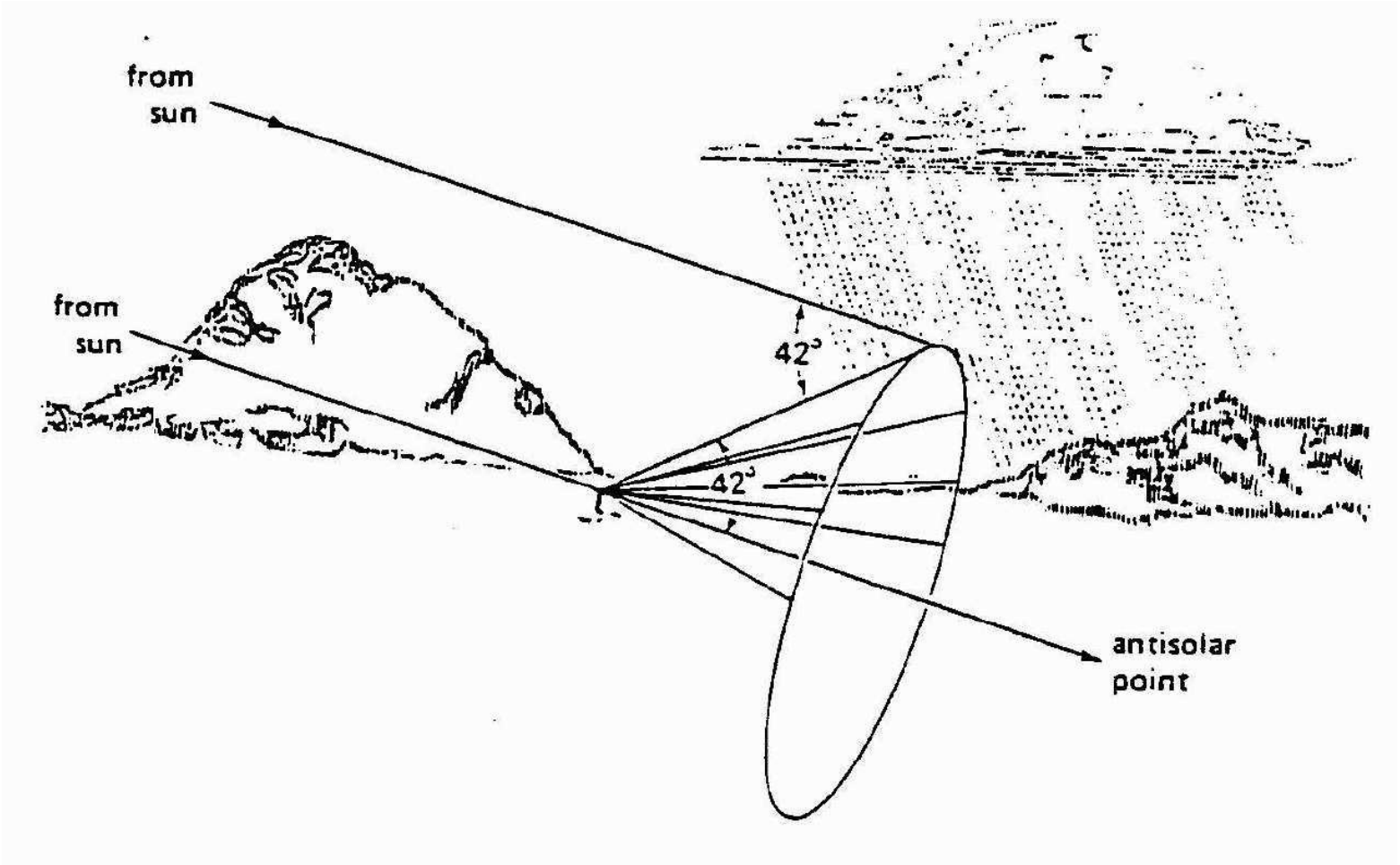

Absorption of elastic channel partial waves

Any excitation of colliding nuclei takes out them from the elastic channel. Such decreasing of in-coming flux (number of elastically scattered particles) can be simulated by additional imaginary (absorptive) potential $iW(r)$, $iW(r) < 0$ and $iW(r \to \infty) \to 0$.

This potential defines the mean free path of relative motion of nuclei:

$$\lambda_{free} = -\hbar v / 2W(r)$$

which, in turn, defines the probability for the nuclear system to remain in the elastic channel .

Differential cross section for elastic scattering

The *differential cross section* $d\sigma(\Omega)$ for elastic scattering is defined as the ratio of the asymptotic probability current flowing radially into an element of solid angle $d\Omega = \sin\theta d\theta d\varphi$ in the direction of the solid angle $\Omega = \{\theta, \varphi\}$, over the probability current density of the incident wave,

$$d\sigma(\Omega) = \frac{\text{probability current into } d\Omega \text{ in the direction } \Omega}{\text{probability current density of the incident wave}}. \qquad (1.13)$$

The asymptotic current flowing into $d\Omega$ is the current through the area $R^2 d\Omega$ at a large distance R from the scattering centre (cf. Fig. 1.1). It is given by formula (1.12) with $r = R$. Together with the current density of the incident wave (1.11) the definition (1.13) yields for the differential cross section per unit solid angle the formula

$$\frac{d\sigma}{d\Omega} = \frac{j_r R^2}{|\mathbf{j}_{\text{in}}|} = |f(\Omega)|^2. \qquad (1.14)$$

For a spherical potential the scattering solution $\psi(\mathbf{r})$ is symmetric about the z-axis, i.e. independent of the azimuthal angle φ. The scattering amplitude is thus a function of θ only, $f(\Omega) = f(\theta)$.

P. Fröbrich, R. Lipperheide, Theory of Nuclear Reactions, Clarendon Press. 1996

Estimation of nuclear radius by the elastic scattering of neutrons

Incident beam of neutrons is described by a plane wave which is expended in the angular momentum eigenstates (we neglect spin)

$$e^{ikz} \approx \frac{\sqrt{\pi}}{kr}\sum_{\ell=0}^{\infty}\sqrt{2\ell+1}\,i^{\ell+1}\left[e^{-i(kr-\ell\pi)} - e^{+i(kr-\ell\pi)}\right]Y_\ell^0(\theta)$$

The scattering process modifies the wave function at small r; in turn this leads to a change of the outgoing wave far away from the target nucleus.

$$e^{ikz} \approx \frac{\sqrt{\pi}}{kr}\sum_{\ell=0}^{\infty}\sqrt{2\ell+1}\,i^{\ell+1}\left[e^{-i(kr-\ell\pi)} - \eta\, e^{+i(kr-\ell\pi)}\right]Y_\ell^0(\theta)$$

η is the amplitude of the outgoing wave and it characterizes the scattering process

$$\varphi(r) = e^{ikr} + f(\theta)\,\frac{e^{-ikr}}{r}$$

Nearside and farside scattering

The significance of the terms nearside and farside is perhaps more obvious if one looks at the trajectories that can contribute to a given scattering angle, as indicated in Figure

M.E. Brandan, G.R. Satchler / Physics Reports 285 (1997) 143–243

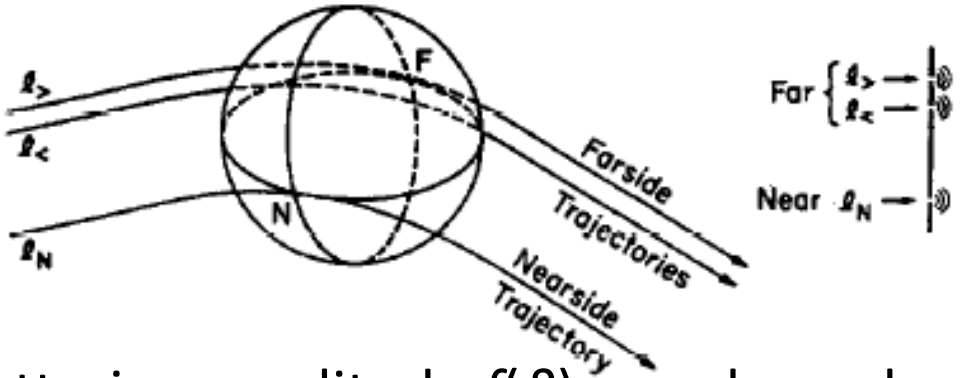

The quanta1 scattering amplitude $f(\vartheta)$ can always be decomposed into two parts by using the partial-wave expansion

$$f(\theta) = i\frac{\sqrt{\pi}}{k}\sum_{\ell}\sqrt{(2\ell+1)}\,(1-\eta_{\ell})\,Y_{\ell}^{0}(\theta)$$

Its square is differential cross section for elastic scattering

$$\left(\frac{d\sigma}{d\Omega}\right)_{\text{el}} = \lfloor f(\vartheta)\,\rfloor^{2}$$

It is known that the probability of penetration is one-half at the top of an inverted harmonic-oscillator potential. It is therefore convenient to define the interaction barrier for the lth partial wave as the energy E_l at which the absorption probability $P(E_l, l)$ is one-half. While such a definition is model independent, it assumes a simple physical meaning in the ingoing-wave strong-absorption model[8] with parabolic barriers.

Interaction barrier as a threshold

In charged-particle nuclear reactions, it is of interest to measure the height of the barrier between the interacting nuclei. Such a measurement provides information on the fusion process,[1] which is an important intermediate step in the production of superheavy nuclei by heavy-ion reactions. It may also facilitate the study of distortion effects[2-6] and of the dependence of the barrier height on the charges and shapes of the interacting nuclei.[7]

With such a definition, the barriers can be readily obtained by analyzing the elastic scattering or reaction cross-section data with an optical model or by parametrizing the phase shifts. For a given incident energy E, one finds the value of l_b for which the absorption probability is given by $1 - |\eta_{l_b}|^2 = \frac{1}{2}$. It can then be said that the interaction barrier for the l_bth partial wave is the incident energy E. If data are available for different energies, the interaction barrier for various values of l can be obtained.

Of particular interest is the interaction barrier for the s wave which is traditionally called the "Coulomb barrier." We wish to present in this article another way to measure this barrier by employing a simple analytic expression for the total reaction cross section obtained in the ingoing-wave strong-absorption model.

Nucleus-nucleus interaction potential

We consider two nuclei with uniform charge distribution whose shapes are specified by the surfaces

$$R_i(\theta,\varphi) = R_{i0}(1+\beta_i Y_{20}), \qquad i = 1, 2 \qquad (1)$$

with $R_{i0} = 1.2\, A_i^{\frac{1}{3}}$ fm. A straightforward calculation shows that when their centers are separated by a distance r and their symmetry axes are parallel, the electrostatic potential energy is given up to the second order in β by [13]

Nucleus-nucleus interaction potential

$$V_C(R,\alpha_1,\alpha_2) = \frac{Z_1 Z_2}{R} e^2$$

$$+ \frac{Z_1 Z_2}{R^3} e^2 \left\{ \left(\frac{9}{20\pi} \right)^{1/2} \sum_{i=1}^{2} R_{0i}^2 \beta_2^{(i)} P_2(\cos\alpha_i) + \frac{3}{7\pi} \sum_{i=1}^{2} R_{0i}^2 \left[\beta_2^{(i)} P_2(\cos\alpha_i) \right]^2 \right\}$$

$$V_{nucl}(R,\alpha_1,\alpha_2) = \int \rho_1^{(0)}(\vec{r} - \vec{R}) f_{eff} \left[\rho_1^{(0)} + \rho_2^{(0)} \right] \rho_2^{(0)}(\vec{r}) d^3\vec{r}$$

$$\rho_i^{(0)}(\vec{r},\vec{R}_i,\alpha_i,\theta_i,\beta_{2^{(i)}}) = \left\{ 1 + \exp\left[\frac{\left|\vec{r} - \vec{R}_i(t)\right| - R_{oi}(1 + \beta_2^{(i)} Y_{20}(\theta_i,\alpha_i))}{a} \right] \right\}^{-1}.$$

$$V_{rot} = \hbar^2 \frac{l(l+1)}{2\mu[R(\alpha_1,\alpha_2)]^2}$$

Dynamics of capture of projectile by target-nucleus

$$\sigma_{cap}(E_{lab}, L; \alpha_1, \alpha_2) = (2L+1)\, T(E_{lab}, L; \alpha_1, \alpha_2)$$

$$T(E_{lab}, L; \alpha_1, \alpha_2) = \begin{cases} 1, & if \ L_{\min} \le L \le L_{dyn} \\ 0, & if \ L < L_{\min} \ or \ L > L_{dyn} \end{cases}$$

L_{dyn} and L_{min} are determined by dynamics of collision and calculated by solution of equations of motion for the collision trajectory:

$$\frac{d\left(\mu(R)\dot{R}\right)}{dt} + \gamma_R(R)\dot{R}(t) = -\frac{\partial V(R)}{\partial R} - \dot{R}^2 \frac{\partial \mu(R)}{\partial R}$$

$$\frac{dL}{dt} = \gamma_\theta(R)R(t)\left[\dot{\theta}R(t) - \dot{\theta}_1 R_{1eff} - \dot{\theta}_2 R_{2eff}\right]$$

$$L_0 = J_R\dot{\theta} + J_1\dot{\theta}_1 + J_2\dot{\theta}_2 , \qquad E_{rot} = \frac{J_R\theta^2}{2} + \frac{J_1\theta_1^2}{2} + \frac{J_2\theta_2^2}{2}$$

Description of the nucleus-nucleus collision at energies < 10A MeV as the 3 stage process.

$$\sigma_{ER}(E_{Lab}, L) = \langle \sigma_{cap}(E_{Lab}, L)\, P_{CN}(E_{Lab}, L)\, W_{surv}(E_{Lab}, L) \rangle_{\{\alpha\}}$$

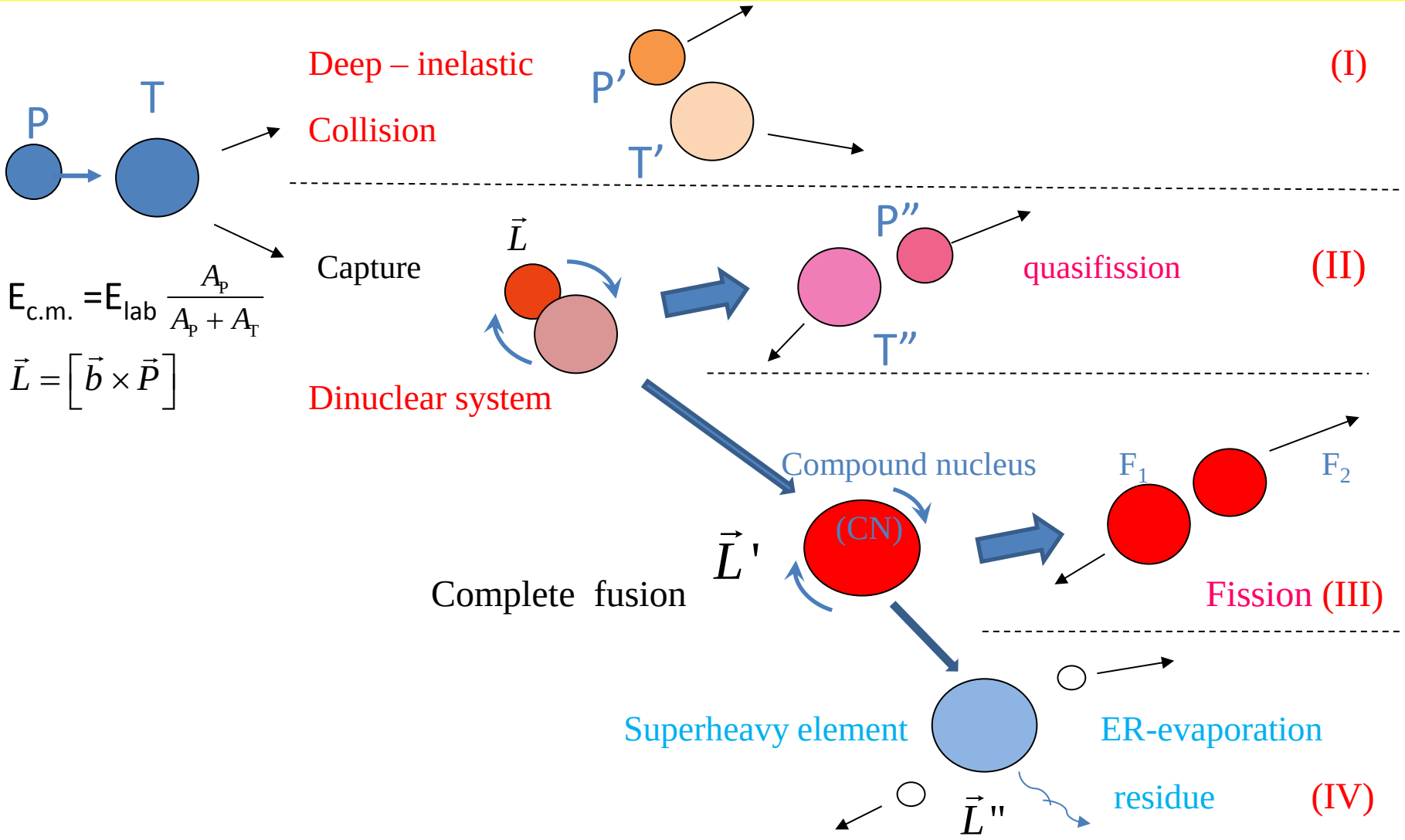

Partial cross sections of compound nucleus (CN), fusion-like (FL), damped (D), quasielastic (QE), Coulomb

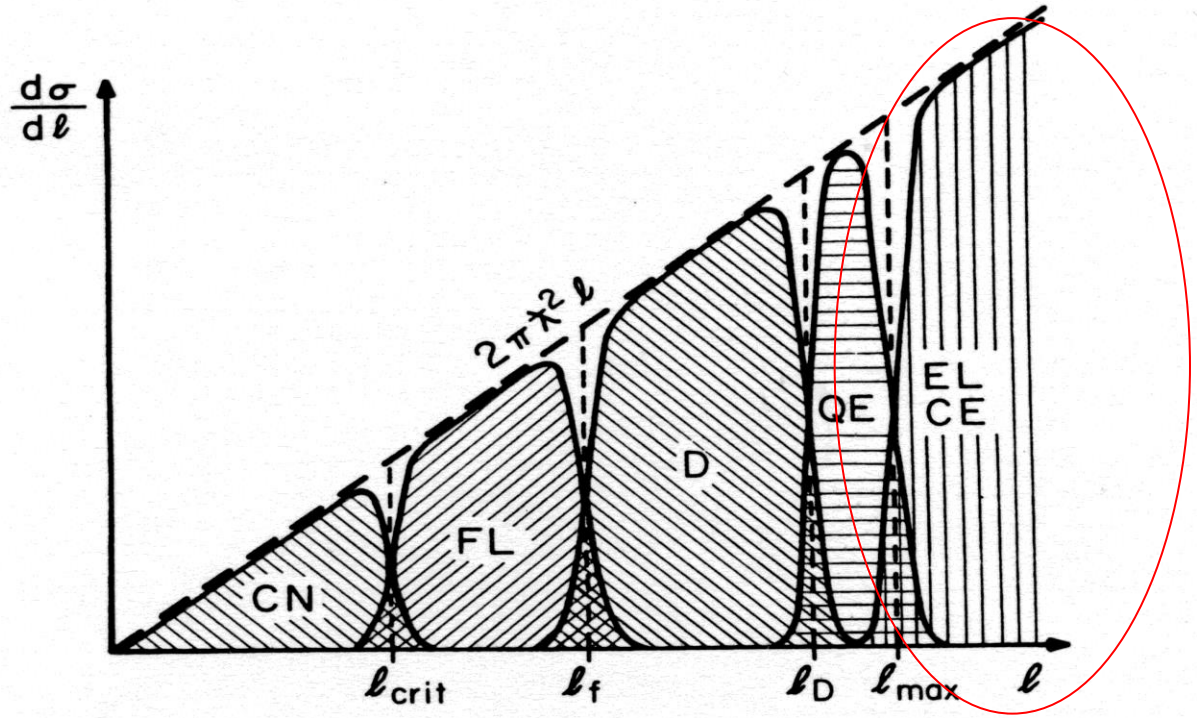

Figure 39. Schematic illustration of the l dependence of the partial cross section for compound-nucleus (CN), fusion-like (FL), damped (D), quasielastic (QE), Coulomb-excitation (CE), and elastic (EL) processes. The long-dashed line represents the geometrical partial cross section $d\sigma/dl = 2\pi\lambda^2 l$. Vertical dashed lines indicate the extensions of the various l windows in a sharp cutoff model with the characteristic l values noted at the abscissa. Hatched areas represent the diffuse l windows assumed in a smooth cutoff model.

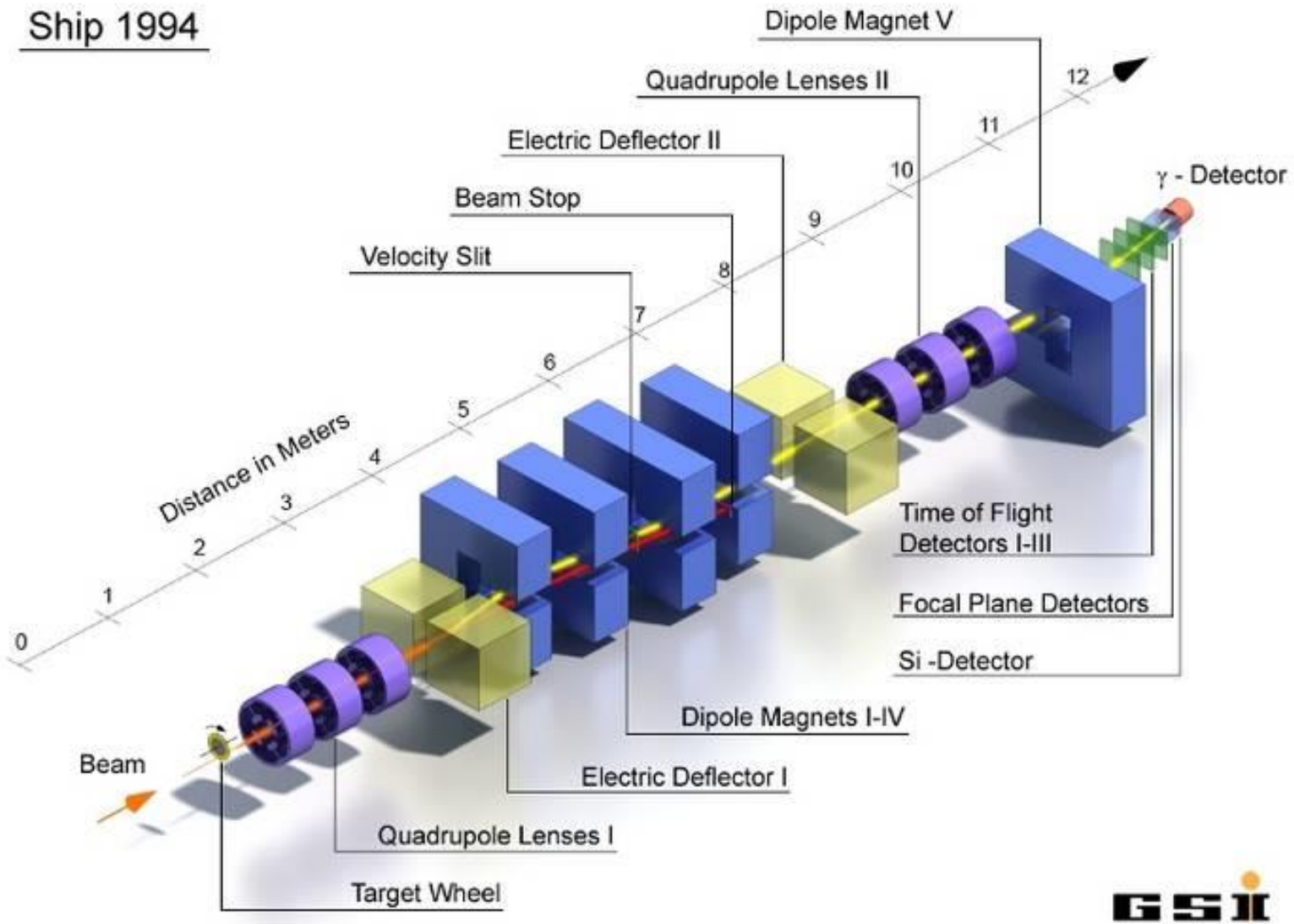

S. Hofmann et al, Rev. Mod. Phys., 72, 733-767 2000

Velocity separator SHIP

SHIP

Separation time:	1 – 2 µs
Transmission:	20 – 50 %
Background:	10 – 50 Hz
Det. E. resolution:	18 – 25 keV
Det. Pos. resolution:	150 µm
Dead time:	25 µs

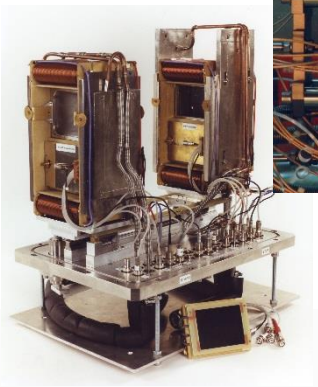

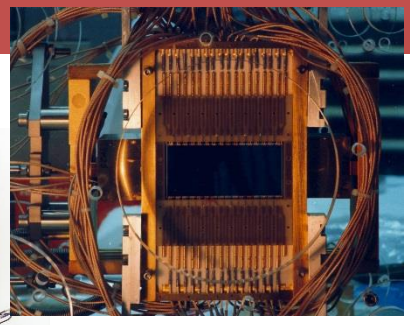

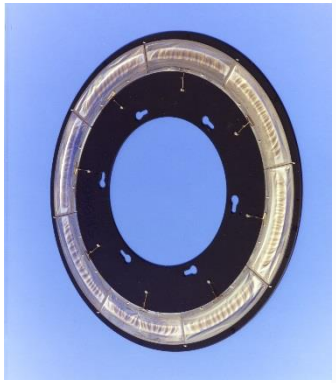

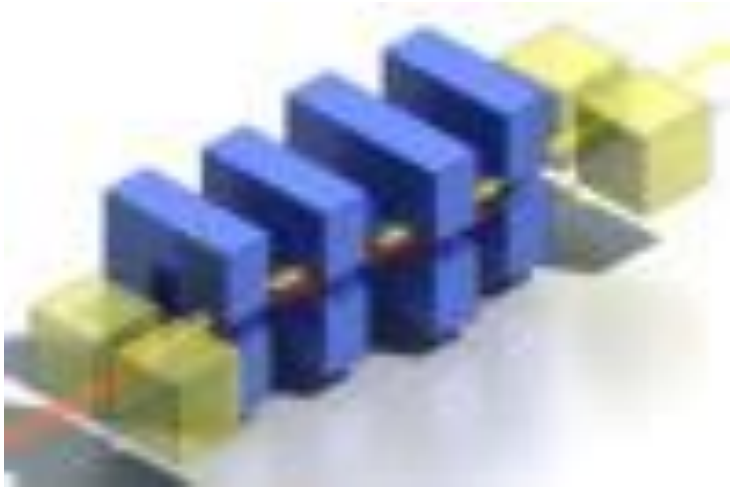

Velocity filter

he reaction products leave the target with velocities which are smaller than the velocity of the projectiles passing the target without interaction. This is due to the conservation of momentum:
The heavy evaporation residues have the same momentum as the light projectiles and therefore less velocity. The velocity of the compound nucleus (V_{CN}) is much smaller than velocities of other products.

$$V_{CN} = [M_p/(M_p+M_t)]\cdot V_p$$

A velocity filter exploits this fact to separate the reaction products

Velocity filter

The comparison of the (magnetic) Lorentzian force and the electric force of perpendicular magnetic and electric fields (crossed fields) yields a velocity dependence in the sense that for each velocity v_i a combination of forces can be found with a resulting force F_{tot}:

$F_{mag} = q \cdot v \cdot B$

$F_{el} = q \cdot E$

$F_{mag} = F_{el} \rightarrow F_{tot} = 0$

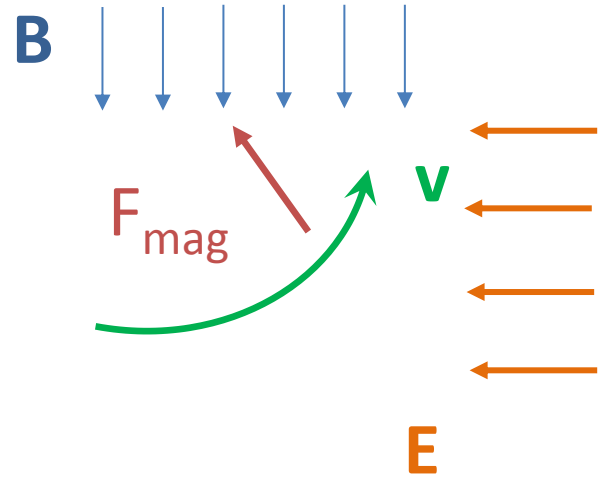

Time of flight detectors

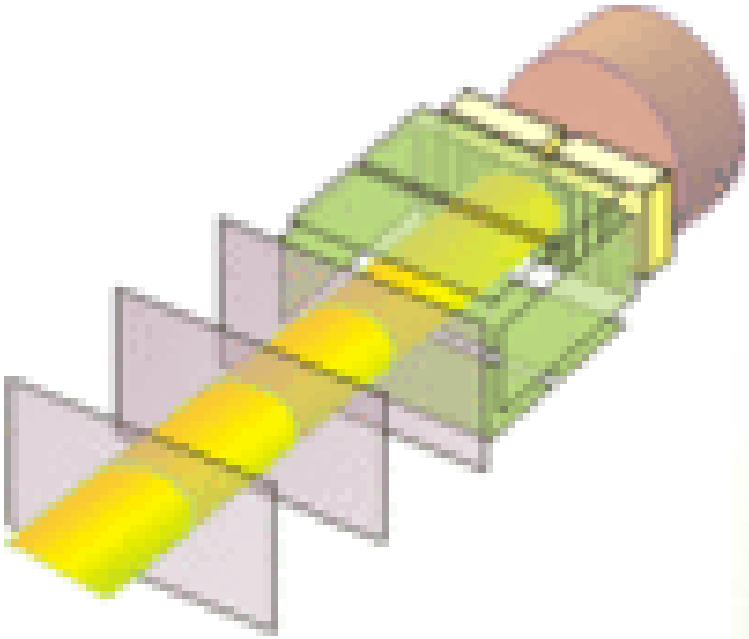

Position-Time Correlation

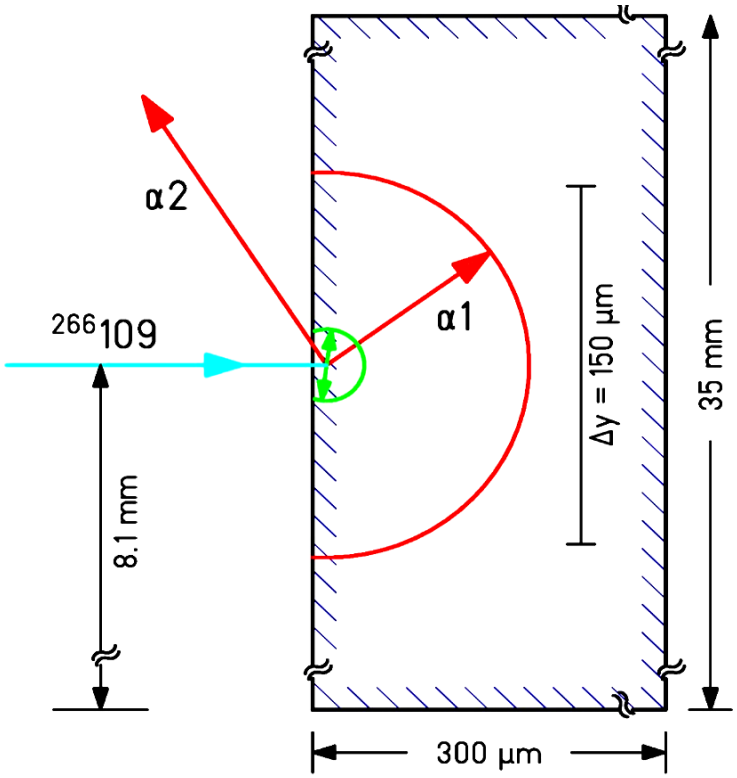

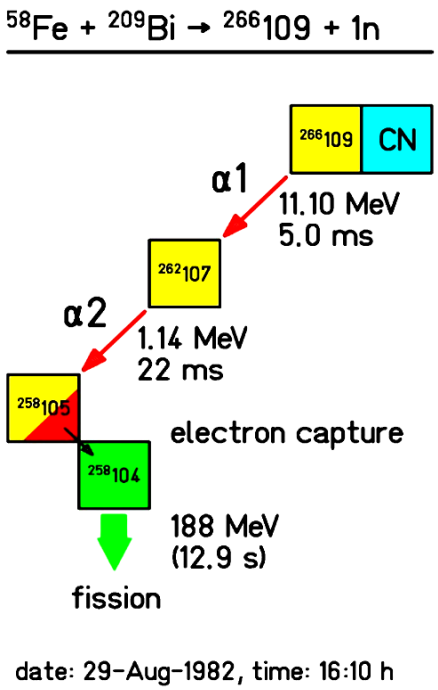

Detector: 80 mm × 35 mm × 300 µm
Pixel: 5 mm × 150 µm → 3700 pixels
ΔE_α: 14 keV (FWHM)

S.Saro, **Large size foil-microchannel plate timing detectors**
Nucl. Instr. Methods in Phys. Research A 381 (1996) 520

Excitation functions of the evaporation residue cross section at synthesis of superheavy elements

Projectiles

^{50}Ti, ^{54}Cr, ^{58}Fe, ^{64}Ni, ^{70}Zn

+ ^{208}Pb

Target

^{48}Ca + ^{244}Pu

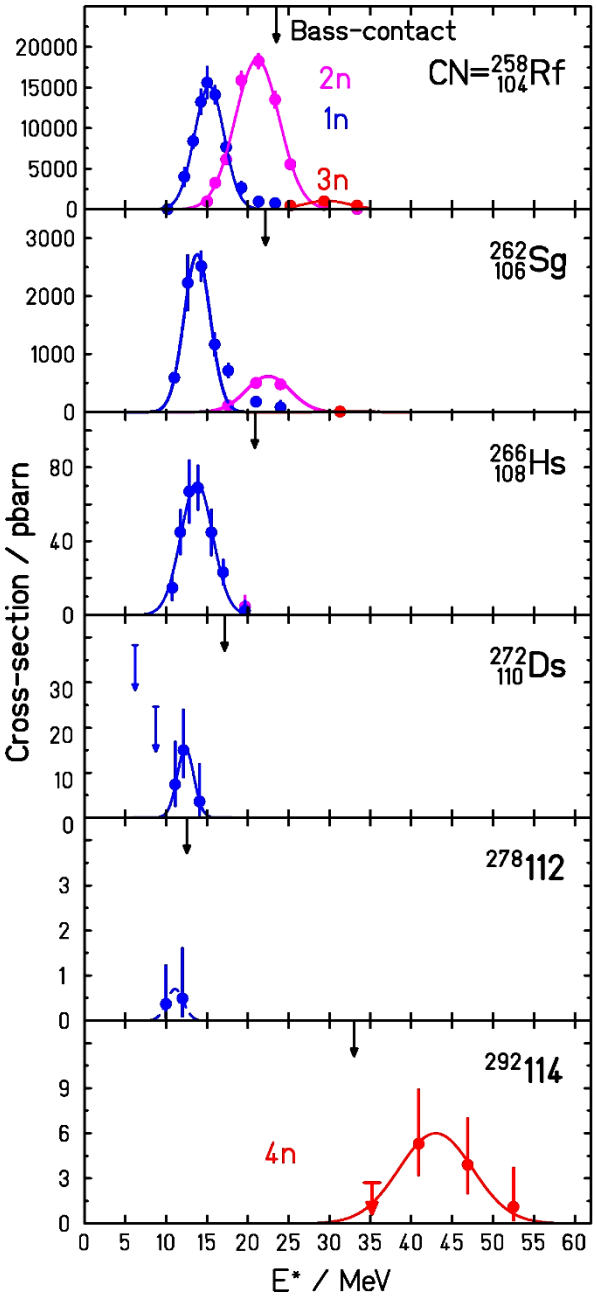

GSI

Cold fusion

Dubna

Hot fusion

Capture and fusion cross sections for the $^{48}Ca+^{238}U$ reaction.

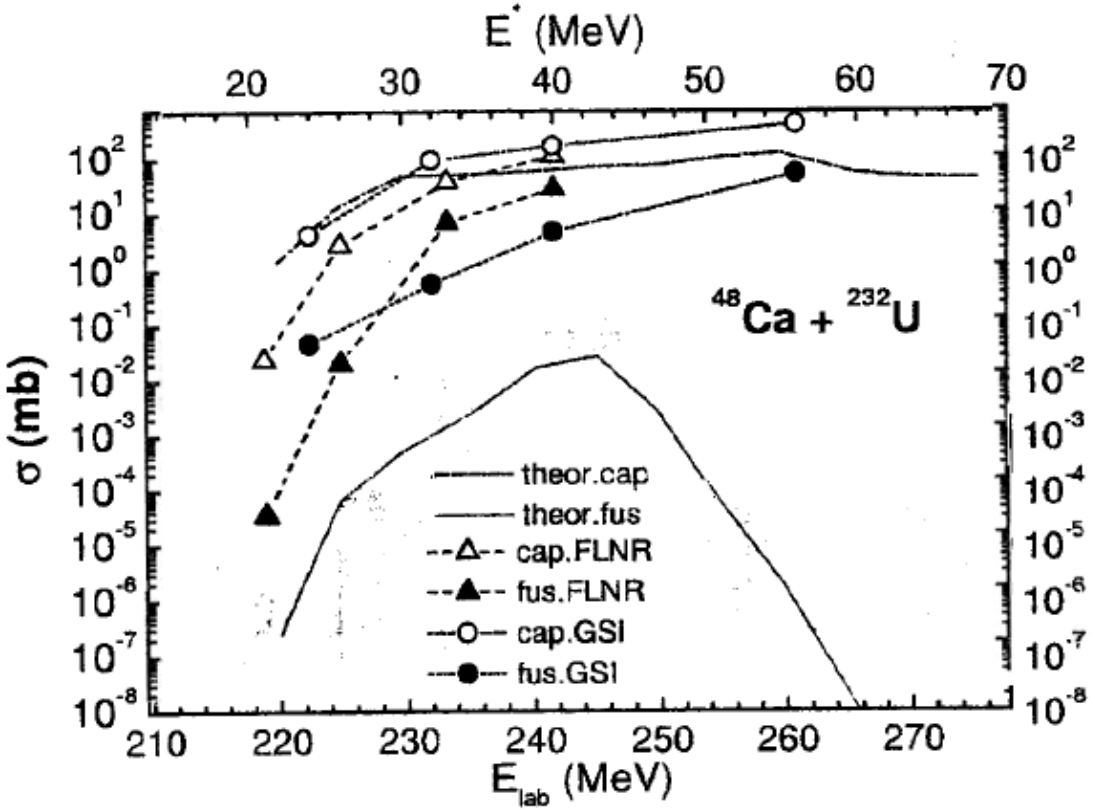

W.Q. Shen et al Phys.Rev. C**36**. 115 (1987) GSI experiment

Fig.1. Comparison the calculated excitation functions of capture (dashed-dotted curve) and fusion (solid curve) with the ones extracted from the experimental data for capture (dashed curve with open circles from [14], dashed curve with open triangles [15]) and fusion (dashed curve with solid circles from [14], dashed curve with solid triangles from [15]). The upper abscissa axe shows excitation energy of compound nucleus.

G.G. Adamian, G. Giardina, A.K. Nasirov, in Cont. of "XIV Int. Workshop on Nuclear Fission" Physics, Obninsk, 1998, Russia, 2000

Capture and fusion cross sections for the $^{48}Ca+^{238}U$ reaction.

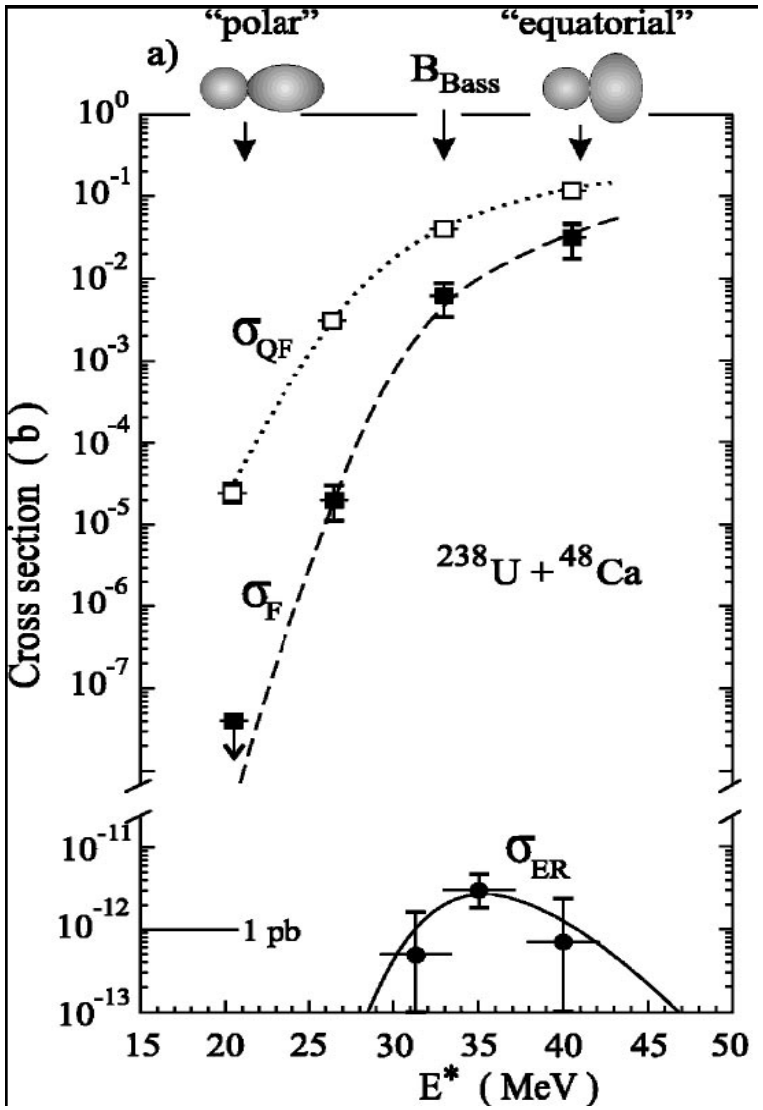

Yu.Ts Oganessian et al,Phys.Rev.C **70** 064609 (2004)

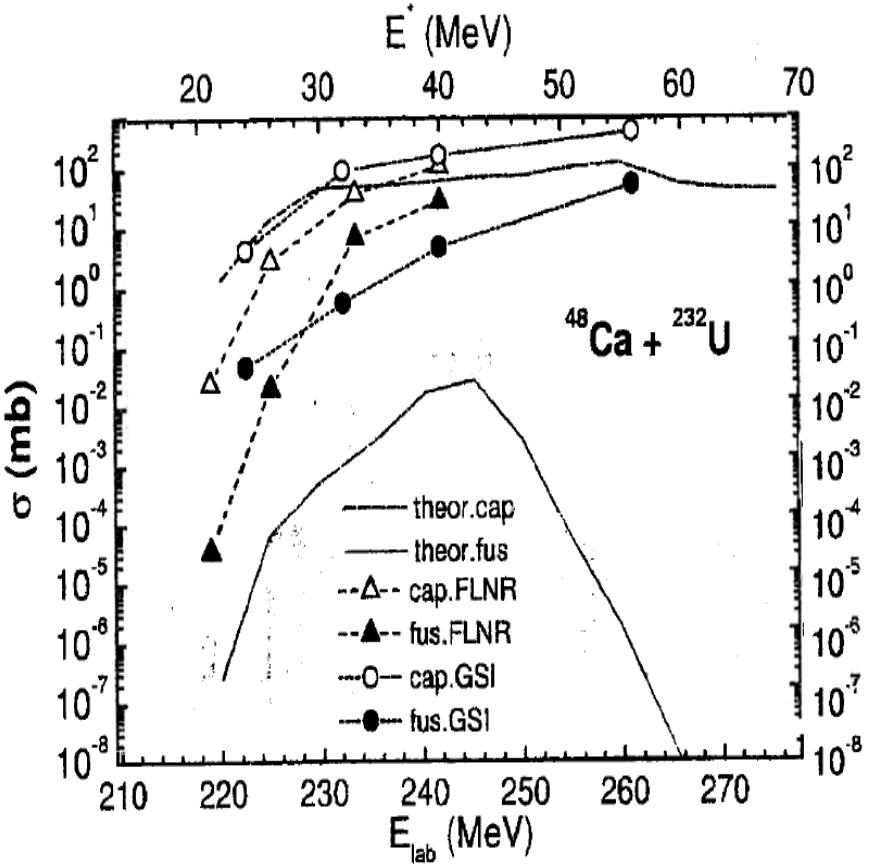

W.Q. Shen et al Phys.Rev. C**36**. 115 (1987) GSI experiment

G.G. Adamian, G. Giardina, A.K. Nasirov, in Cont. of "XIV Int. Workshop on Nuclear Fission" Physics, Obninsk, 1998, Russia, 2000

Results of calculation and comparison of them with the experimental data for the "cold" $^{64}Ni+^{208}Pb$ and $^{70}Zn+^{208}Pb$ reactions.

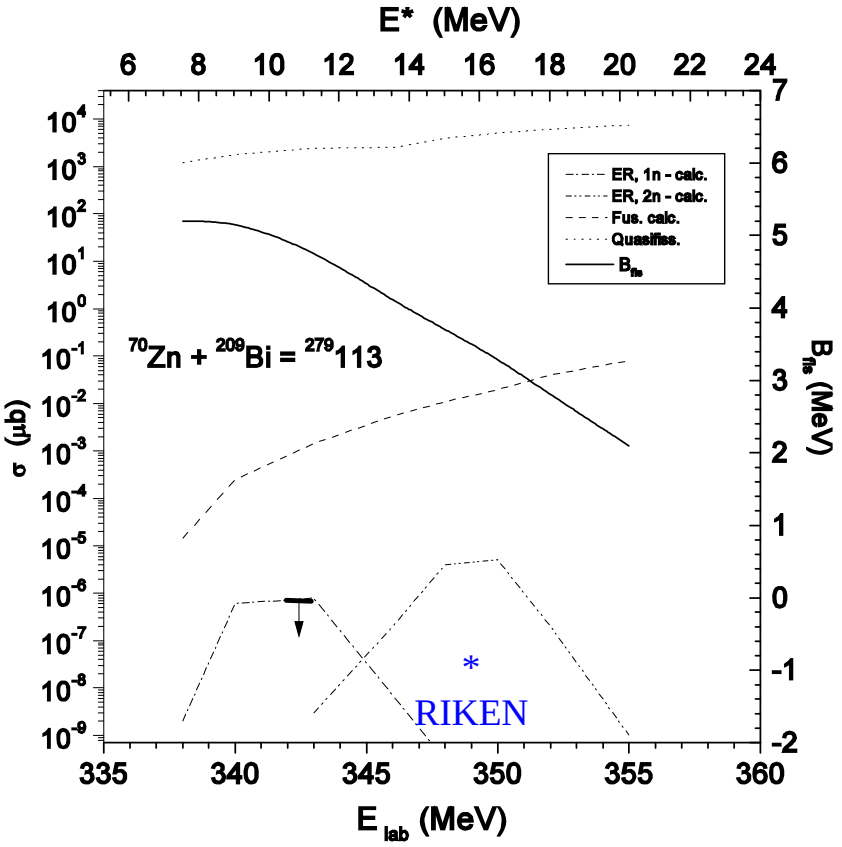

G.Giardina, et al.
Eur. Phys. J. A **8**, 205–216 (2000)

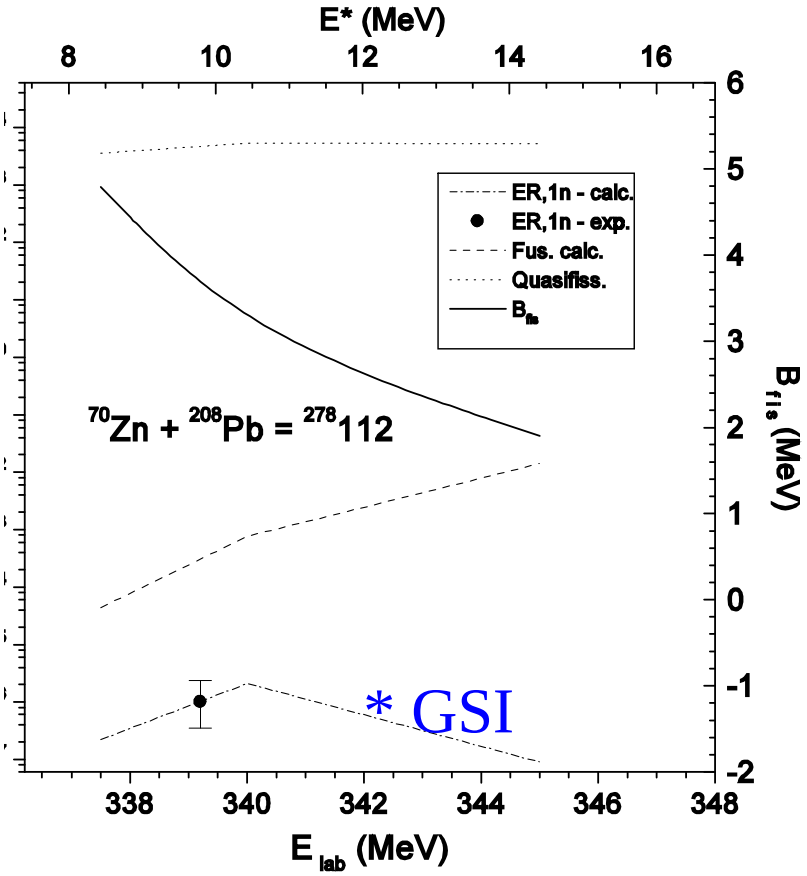

S. Hofmann,
Rep. Progr. Phys. **61**, 639 (1998);

Comparison of conditions at cold and hot fusion

$$\sigma_{ER}(E_{Lab}, L) = \langle \sigma_{cap}(E_{Lab}, L)\, P_{CN}(E_{Lab}, L)\, W_{surv}(E_{Lab}, L) \rangle$$

Hot fusion	Cold Fusion	Main reason
$\sigma_{cap}(E_{Lab}, L)$ >	$\sigma_{cap}(E_{Lab}, L_{\sigma})$:	$B_{qfis} > B_{qfis}$
$P_{CN}(E_{Lab}, L)$ >	$P_{CN}(E_{Lab}, L)$:	$B_{fus} < B_{fus}$
$W_{surv}(E_{Lab}, L)$ <	$W_{surv}(E_{Lab}, L)$:	$E^*_{CN} > E^*_{CN}$

SHE experiments showed: $\sigma_{ER}(E_1) > \sigma_{ER}(E_2)$

But recent experiment $^{48}Ca + ^{238}U$ showed opposite $\sigma_{ER}(E_1) < \sigma_{ER}(E_2)$

The estimation of the nucleus radius by the elastic scattering of neutrons

The diffraction pattern of neutrons scattered from nuclei. The classical turning point for collision with momentum p=$\hbar$k and angular momentum $\hbar\ell$ occurs when

$k^2 = \ell(\ell+1)/R^2 \approx (\ell+1/2)^2/R^2$

We suppose that neutrons which pass within a distance R of the nucleus are absorbed then there will be not outgoing wave for small angular momentum,

$\eta_\ell = 0$ for $\ell < k R - \frac{1}{2}$,

while for large angular momentum, the outgoing wave will be as in the plane wave:

$\eta_\ell = 1$ for $\ell > k R - \frac{1}{2}$

The estimation of the nucleus radius by the elastic scattering of neutrons

Thus the cross section is found by

$$\frac{d\sigma}{d\Omega} = \frac{\pi}{k^2}\left|\sum_{\ell=0}^{kR-1/2}\sqrt{2\ell+1}Y_\ell^0(\theta)\right|^2$$

If *kR* is small the sum has only a few terms and we have small cross section; if *kR* is large we may use the analytical approximation for the spherical harmonics,

for large θℓ*:*

$$Y_\ell^0 = \frac{\sin\left[\left(\ell+1/2\right)\theta+\frac{\pi}{4}\right]}{\pi\sqrt{\sin\theta}}$$

for small θℓ*:*

$$Y_\ell^0 \approx \sqrt{\frac{(2\ell+1)}{4\pi}}\left(1-\ell(\ell+1)\theta^2/2\right)$$

Then the sum may be is approximated by the integral

$$\frac{d\sigma}{d\Omega} = \frac{\pi}{k^2}\left|\int_0^{kR-1/2}\frac{d\ell}{\pi}\frac{\sqrt{2\ell+1}}{\sin\theta}\sin\left[\left(\ell+1/2\right)\theta+\frac{\pi}{4}\right]\right|^2$$

The estimation of the nucleus radius by the elastic scattering of neutrons

For large values of $Rk\vartheta >> 1$

$$\frac{d\sigma}{d\Omega} = \frac{2R}{\pi k\theta^2 \sin\theta}\cos^2\left(Rk\theta + \frac{\pi}{4}\right)^2$$

For small values of $Rk\vartheta << 1$

$$\frac{d\sigma}{d\Omega} = \frac{k^2R^4}{4}\left(1 - \left(Rk\theta/2\right)^2\right)^2$$

Estimations showed that cross section has maximum at the forward direction and its minimum is at angle

$\theta_{min} \approx \frac{5\pi}{4kR} \approx 15°$. At k=2 fm^{-1}, we have R=7.5 fm for Pb

Total cross section of elastic scattering

The differential cross section

$$\frac{d\sigma}{d\Omega} = |f(\theta)|^2 \tag{1.40}$$

is now a double sum over the angular momenta l, in which the contributions of different angular momenta interfere,

$$\frac{d\sigma}{d\Omega} = \frac{1}{4k^2} \sum_{l,l'=0}^{\infty} (2l+1)(2l'+1)(S_l - 1)(S_{l'}^* - 1) P_l(\cos\theta) P_{l'}(\cos\theta). \tag{1.41}$$

The total elastic scattering cross section (1.15) is obtained by integrating expression (1.41) over angles. Using the orthogonality relation (1.23) for the Legendre polynomials we find

$$\sigma_{\text{el}} = 2\pi \int_{-1}^{1} d(\cos\theta) \frac{d\sigma}{d\Omega} = \frac{\pi}{k^2} \sum_{l=0}^{\infty} (2l+1)|S_l - 1|^2, \tag{1.42}$$

where $S_\ell = e^{2i\delta_\ell}$, so cross section is determined by phase shift which depends on the peculiarities of the interaction potential.

A. Messiah , Quantum Mechanics, Vol. 1.
P. Fröbrich, R. Lipperheide, Theory of Nuclear Reactions, Clarendon Press. 1996

Quasielastic transfer in the $^{136}Xe+^{64}Ni$ reaction

M. Sefarraza, *et al.*,
Phys.Rev. C 55 (1997) p.2541

Angular distributions normalized to Rutherford scattering for the "elastic" and low-lying (2^+ and 4^+) inelastic excitations of the target and projectile. The bold curve corresponds to the sum of the elastic and inelastic distributions of the coupled channel Born approximation calculation.

An effective interaction radius *R* can be determined based on ''quarter-point recipe" [Bass] which assumes

$$\frac{\sigma_R(\theta_{gr})}{\sigma_{Rutherford}(\theta_{gr})}=1/4$$

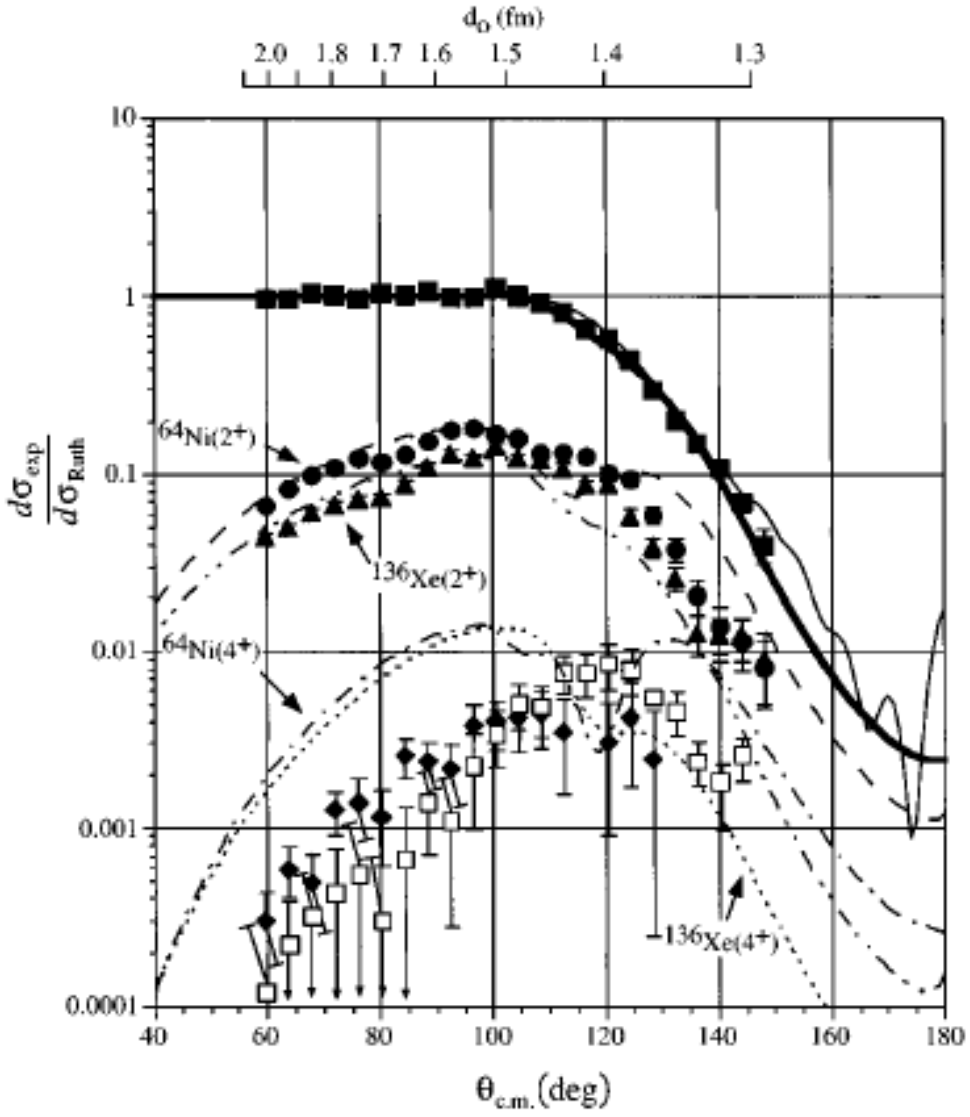

Main characteristics of elastic collisions and rainbow scattering

- The product mass and charge numbers are very close or the same values as ones of the projectile and target nuclei;
- Angular distribution of the reaction products extends in the wide range $0 < \theta < \pi/2$ but its maxima are placed near grazing angle and rainbow angles;
- Energy loss is small and consists some MeV's;
- The cross section of elastic scattering is very large in comparison with inelastic and deep-inelastic collisions which take place at smaller values of angular momentum.

Classification of reactions by impact parameter.

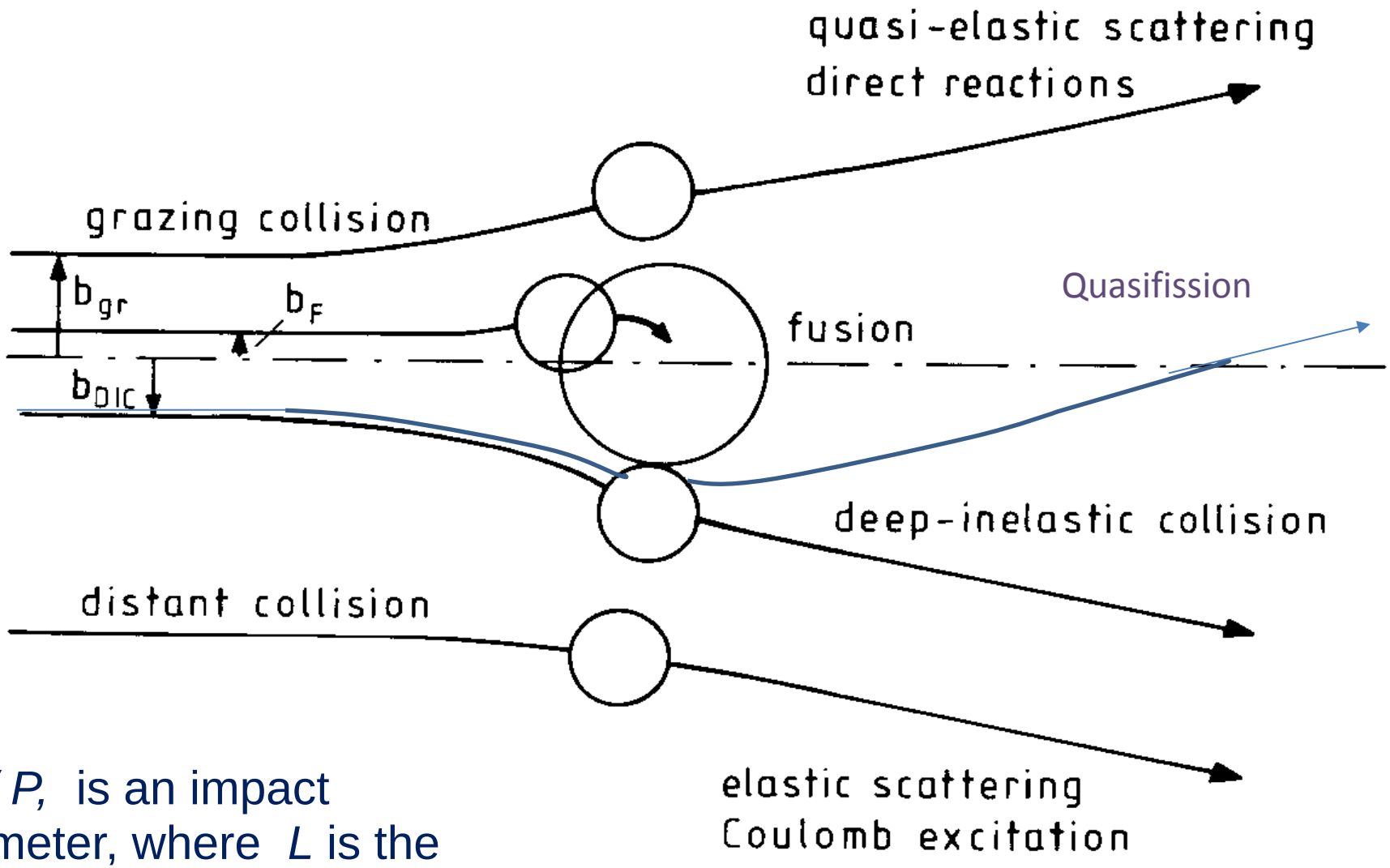

b=L / P, is an impact parameter, where *L* is the orbital angular momentum and *P* is momentum of relative motion

Semiclassical interpretation of potential scattering

- The wavelengths associated with heavy-ion scattering are usually short enough, and consequently the number of partial waves involved is sufficiently large, that use of the language of semiclassical trajectories becomes meaningful and very useful for understanding the characteristics of the scattering.
- The presence of absorption plays a very important role in determining the outcome of the collision. but in practice does not destroy the underlying trajectory picture. Qualitatively, absorption can be thought of as simply damping the flux as the system traverses the classical path.
- Description of the deep-inelastic collisions allows to analyze the behavior of interacting system formed at trajectories corresponding to the absorbed partial waves.

Heavy ions are many body system

Atomic nucleus is a quantum object which consists from protons and neutrons binding by strong nucleon-nucleon interaction. The reaction taking place in collisions of atomic nuclei should be described adequately. The application of classical picture requires consideration of nucleus as localized wave packets. The role of the electron shell is not so important in nucleus-nucleus interaction because of smallness of the electron's mass $m_e/m_N=0.0005$

.

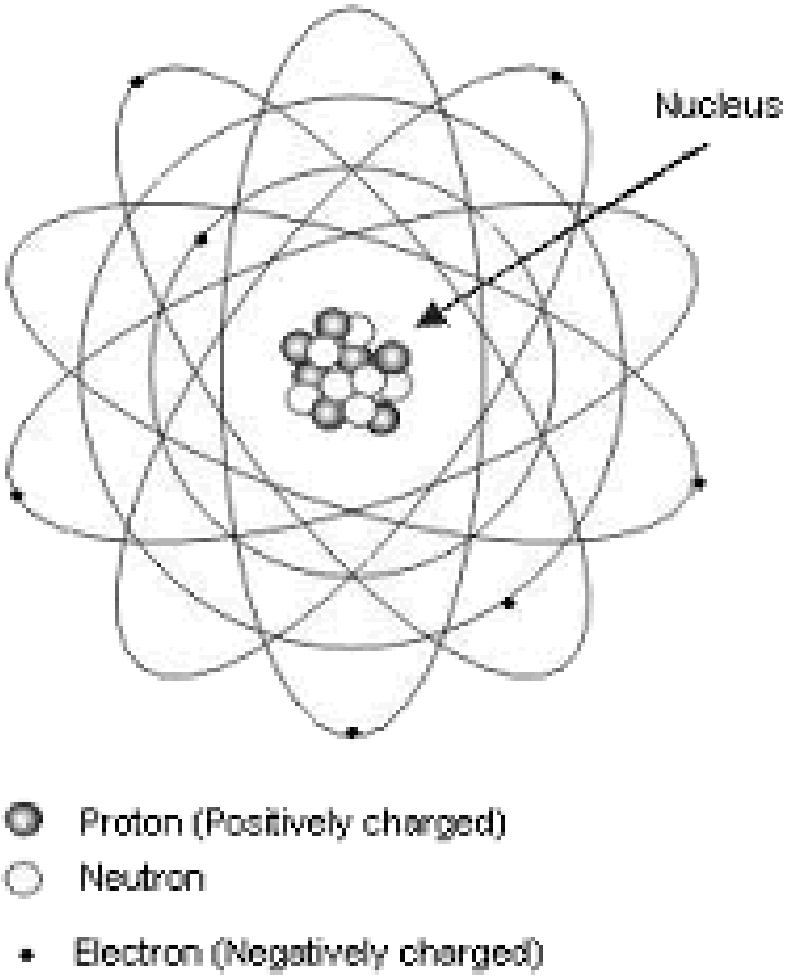

Basic quantities for colliding nuclei

$E_{c.m.}$, L=[b x P]

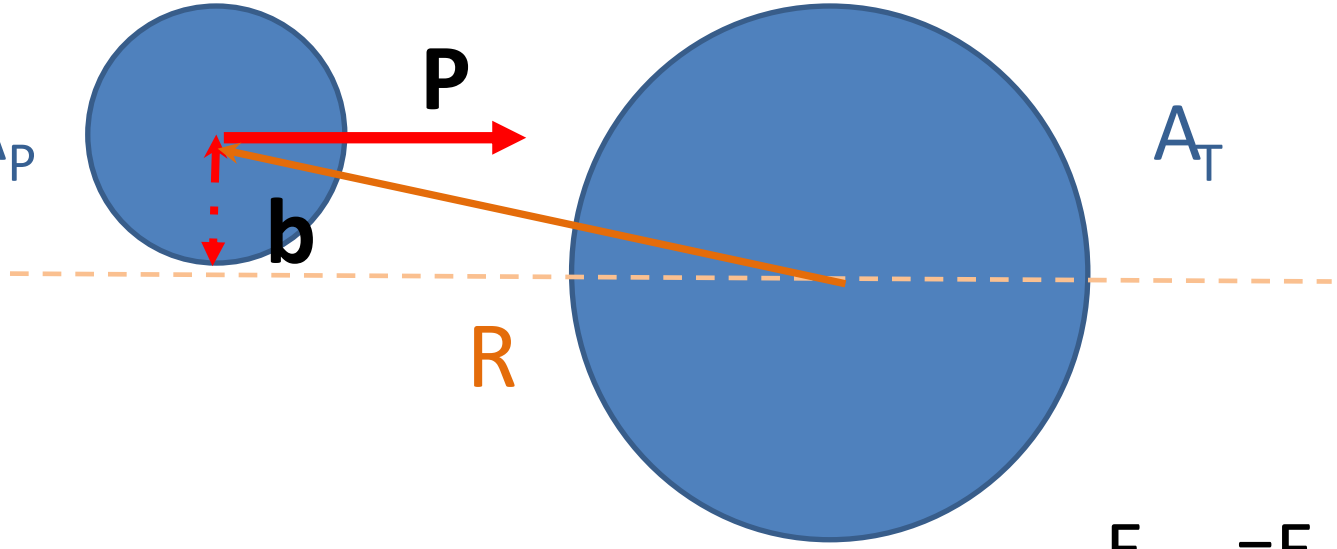

$E_{c.m.}=E_{lab}\ A_T\ /(A_P+A_T)$

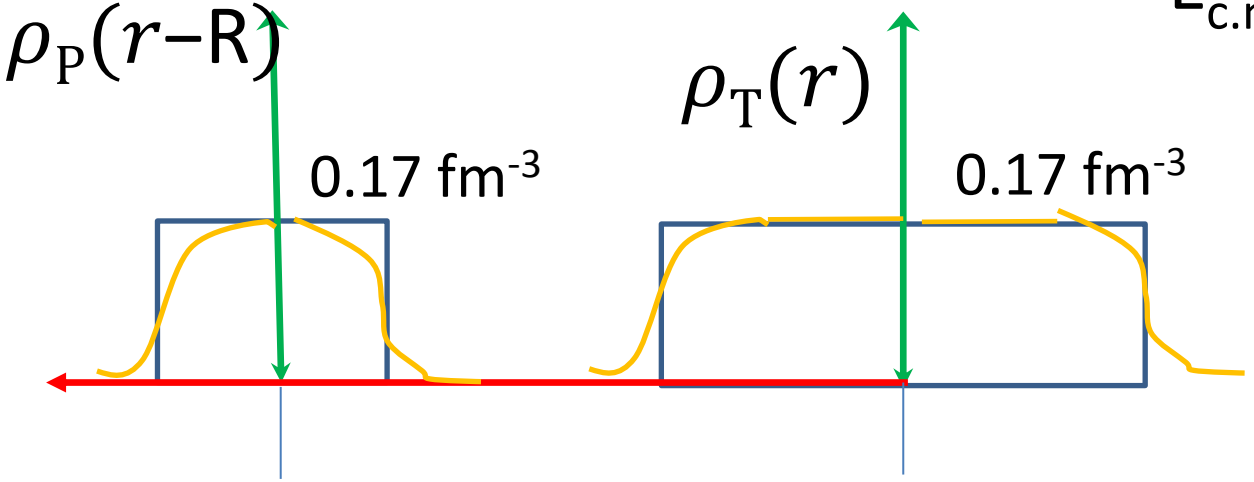

Adequacy of the classical description the reaction dynamics in heavy ion collisions

The spread of energies in a wave packet of width ΔR may be estimated by

$$\Delta E = \frac{\Delta P^2}{2M} ,$$

where M is a reduced mass of the colliding nuclei $M = \frac{M_1 M_2}{M_1 + M_2}$. From the Heisenberg uncertainty principle for the coordinate and momentum we have

$$\Delta P \Delta R \geq \frac{\hbar}{2}$$

that allows us to find connection between widths of energy and space coordinate $\Delta E = \frac{\hbar^2}{2 \cdot 4\, M(\Delta R)^2} = \frac{(\hbar c)^2}{8A\ \mathrm{m}_N\, c^2 (\Delta R)^2} \cong \frac{(197)^2 (\mathrm{MeV\ fm})^2}{8\ A\ 939\ \mathrm{MeV} (\Delta R)^2} \cong \frac{5\ \mathrm{MeVfm}^2}{A(\Delta R)^2}$

In the last expression $A = \frac{A_1 A_2}{A_1 + A_2}$. Thus, for example ^{16}O+^{208}Pb reaction we have A=14 and

$$\Delta E (\Delta R)^2 \geq 0.3 \ \mathrm{MeV\ fm}^2.$$

As light as oxygen may be localized to within 0.5 fm by a wave packet with an energy spread of 1 MeV. For heavier ions the energy spread decreases like A^{-1}. We conclude that a classical description of the relative motion is appropriate.

The conditions of application of the classical approaches

The most important parameter pertaining to semiclassical considerations is the reduced wave length $\lambda\!\!\!^{-}$ of the system of two interacting heavy ions

$$\lambda\!\!\!^{-}(r) = \frac{\hbar}{P(r)} = \frac{\hbar}{\sqrt{2\mu(E_{\text{c.m.}} - V(r))}} \qquad (1)$$

Here, μ is the reduced mass; $P(r)$ is momentum of relative motion; $E_{\text{c.m.}}$ and $V(r)$ are the center-of-mass energy and the interaction potential, respectively. The classical approximation is generally valid if the radius R of curvature of the trajectory to be large

$$\frac{\lambda\!\!\!^{-}}{R} \ll 1 \qquad (2)$$

The condition for the centrifugal forces is found as $\frac{\mu v^2}{R} = \left|\text{grad } V(r)\right|$.

Putting R found here into (2) we have $\frac{\lambda\!\!\!^{-}\left|\text{grad } V(r)\right|}{\mu v^2} \ll 1$ (3)

Finding $\left|\text{grad } V\right|$ from (1) we find condition for wave length $\left|\text{grad } \lambda\!\!\!^{-}\right| \ll 1$, which means that the wave transverse size is large in comparison with $\lambda\!\!\!^{-}$.

Application of classical physics to description of Coulomb scattering in heavy ion collisions

The smallness of the wave length of the relative motion in heavy ion collisions in comparison with the size of colliding nuclei allows to use the classical physics presentations to study dynamics of heavy ion trajectory determined by Coulomb and nuclear forces.

$$\frac{p_r^2}{2\mu} + \frac{l(l+1)\hbar^2}{2\mu r^2} + \frac{Z_1 Z_2 e^2}{r} = E. \qquad (4)$$

The criterion of application of the classical mechanics to the Coulomb trajectory is ratio of the wave length of the relative motion to the closest distance between nuclear centers r_{min} :

$$\frac{\lambda\!\!\!^{-}}{r_{min}} \ll 1. \qquad (5)$$

$$r_{min} = \frac{Z_1 Z_2 e^2}{E}.$$

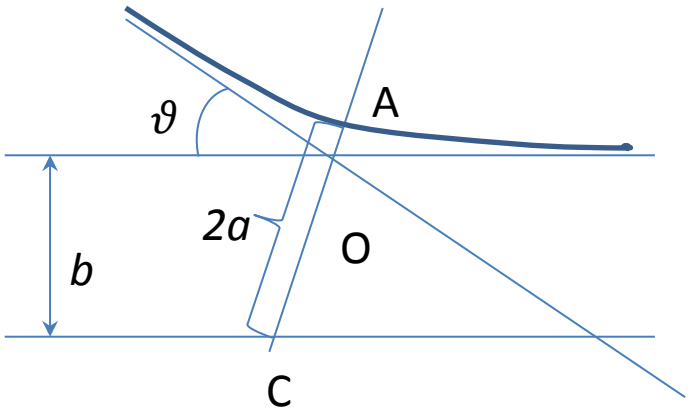

Study of the inelastic and deep-inelastic collisions of heavy ions at Coulomb barrier energies (E_{lab}=5-10 MeV/nucleon)

It is natural that the stronger the absorption, the smaller the chance to observe the rainbow pattern. Due to the strong absorption, most of the elastic HI scattering is dominated by the surface scattering and the information about the nucleus-nucleus interaction is obtained for peripheral trajectories only. Here, the term "surface" means the region where the nuclear forces begin to act strongly. It corresponds to the distance:

$$R_{\mathrm{sa}} = r_0(A_1^{1/3} + A_2^{1/3}) + \Delta.$$

$$r_0 \approx 1.1 \ \mathrm{fm},$$

Values of Δ between 2 and 3 fm are typical separations at bombarding energies with E/A = l0-20MeV.

P.J. Siemens, A.S. Jensen, Elements of Nuclei , Addison Wesley Publ. Comp. 1987

Grazing angular momentum ℓ_{gr}

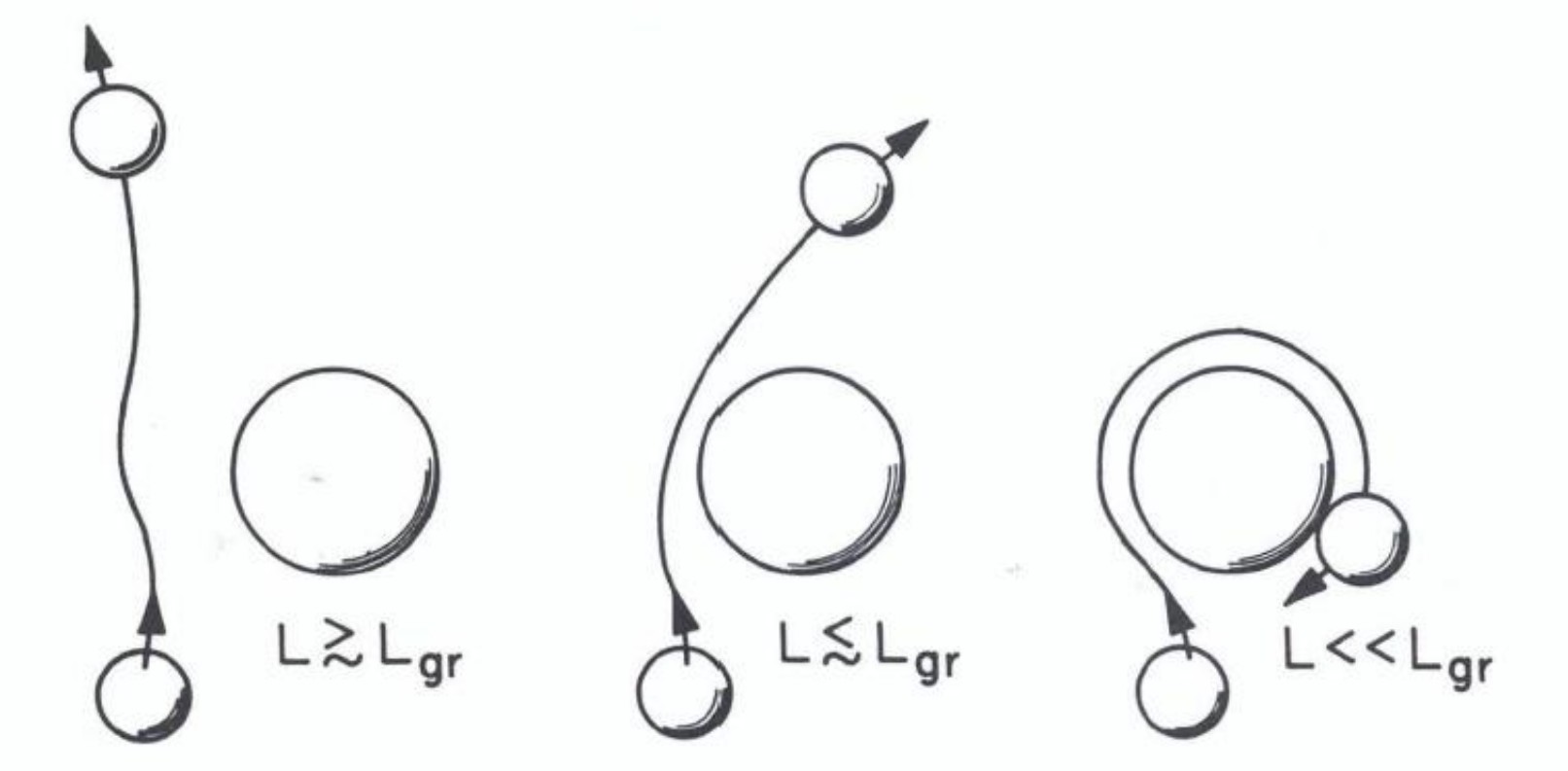

Philip J. Siemens and Aksel S. Jensen, Elements of Nuclei.
Many- Body Physics with the Strong Interaction, Addison –Wesley Publishing Company, 1987.

Scheme of setup COMBAS of the Flerov Laboratory of Nuclear Reaction at Joint Institute for Nuclear Research to register the binary reaction products in coincidence.

http://flerovlab.jinr.ru/linkc/eng_1/corset.html

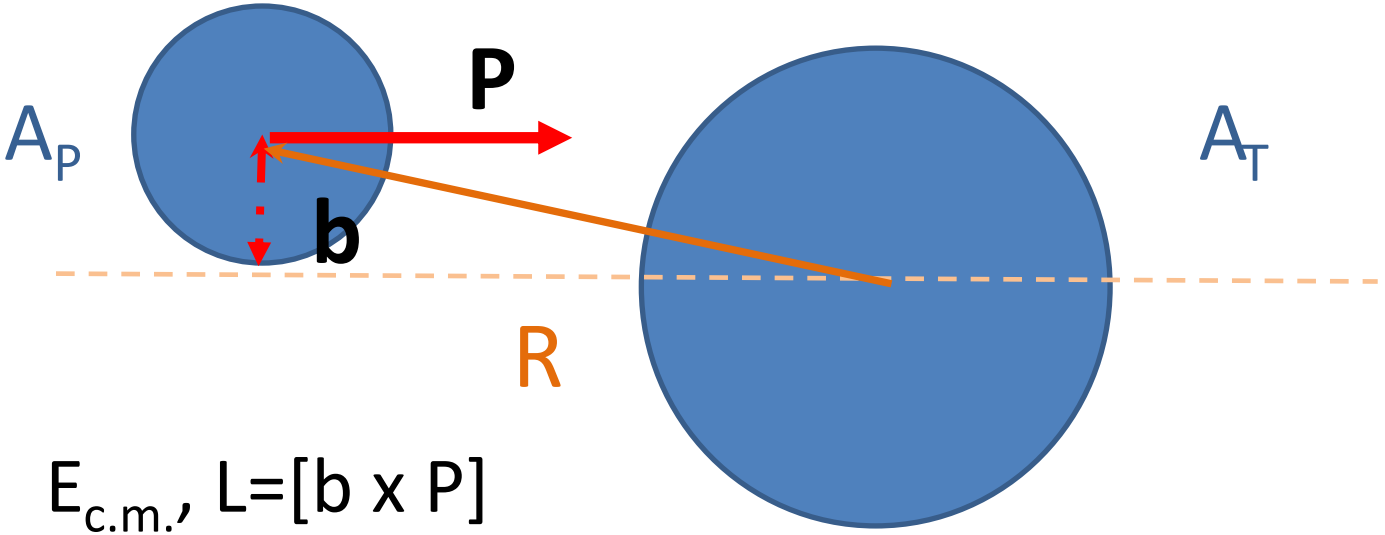

$E_{c.m.}$, L=[b x P]

Dependence of the reaction types on the initial beam energy and orbital angular momentum.

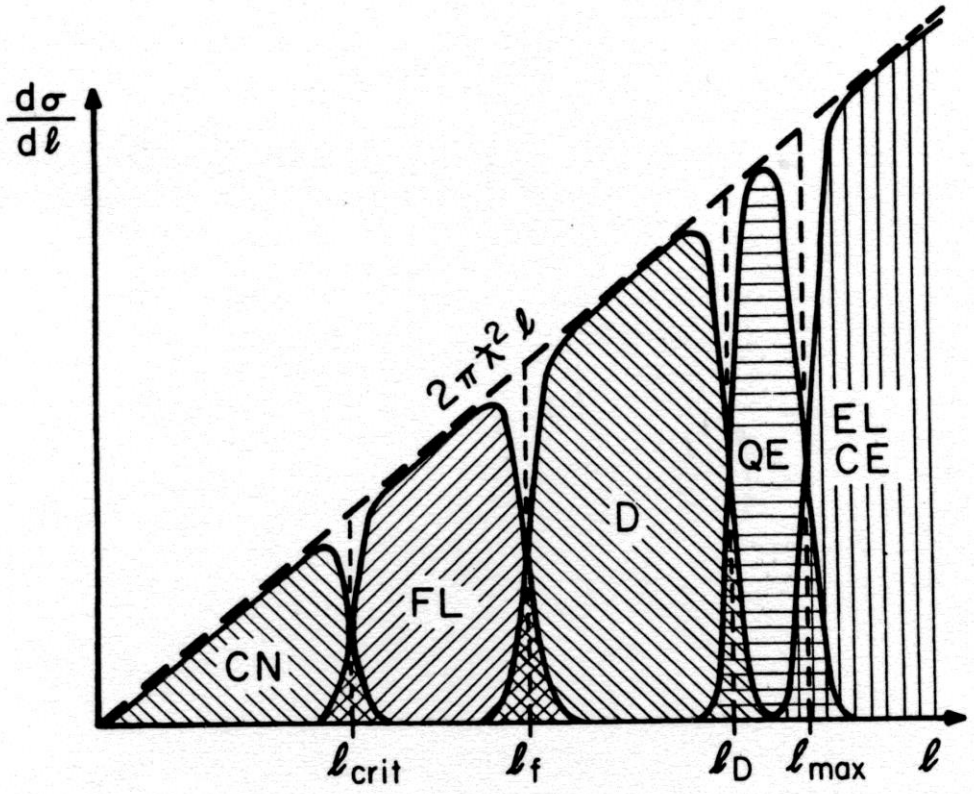

Figure 39. Schematic illustration of the l dependence of the partial cross section for compound-nucleus (CN), fusion-like (FL), damped (D), quasielastic (QE), Coulomb-excitation (CE), and elastic (EL) processes. The long-dashed line represents the geometrical partial cross section $d\sigma/dl = 2\pi\lambda^2 l$. Vertical dashed lines indicate the extensions of the various l windows in a sharp cutoff model with the characteristic l values noted at the abscissa. Hatched areas represent the diffuse l windows assumed in a smooth cutoff model.

Importance of correct separation of fusion-fission fragments from the quasifission and fast-fission products

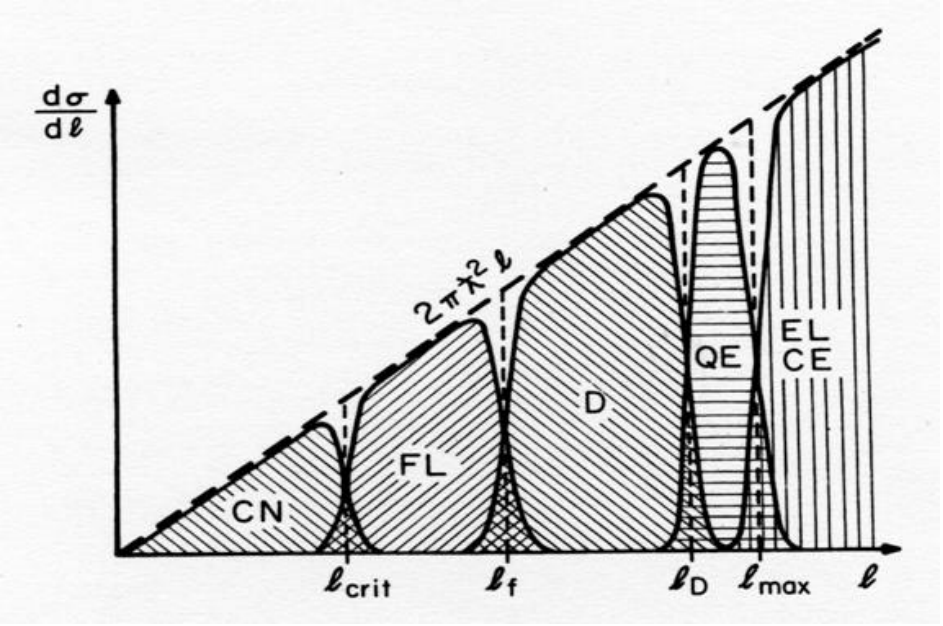

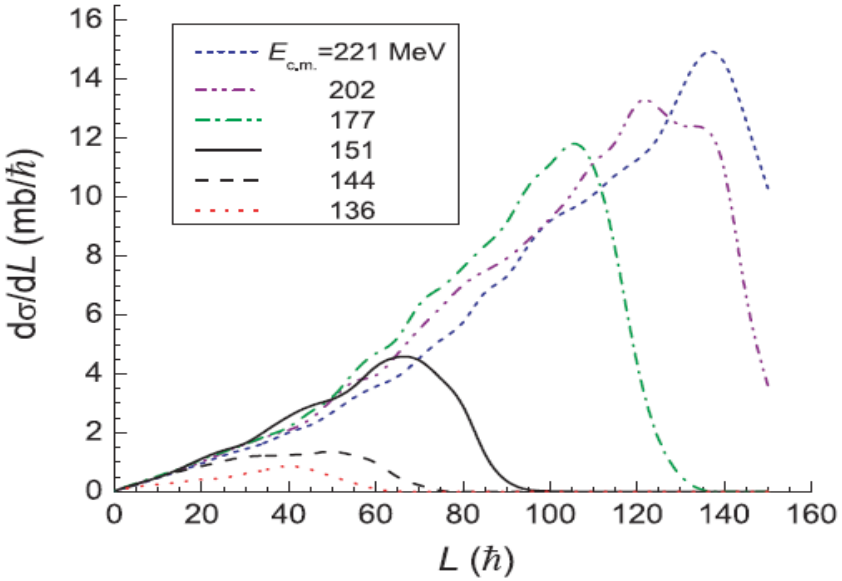

Well known approach is that angular momentum distribution allows us to differ products of reaction channels if it is possible to estimate key values of angular momentum, as ℓ_{crit}, ℓ_{f}, $\ell_{D.}$

The total cross section of inelastic collisions

The total cross section for reactions dominated by the strong interaction (inelastic collisions) may be estimated by expression

$$\sigma_{geom} = \frac{\pi}{k^2}\sum_{0}^{\ell_{gr}}(2\ell+1) = \frac{\pi}{k^2}(\ell_{gr}+1)^2$$

$$\approx \pi {r_0}^2\left({A_1}^{1/3} + {A_2}^{1/3}\right)^2\left(1 - {U_C}/{E}\right)$$

This is called the geometric cross section.

Trajectories with angular momenta larger than ℓ_{gr} will still lead to Coulomb scattering. Trajectories with angular momenta near ℓ_{gr} are likely to lead to inelastic reactions, but they may also lead to elastic scattering.

The elastic scattering angle corresponding to these trajectories will be reduced by the attractive nuclear force between the target and projectile. Thus there is, classically, a maximum angle of deflection ϑ_r corresponding to a Coulomb trajectory with angular momentum just larger than ℓ_{gr} .

Deep inelastic collisions : macroscopic view seems to be OLD ?!

diffusion effects on nucleons

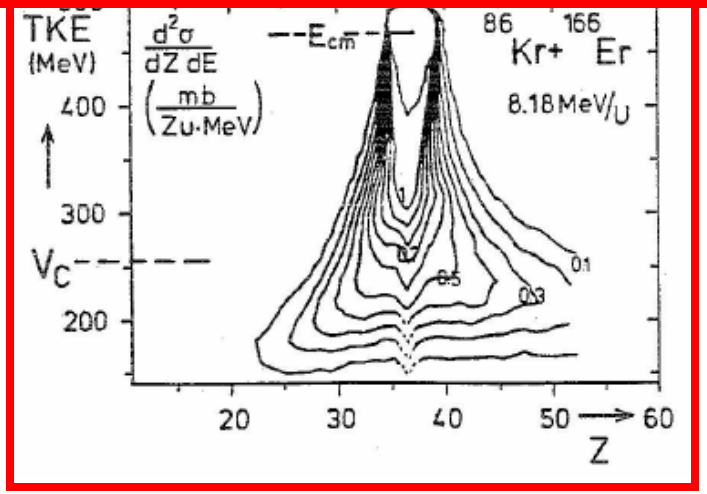

angular dependence of energy loss

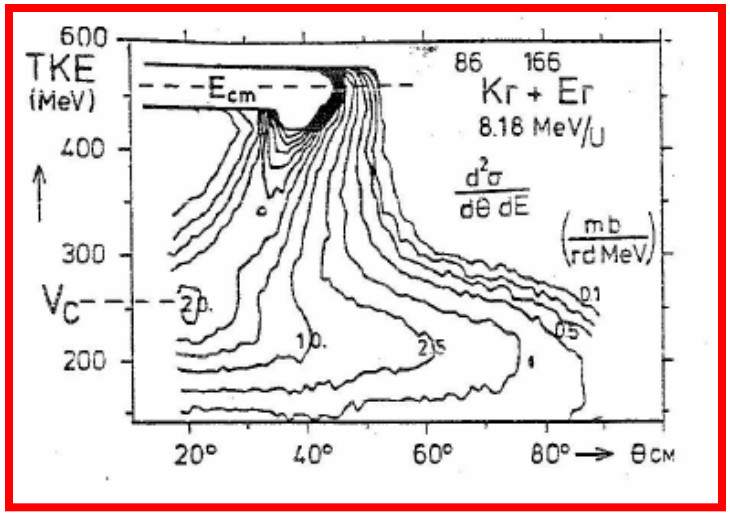

concept of dinuclear system

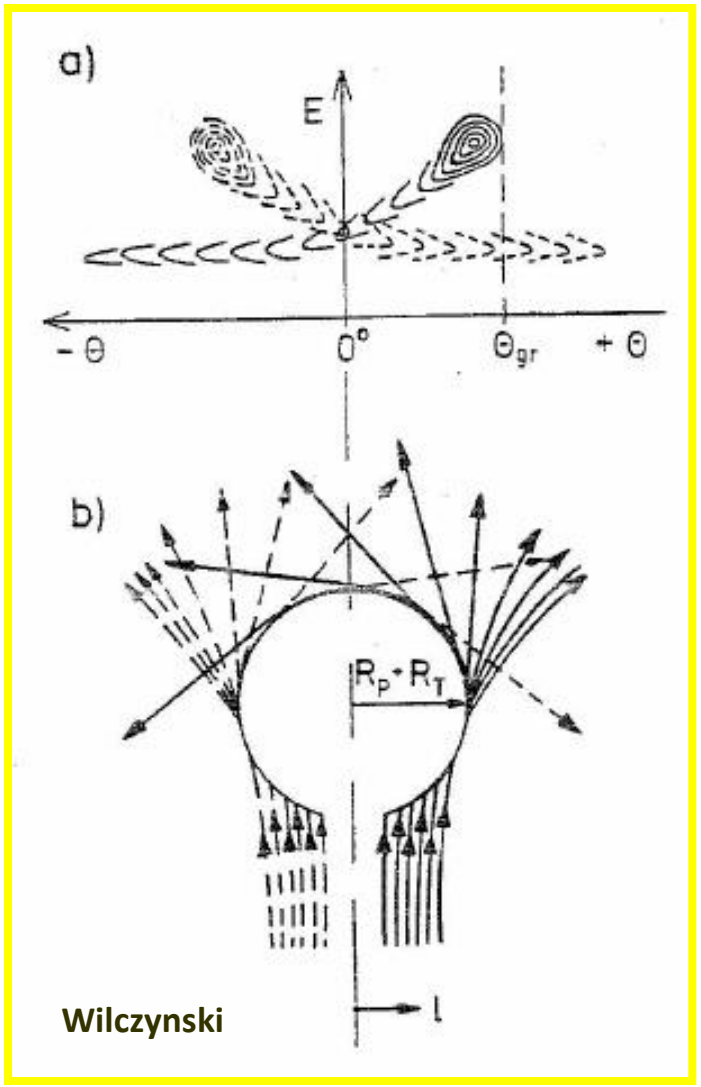

Energy-integrated mass spectra for the reaction $^{238}U + ^{48}Ca$ measured at four incident energies (4.7, 4.9, 5.2, 5.7 MeV/u), with two ionisation chambers in coincidence.

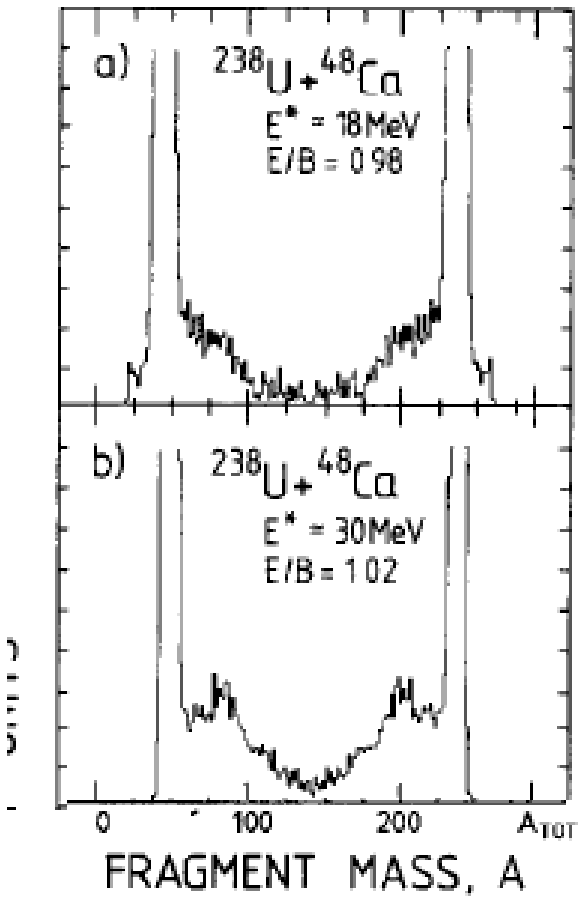

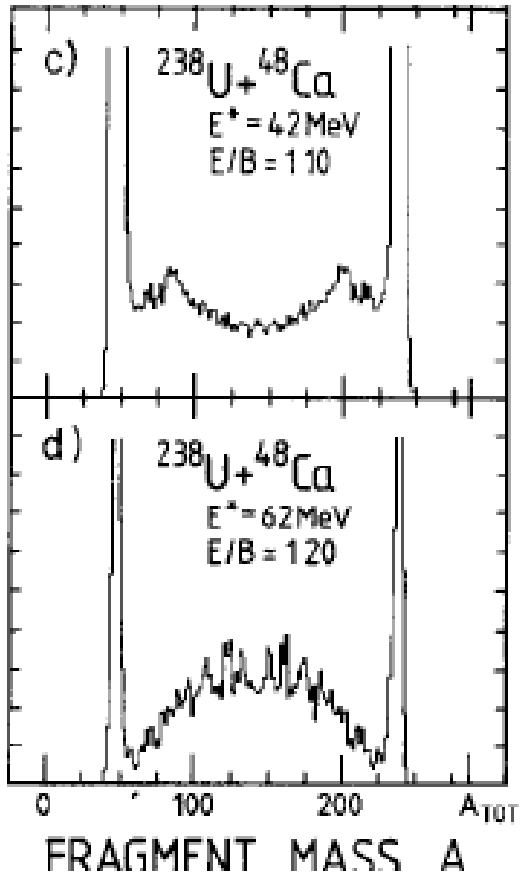

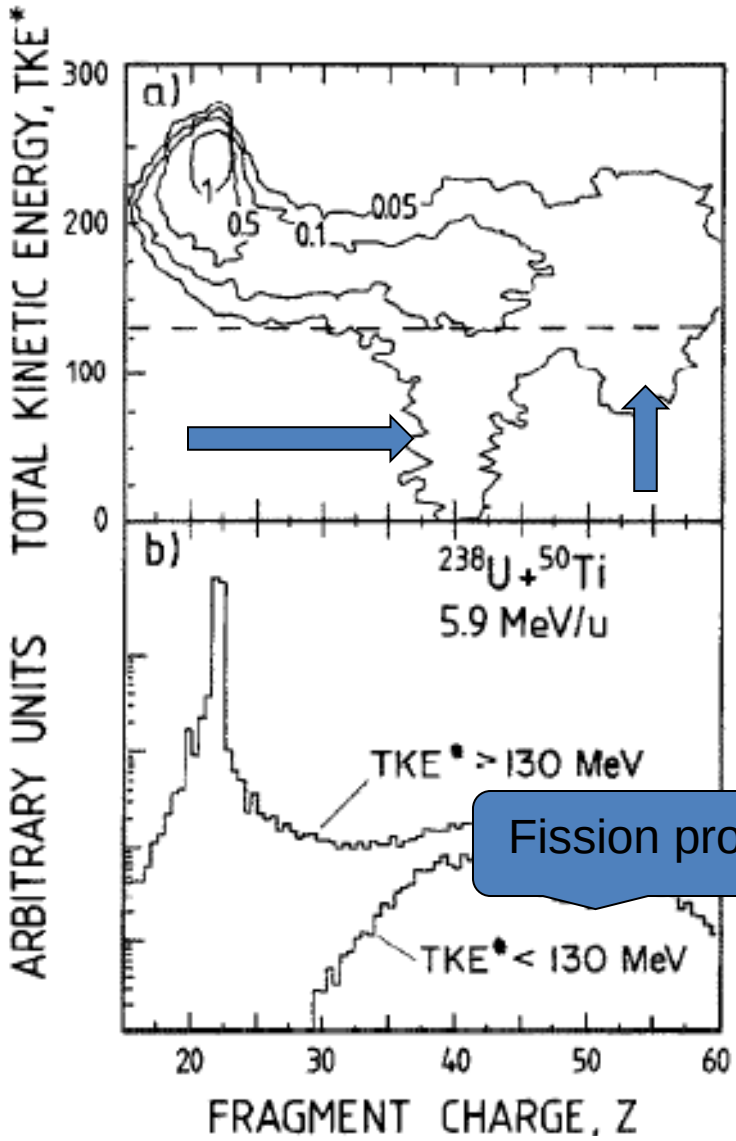

Fission products

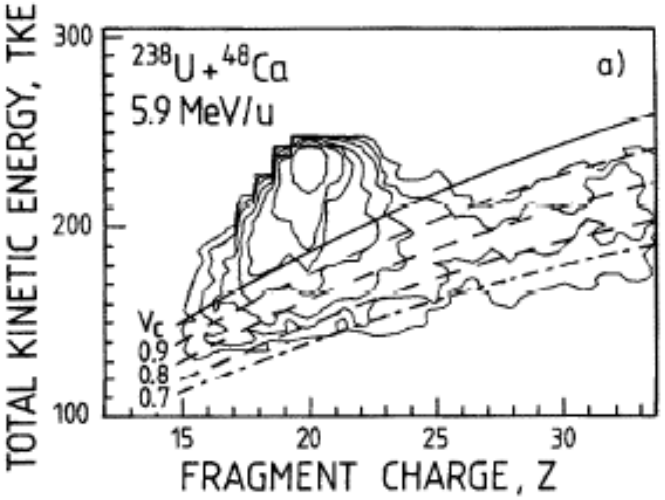

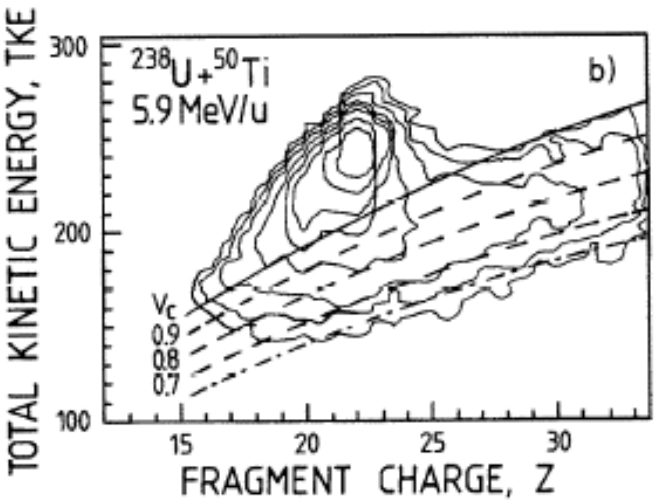

$$\mathrm{TKE}^* = \mathrm{TKE} + \frac{Z_P Z_T e^2}{r_0(A_P^{\frac{1}{3}} + A_T^{\frac{1}{3}})} - \frac{Z_{PL} Z_{TL} e^2}{r_0(A_{PL}^{\frac{1}{3}} + A_{TL}^{\frac{1}{3}})},$$

Energy-mass distribution of the reaction products in the ^{238}U (7.5 MeV/u) + ^{35}Cl reaction

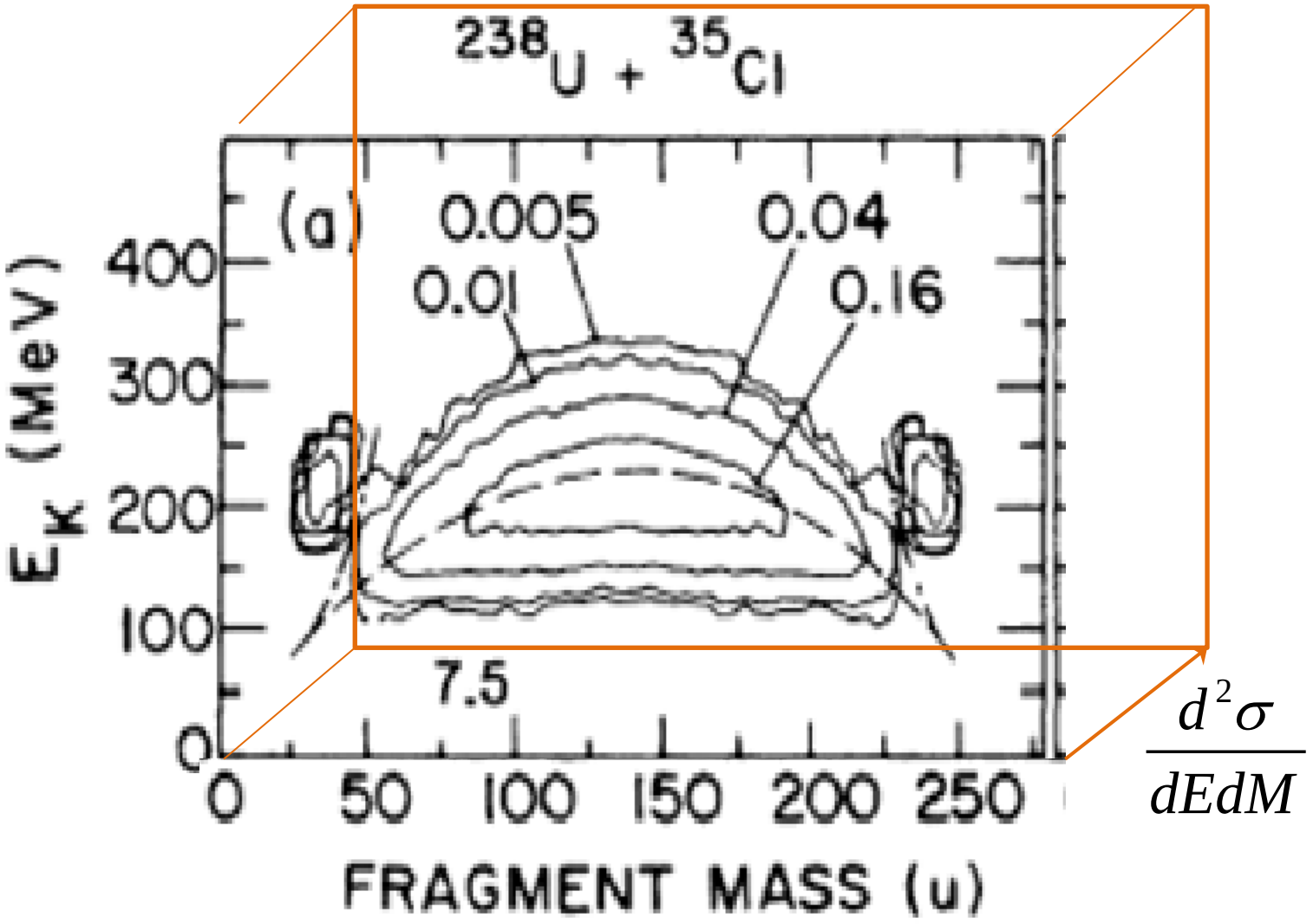

Mixing of the distribution of fragment masses versus total kinetic energy

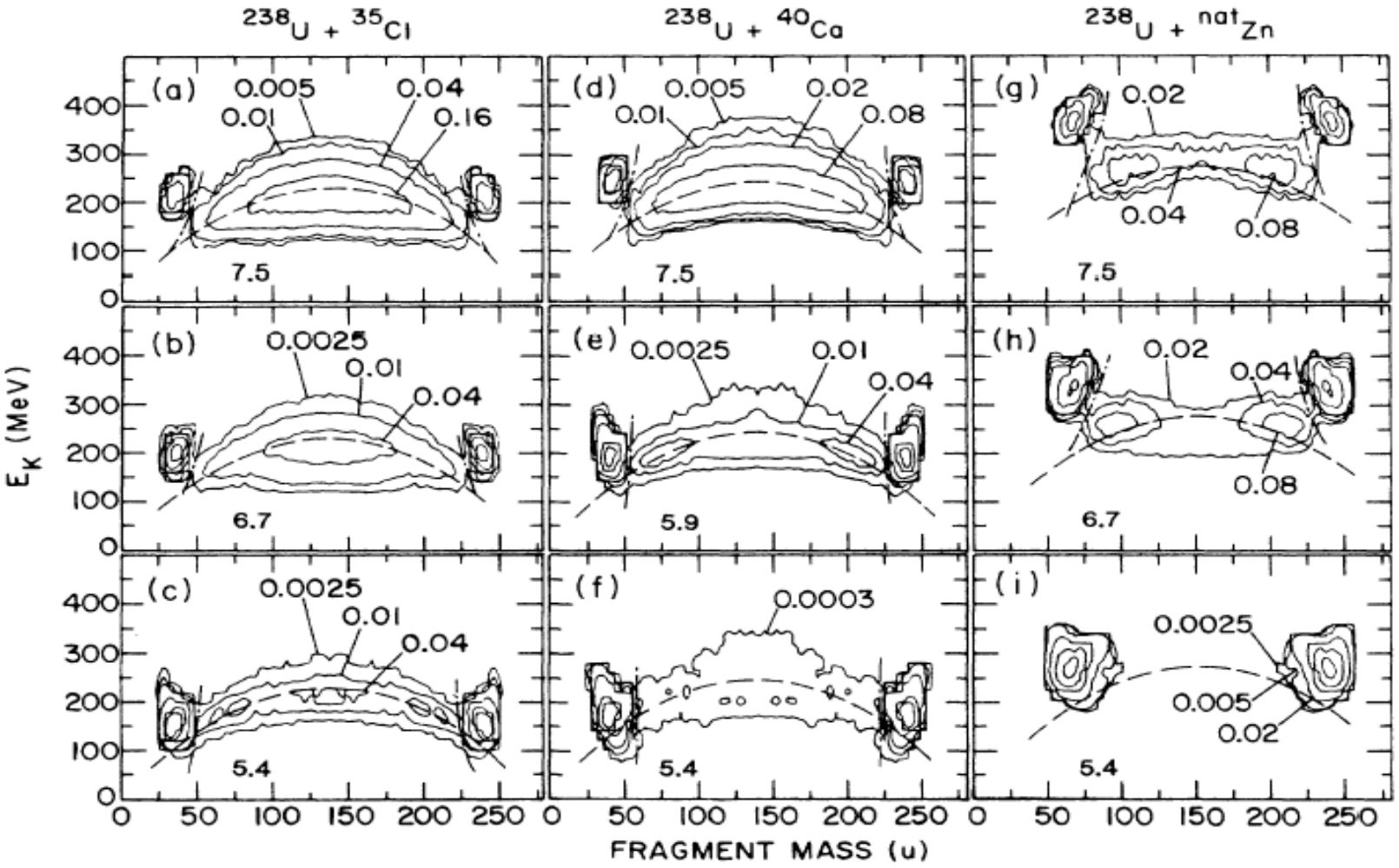

W.Q. Shen et al (GSI) Phys.Rev.C**36**, 115 (1987)

Charge and mass transfer from light ^{64}Ni to ^{238}U is hindered in the ^{64}Ni + ^{238}U reaction

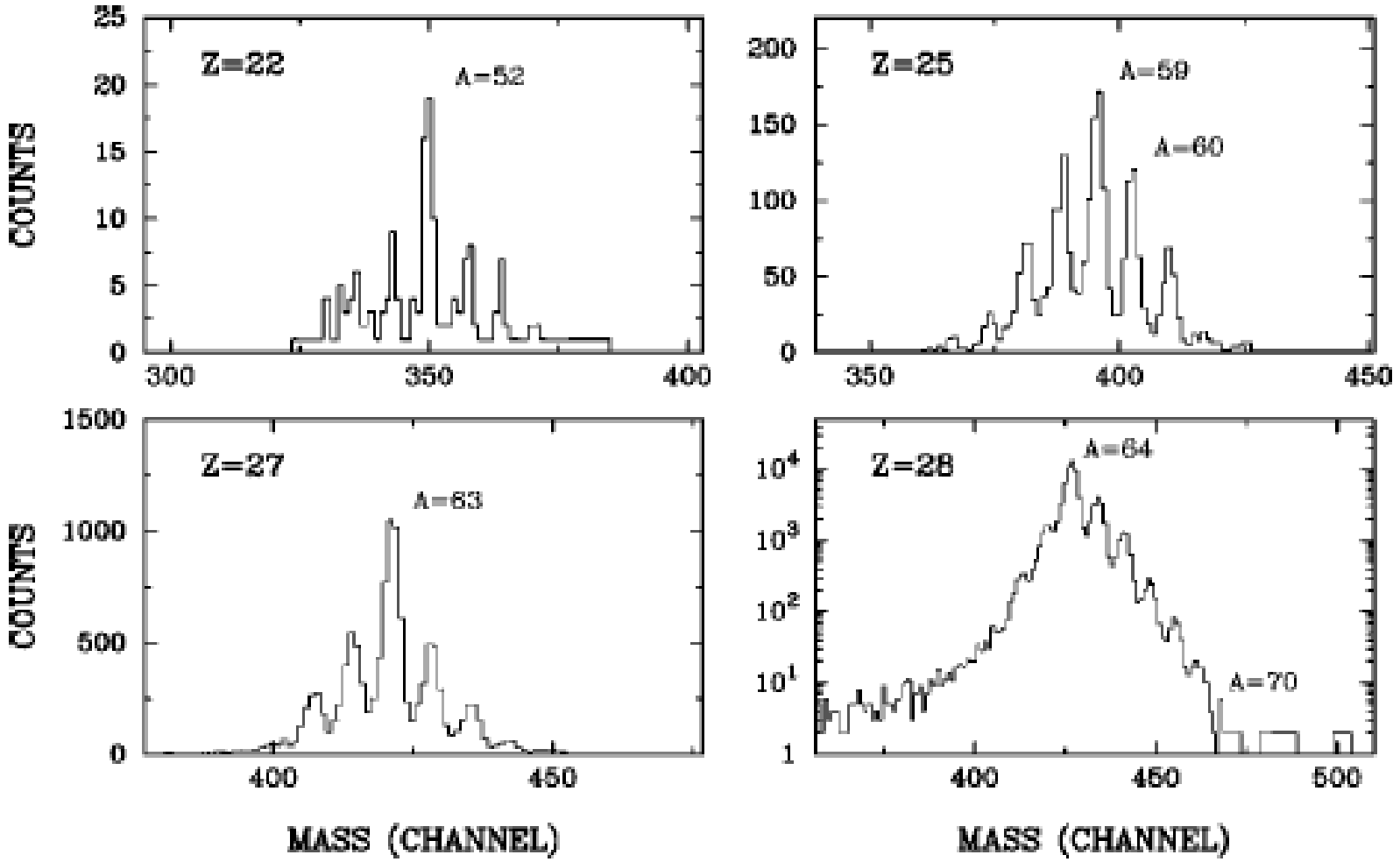

PHYSICAL REVIEW C 81, 034611 (2010)

Competition between fusion-fission and quasifission processes in the $^{32}S + ^{184}W$ reaction

H. Q. Zhang,* C. L. Zhang, C. J. Lin, Z. H. Liu, and F. Yang
China Institute of Atomic Energy, Post Office Box 275, Beijing 102413, People's Republic of China

A. K. Nasirov†
Joint Institute for Nuclear Research, RU-141980 Dubna, Russia

G. Mandaglio, M. Manganaro, and G. Giardina
Dipartimento di Fisica dell' Università di Messina, 98166 Messina, and Istituto Nazionale di Fisica Nucleare, Sezione di Catania, Italy

(Received 5 June 2009; revised manuscript received 21 February 2010; published 24 March 2010)

$$\sigma_{\mathrm{ER}}(E) = \sum_{l=0}^{\infty}(2l+1)\sigma_{\mathrm{fus}}^{(l)}(E)W_{\mathrm{sur}}(E,l). \quad (1)$$

The entrance channel effects can be studied [16] by analyzing the partial fusion cross section $\sigma_{\mathrm{fus}}^{l}(E)$, which is defined by the expression

$$\sigma_{\mathrm{fus}}^{(l)}(E) = \sigma_{\mathrm{capture}}^{(l)}(E)P_{\mathrm{CN}}(E,l). \quad (2)$$

The theoretical cross section for capture includes the contributions of all fragment yields from full momentum transfer reactions:

$$\sigma_{\mathrm{cap}}(E_{\mathrm{c.m.}}) = \sigma_{\mathrm{ER}}(E_{\mathrm{c.m.}}) + \sigma_{\mathrm{f}}(E_{\mathrm{c.m.}}) + \sigma_{\mathrm{qf}}(E_{\mathrm{c.m.}}) + \sigma_{\mathrm{fast\,fission}}(E_{\mathrm{c.m.}}), \quad (3)$$

where σ_{ER}, σ_{f}, σ_{qf}, and $\sigma_{\mathrm{fast\,fission}}$ are the evaporation residue, fusion-fission, quasifission, and fast-fission cross sections, respectively.

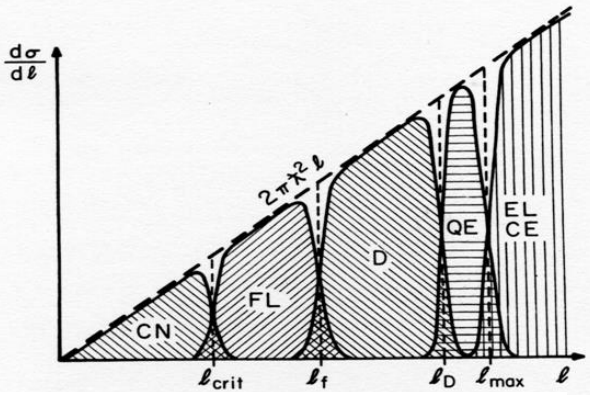

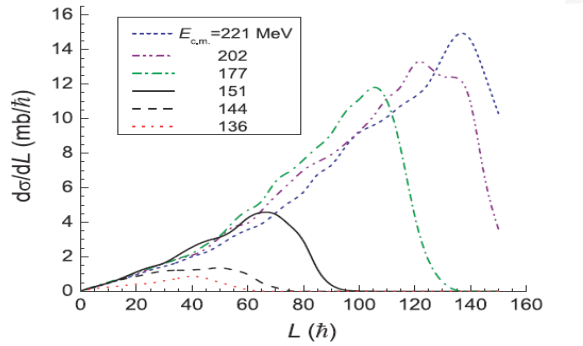

About ambiguity of separation of fusion-fission (ff) and quasifission (qf) products at the analysis of experimental data.

The pure cross section of the complete fusion must include only evaporation residues and fusion-fission cross sections,

$$\sigma_{\rm fus}^{\rm (pure)} = \sigma_{\rm ER} + \sigma_{\rm ff}. \quad (4)$$

The experimental value of $\sigma_{\rm fus}$ is reconstructed from the detected cross sections of fissionlike fragments $\tilde{\sigma}_{\rm ff}$ and evaporation residues $\sigma_{\rm ER}$:

$$\sigma_{\rm fus}^{\rm (exp)} = \tilde{\sigma}_{\rm ff} + \sigma_{\rm ER}. \quad (5)$$

But fissionlike fragments can be a mixture of the contributions of fusion-fission ($\sigma_{\rm ff}$), quasifission ($\sigma_{\rm qf}$), and fast-fission ($\sigma_{\rm fast\,fis}$) products:

$$\tilde{\sigma}_{\rm ff} = \sigma_{\rm ff} + \sigma_{\rm qf} + \sigma_{\rm fast\,fis}. \quad (6)$$

The ratio between contributions of different binary channels is a function of the initial values of the beam energy and the orbital angular momentum for the given reaction.

Fission fragment angular distribution for the $^{32}S+^{184}W$ reaction. Incident energies are shown in the figure. The experimental data are shown with the fitting curve, which is used to determine the anisotropy A_{exp} of the fragment angular distribution and mean square values of angular momentum from these events.

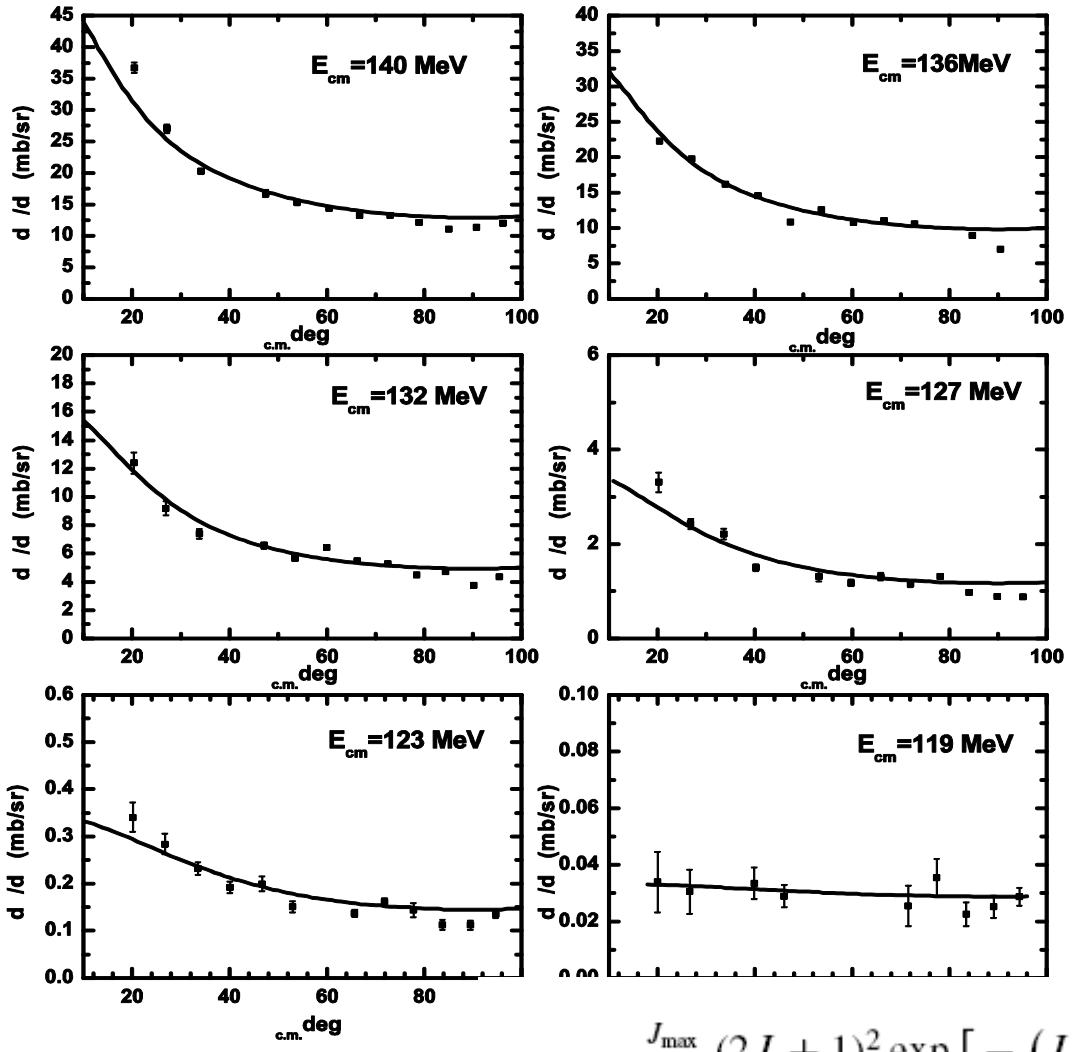

H. Q. Zhang et al,
Phys. Rev. C 81, 034611 (2010)

$E_{c.m.}$ (MeV)	E^*_{CN} (MeV)	$\sigma_{capture}$ (mb)	$\mathcal{A}_{exp}$	K_0^2
118.8	37.2	0.04	1.51	114.71
123.1	41.5	2.35	2.16	124.35
127.3	45.8	22.97	2.27	132.09
131.5	50.0	81.01	2.74	140.01
135.8	54.3	132.27	3.06	148.67
141.1	58.5	189.33	3.28	157.35
144.4	61.8	237.06	3.80	155.09

$$A_{\exp} = W(0^\circ)/W(90^\circ)$$

$$A_{theor} = 1 + \frac{\langle \ell^2 \rangle}{4\langle K_0^2 \rangle}$$

$$\langle K_0^2 \rangle = \langle J_{eff} T \rangle / \hbar^2$$

I. Halpern and V. M. Strutinski,

$$W(\theta) = \sum_{J=0}^{J_{max}} \frac{(2J+1)^2 \exp\left[-\left(J+\frac{1}{2}\right)^2 \sin^2\theta/4K_0^2\right] J_0\left[i\left(J+\frac{1}{2}\right)^2 \sin^2\theta/4K_0^2\right]}{\mathrm{erf}\left[\left(J+\frac{1}{2}\right)/(2K_0^2)^{1/2}\right]},$$

Interpretation of the experimental data presented as fusion-fission data in the $^{32}S+^{184}W$ reaction

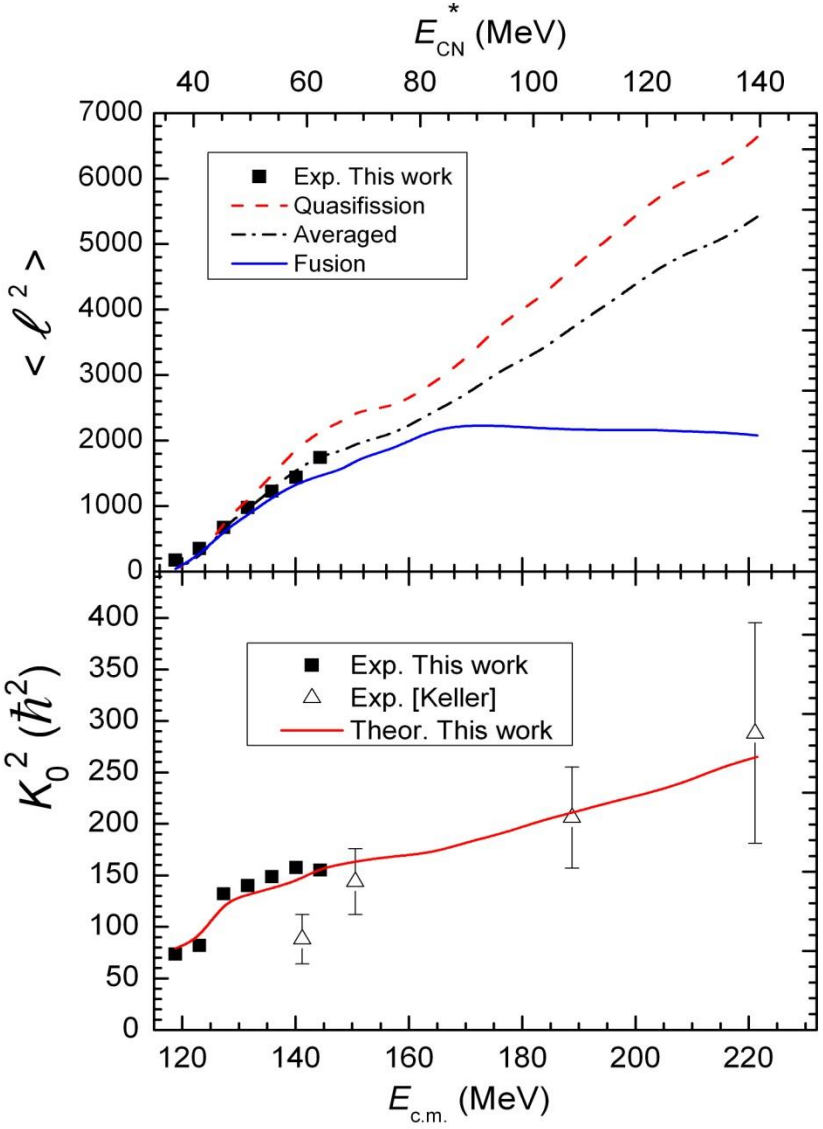

$$\left\langle \ell^2 \right\rangle = \frac{\sigma_{\text{fus}} \left\langle \ell^2 \right\rangle_{\text{fus}} + \sigma_{\text{qf}} \left\langle \ell^2 \right\rangle_{\text{qf}}}{\sigma_{\text{fus}} + \sigma_{\text{qf}}}$$

$$\left\langle \ell^2(E) \right\rangle_{\text{fus}} = \int_0^{\pi/2} \sin\alpha_P \int_0^{\pi/2} \ell^2_{\text{fus}}(E, \alpha_T, \alpha_P) \sin\alpha_T \, d\alpha_P \, d\alpha_T$$

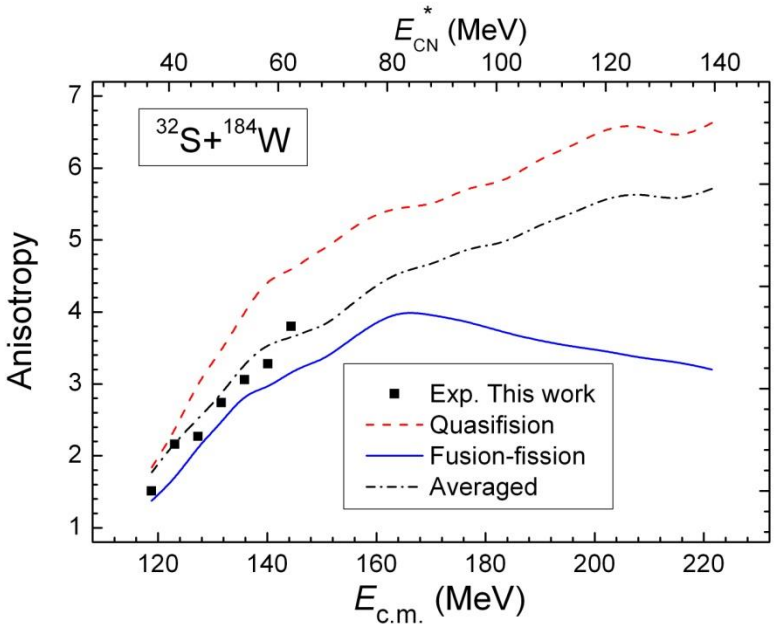

Dependence of competition between complete fusion and quasifission on energy and orbital angular momentum allows us to determine the angular momentum distribution of dinuclear system and compound nucleus.

$$P_{\rm CN}[E^*_{\rm DNS}(Z,A,\ell);\{\alpha_i\}]$$
$$= \sum_{Z_{\rm sym}}^{Z_{\rm max}} Y_Z[E^*_{\rm DNS}(Z,A,\ell)] P^{(Z)}_{\rm CN}[E^*_{\rm DNS}(Z,A,\ell);\{\alpha_i\}],$$

where $E^*_{\rm DNS}(Z,A,\ell) = E^*_{\rm DNS}(Z_{\rm P},A_{\rm P},\ell) + \Delta Q_{\rm gg}(Z)$

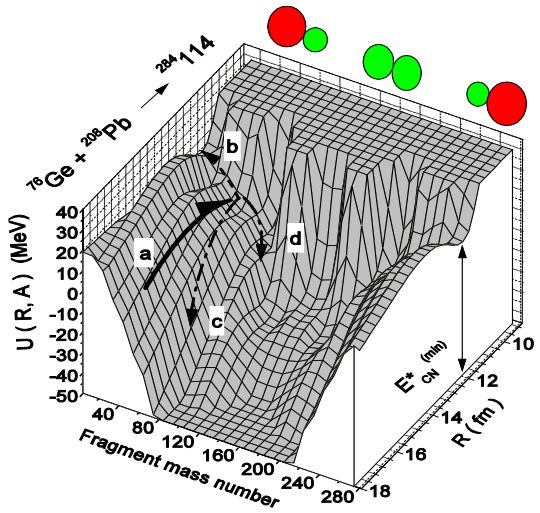

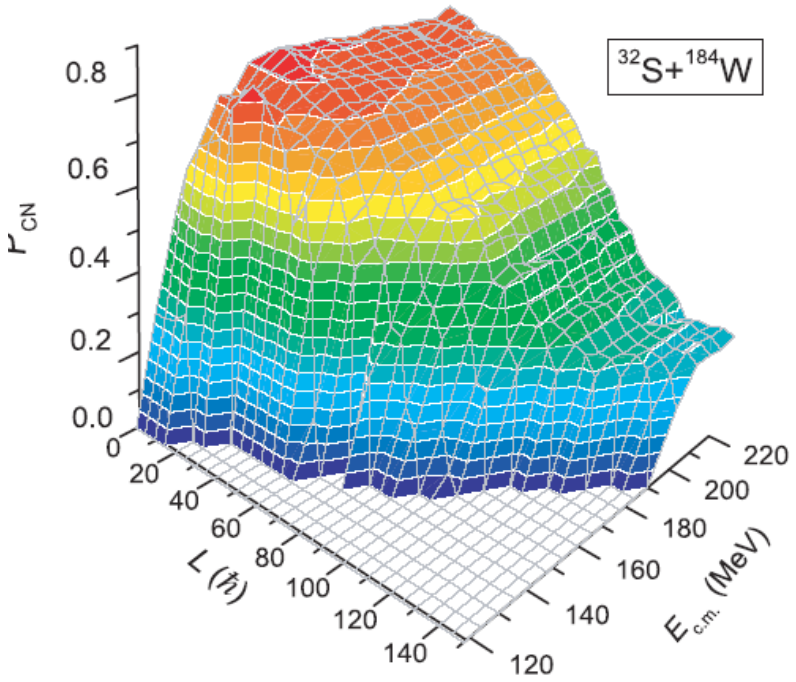

FIG. 10. (Color online) The presentation of the fusion probability $P_{\rm CN}$ for the ^{32}S + ^{184}W reaction as a function of collision energy $E_{\rm c.m.}$ and initial angular momentum L.

$$P^{(Z)}_{\rm CN}(E^*_{\rm DNS}) \approx \frac{\Gamma^{(Z)}_{\rm fus}(B^*_{\rm fus}, E^*_{\rm DNS})}{\Gamma^{(Z)}_{\rm (qf)}(B_{\rm qf}, E^*_{\rm DNS}) + \Gamma^{(Z)}_{\rm (fus)}(B^*_{\rm fus}, E^*_{\rm DNS}) + \Gamma^{(Z)}_{\rm sym}(B_{\rm sym}, E^*_{\rm DNS})},$$

Dependence of competition between complete fusion and quasifission on energy and orbital angular momentum

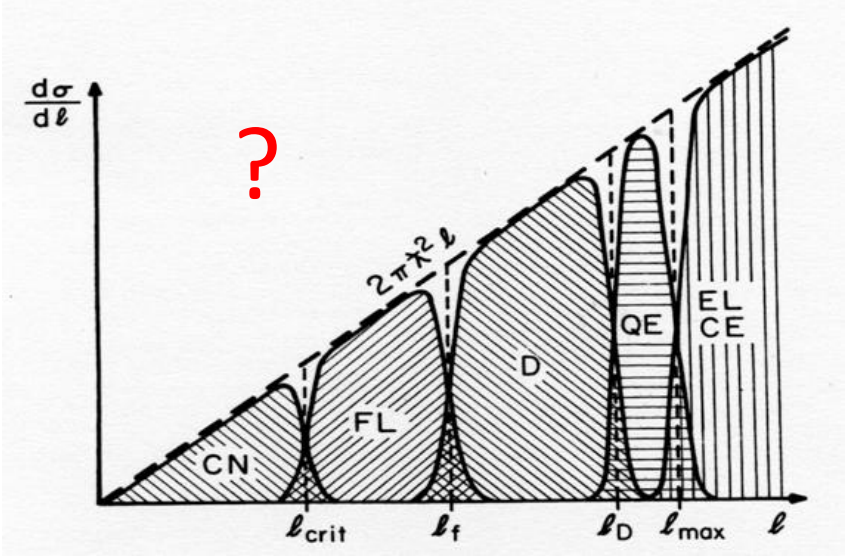

$^{48}Ca+^{154}Sm$

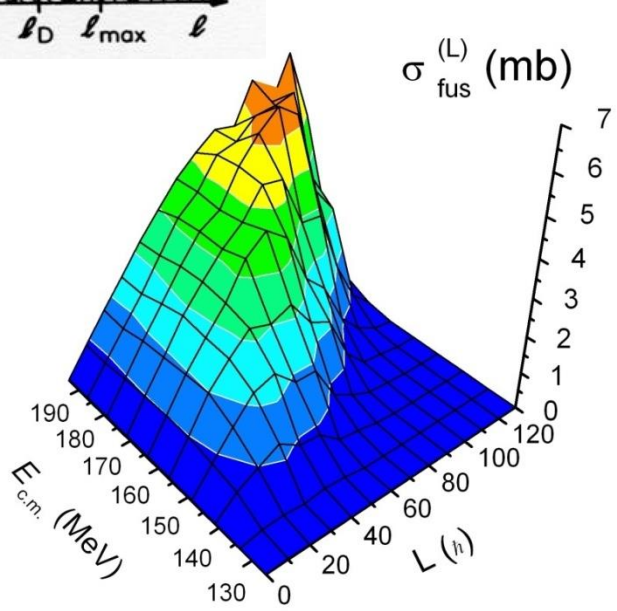

!

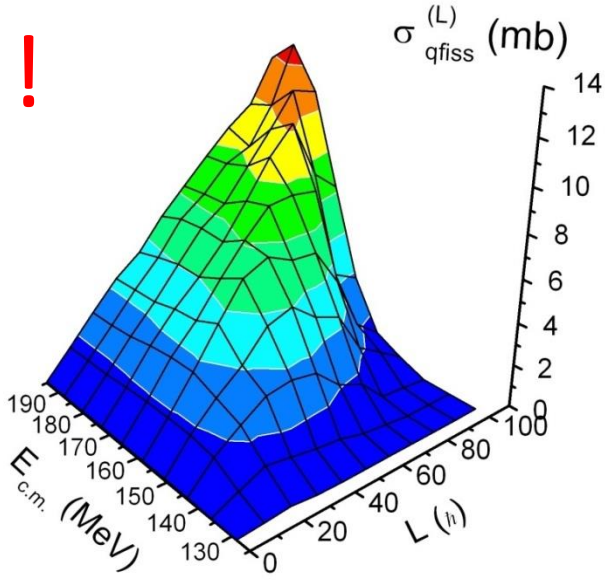

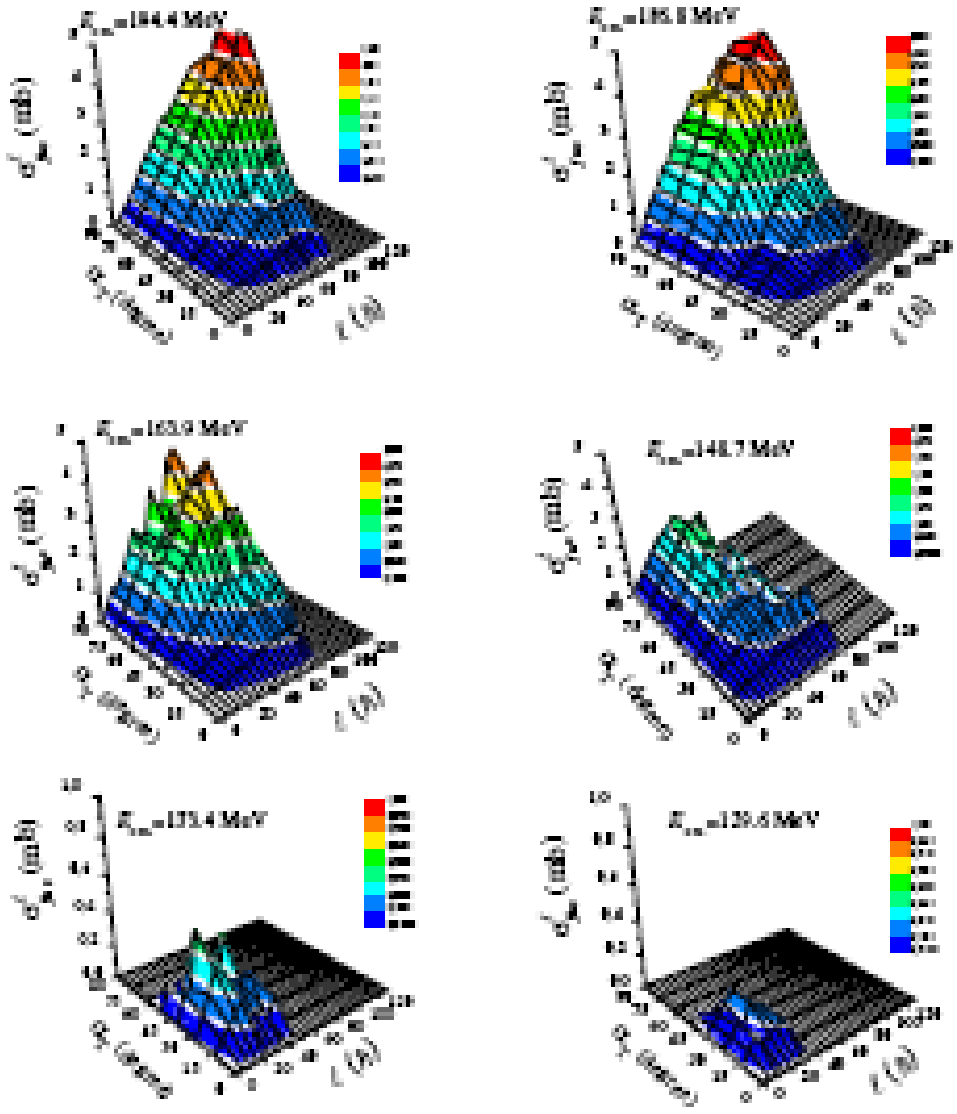

Fig. 5. (Color online) Partial fusion cross section as a function of the orientation angle α_T of the target-nucleus and initial orbital angular momentum ℓ, at various values of the collision energy $E_{c.m.}$. Note that the scale of the panels at $E_{c.m.}$ = 129.6 and 133.4 MeV is five times smaller than that of other panels to better show the structure of the σ^{ℓ}_{fus} shape.

Angular momentum distribution of compound nuclei formed in collisions with different orientations of the target ^{154}Sm at different values of the beam energy.

G. Fazio et al. Jour. Phys. Soc. of Japan., Vol. 77, No. 12, No. 12, December, 2008, 124201

Interpretation of the measured capture and fusion excitation functions by description of evaporation residue cross sections.

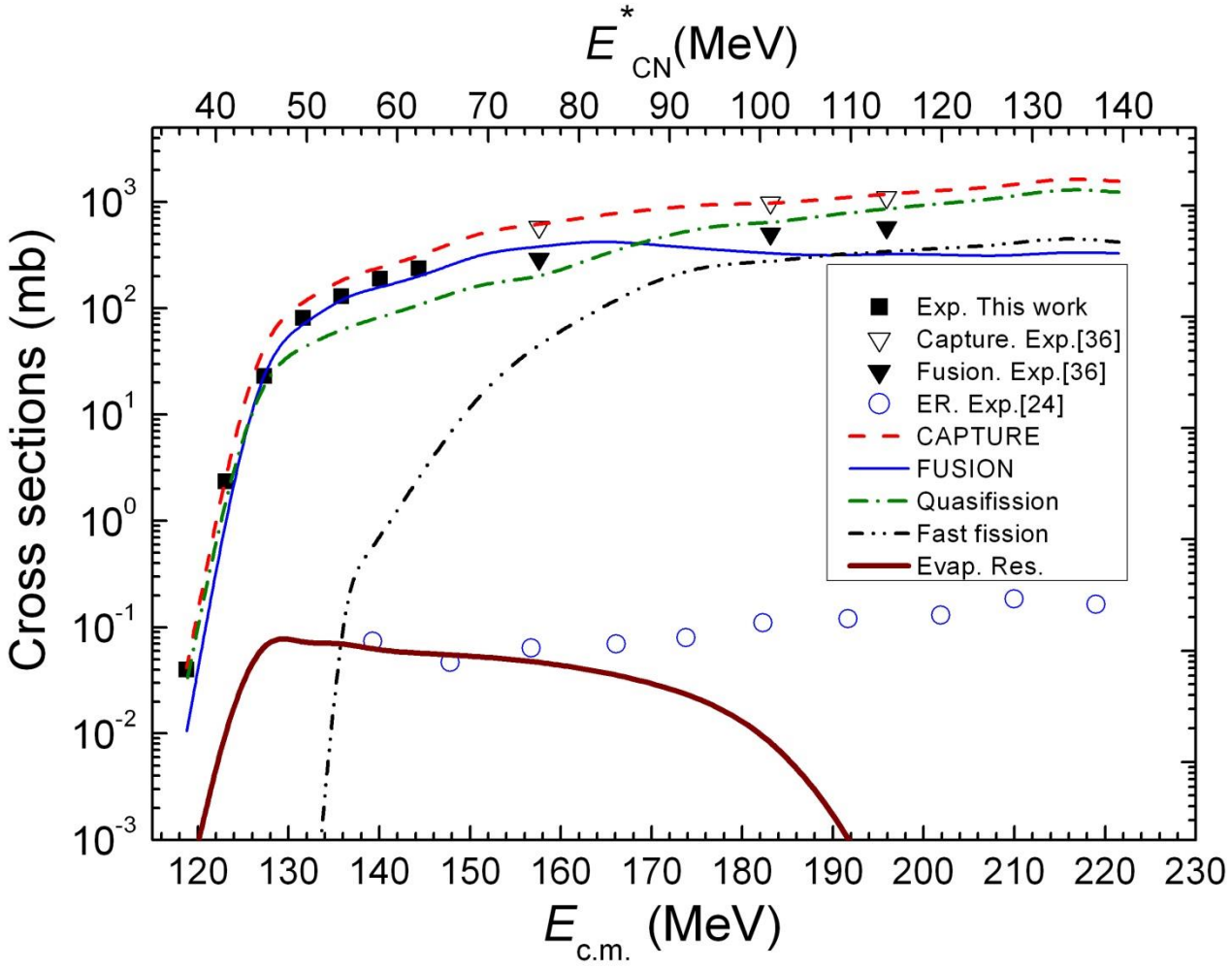

Characteristic Properties of Deeply Inelastic Collisions and Quasifission reactions

In this section we discuss an experimental evidence is provided for the characteristic reaction patterns of strongly damped collisions. Apart from their basic two-body nature ($A + X \rightarrow B + Y$), other gross properties of these processes, such as angular distributions, cross sections, mass and energy distributions, are discussed, with emphasis on their dependence on the projectile-target system and the bombarding energy.

The binary nature of the deep inelastic collisions and quasifission reactions is proved by the experiments where two reaction fragments are measured in coincidence.

The reaction-product mass distributions are bimodal with centroids near the target and projectile masses.

Non-equilibrium processes in heavy ion collisions

At $A_1 + A_2 \rightarrow A_1' + A_2'$ usually $E_1^* : E_2^* \neq A_1' : A_2'$ (even at fission!).
At thermodynamic equilibrium must be $T_1 = T_2 \rightarrow E_1^* : E_2^* = A_1' : A_2'$

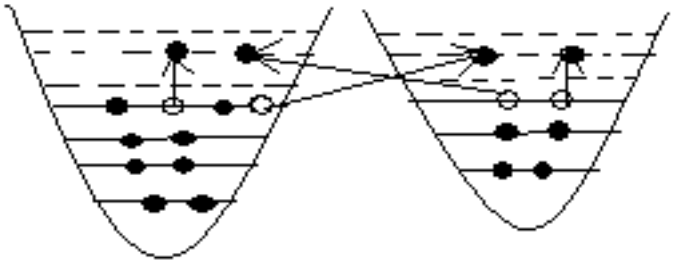

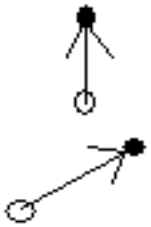

$$T_i = 3.46\sqrt{E_i^* / A_i}$$

i=P,T

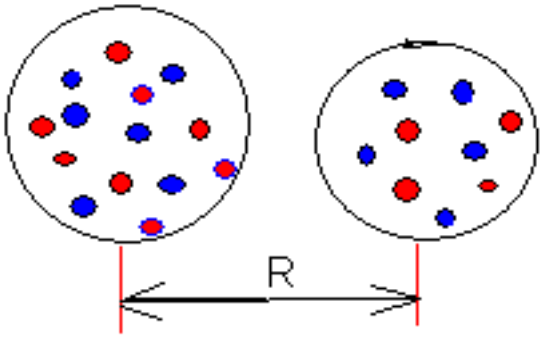

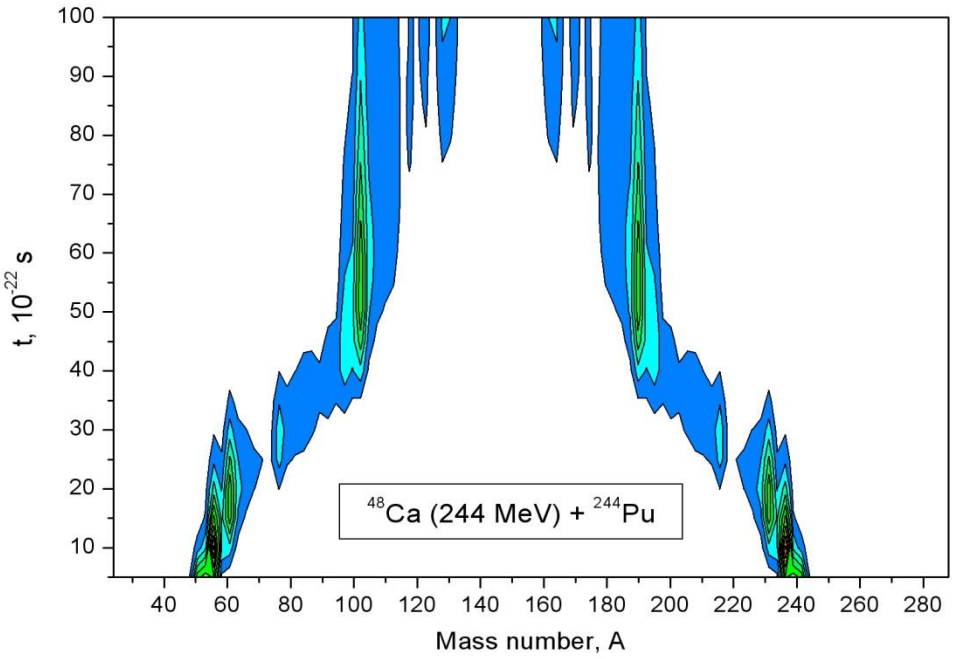

R.V. Jolos, Eur. Phys. Jour. A**7**, 2000, p.115-224

Theoretical methods to describe multinucleon transfer reactions at low energies

2. Hamiltonian.

It is convenient to start with the hydrodynamical Hamiltonian of the many body system written in the form [106]

$$\begin{aligned} H &= \frac{m}{2}\int J(\mathbf{R},\mathbf{r})\frac{1}{\rho(\mathbf{R},\mathbf{r})}J(\mathbf{R},\mathbf{r})d^3\mathbf{r} \\ &+ \frac{\hbar^2}{8m}\int\frac{(\nabla\rho(\mathbf{R},\mathbf{r}))^2}{\rho(\mathbf{R},\mathbf{r})}d^3\mathbf{r} + \frac{1}{2}\int\rho(\mathbf{R},\mathbf{r})v_{eff}(\mathbf{R},\mathbf{r},\mathbf{r}')\rho(\mathbf{R},\mathbf{r}')d^3\mathbf{r}', \end{aligned} \tag{1.1}$$

which can be presented as sum of components of a dinuclear system consisting from the separated nuclei:

$$\begin{aligned} J(\mathbf{R},\mathbf{r}) &= (\rho\mathbf{P}+\mathbf{P}\rho)/2\mu + j_{in}, \\ j_{in}(\mathbf{R},\mathbf{r}) &= j_P(\mathbf{R}-\mathbf{r}) + j_T(\mathbf{r}), \\ \rho(\mathbf{R},\mathbf{r}) &= \rho_P(\mathbf{R}-\mathbf{r}) + \rho_T(\mathbf{r}), \end{aligned} \tag{1.2}$$

$$\hat{H}_{rel}(\mathbf{R};\mathbf{P}) = \frac{\hat{\mathbf{P}}^2}{2\mu} + \hat{\mathcal{V}}(\hat{\mathbf{R}}), \tag{1.4}$$

which consists of the kinetic energy operator and the nucleus-nucleus interaction potential $\hat{\mathcal{V}}(\hat{\mathbf{R}}) = \int \rho_P(\mathbf{R}-\mathbf{r}) v_{eff}(\mathbf{R},\mathbf{r}) \rho_T(\mathbf{r}) d^3\mathbf{r}$. The last two terms in (1.3) describe the internal motion of nuclei and the coupling between relative and internal motions. The intrinsic motion of nucleons in the projectile and target nuclei is presented by the Hamiltonian

$$\begin{aligned}
\hat{H}_{in} &= \frac{m}{2}\int \hat{j}_P(\mathbf{R}-\mathbf{r})\frac{1}{\rho(\mathbf{R},\mathbf{r})}\hat{j}_P(\mathbf{R}-\mathbf{r})d^3\mathbf{r} + \int \hat{\rho}_P(\mathbf{R}-\mathbf{r})\hat{v}_{eff}(\mathbf{R},\mathbf{r},\mathbf{r}')\hat{\rho}_P(\mathbf{R}-\mathbf{r}')d^3\mathbf{r}' \\
&+ \frac{m}{2}\int \hat{j}_T(\mathbf{r})\frac{1}{\rho(\mathbf{R},\mathbf{r})}\hat{j}_T(\mathbf{r})d^3\mathbf{r} + \int \hat{\rho}_T(\mathbf{R},\mathbf{r})\hat{v}_{eff}(\mathbf{R},\mathbf{r},\mathbf{r}')\hat{\rho}_T(\mathbf{R},\mathbf{r}')d^3\mathbf{r}'.
\end{aligned} \tag{1.5}$$

The first and third terms of this expression corresponds to the nucleon kinetic energy in projectile and target; the second and forth terms are their potential energy. The Hamiltonian (1.5) corresponds to a single-particle Hamiltonian of fragments of a dinuclear system

$$\hat{H}_{in}(\xi) = \sum_{i=1}^{A_P}\left(\frac{-\hbar^2}{2m}\Delta_i + \hat{V}_P(\mathbf{r}_i - \mathbf{R}(t))\right) + \sum_{i=1}^{A_T}\left(\frac{-\hbar^2}{2m}\Delta_i + \hat{V}_T(\mathbf{r}_i)\right) + h_{residual}, \quad (1.6)$$

where mean fields V_P and V_T of nuclei are defined by the nucleon distribution according to self-consistency condition:

$$V_P(\mathbf{r}_i - \mathbf{R}(t)) = \int \rho(\mathbf{R}-\mathbf{r}) v_{eff}(\mathbf{R},\mathbf{r},\mathbf{r}')\hat{\rho}(\mathbf{R},\mathbf{r}')d^3\mathbf{r}' \quad (1.7)$$

$$V_P(\mathbf{r}-\mathbf{R}) = -V_{(0)}^{N_P,Z_P}\left\{1+\exp\left[\frac{|\mathbf{r}-\mathbf{R}(t)|-R_P}{a}\right]\right\}^{-1},$$

$$V_T(\mathbf{r}) = -V_{(0)}^{N_T,Z_T}\left\{1+\exp\left[\frac{|\mathbf{r}|-R_T}{a}\right]\right\}^{-1},$$

$$V_{(0)}^N = V_0\left[1-0.63\frac{N-Z}{A}\right],\ V_{(0)}^Z = V_0\left[1+0.63\frac{N-Z}{A}\right],$$

$$V_0 = 53MeV,\ R_i = r_0 A_i^{1/3},\ r_0 = 1.24fm,\ a = 0.63fm.$$

$$\hat{H}(\mathbf{R}(t)) = \hat{H}_{rel}(\mathbf{R}(t)) + \hat{H}_{in}(\mathbf{R}(t)) + \delta\hat{V}(\mathbf{R}(t)),$$

$$\hat{H}_{in}(\mathbf{R}(t)) = \sum_{P} \varepsilon_P \mathrm{a}_P^+ \mathrm{a}_P + \sum_{T} \varepsilon_T \mathrm{a}_T^+ \mathrm{a}_T,$$

$$\delta\hat{V}(\mathbf{R}(t);\xi) = \sum_{i \neq i'} V_{ii'}(\mathbf{R}(t)) \mathrm{a}_i^+ \mathrm{a}_{i'}$$

$$= \sum_{P \neq P'} \Lambda^{(T)}_{PP'}(\mathbf{R}(t)) \mathrm{a}_P^+ \mathrm{a}_{P'} + \sum_{T \neq T'} \Lambda^{(P)}_{TT'}(\mathbf{R}(t)) \mathrm{a}_T^+ \mathrm{a}_{T'} +$$

$$\sum_{T,P} \mathrm{g}_{PT}(\mathbf{R}(t))(\mathrm{a}_P^+ \mathrm{a}_T + h.c.),$$

Hamiltonian for calculation of the transport coefficients

The macroscopic motion of nucleus and microscopic motion of nucleons must be calculated simultaneously.

$$\mathrm{H} = \mathrm{H}_{\mathrm{coll}} + \mathrm{H}_{\mathrm{micr}} + \delta \mathrm{V} \qquad (1)$$

where

$$\mathrm{H}_{\mathrm{coll}} = \frac{\mathrm{P}^2}{2\mu} + \mathrm{U}(\mathrm{R}) \text{ - for the relative motion of nuclei;} \qquad (2)$$

$$\mathrm{H}_{\mathrm{micr}} = \sum_{i_P} \varepsilon_{i_P} \hat{a}^{+}_{i_P} \hat{a}_{i_P} + \sum_{i_T} \varepsilon_{i_T} \hat{a}^{+}_{i_T} \hat{a}_{i_T} \text{ - for nucleons of nuclei;} \qquad (3)$$

$$\delta \mathrm{V} = \sum_{i_P, j_T} g_{i_P j_T}(R)(\hat{a}^{+}_{i_P} \hat{a}_{j_T} + \hat{a}^{+}_{j_T} \hat{a}_{i_P}) + \sum_{i_P, j_P} \Lambda^{(T)}_{i_P j_P}(R) \hat{a}^{+}_{i_p} \hat{a}_{j_p} + \sum_{i_P, j_P} \Lambda^{(P)}_{i_T j_T}(R) \hat{a}^{+}_{i_T} \hat{a}_{j_T} - \qquad (4)$$

nucleon exchange between nuclei and particle – hole excitations in nuclei;

$g_{i_P j_T}$ *and* $\Lambda^{(P)}{}_{i_T j_T}$ *– matrix elements of nucleon exchange between nuclei and particle – hole excitations in them caused by mean field of partner nucleus.*

Master equations for the nucleon occupation numbers and
Equation of motion for the relative distance

$$\begin{cases} i\hbar \dfrac{\partial \hat{n}(t)}{\partial t} = \left[H(\mathbf{R}(t), \hat{n}(t)) \right], & (5) \\ i\hbar \dfrac{\partial \hat{\vec{R}}(t)}{\partial t} = \left[H(\mathbf{R}(t), \hat{\vec{R}}(t)) \right], & (6) \end{cases} \qquad n_i(t) = a_i^+ a_i \qquad i = P, T$$

$$P \equiv (n_P, j_P, l_P, m_P)$$

$$T \equiv (n_T, j_T, l_T, m_T)$$

$$i\hbar \frac{\partial n_i(t)}{\partial t} = \left[H, \tilde{n}(t) \right] - \frac{i\hbar}{\tau} \left[\tilde{n}(t) - \tilde{n}^{eq}(R(t)) \right] \qquad (7)$$

$$\tilde{\mathrm{n}}_i = \tilde{\mathrm{n}}_i^{\mathrm{eq}}(\mathbf{R}(t)) \left[1 - \exp\left(\frac{-\Delta t}{\tau} \right) \right] + n_i(t) \exp\left(\frac{-\Delta t}{\tau} \right) \qquad (8)$$

$$n_i(t) = \tilde{n}_i(t - \Delta t) + \sum_k \overline{W}_{ik}(R(t), \Delta t)[\tilde{n}_k(t - \Delta t) - \tilde{n}_i(t - \Delta t)] \qquad (9)$$

$$\overline{W}_{ik}(\mathbf{R}(t), \Delta t) = \left| V_{ik}(\mathbf{R}(t)) \right|^2, \quad V_{ik}(\mathbf{R}) = \left\langle i \left| V(R) \right| k \right\rangle$$

. G.G. Adamian, et al. Phys. Rev. C**53,** (1996) p.871-879

Evolution operator for the macroscopic and microscopic degrees of freedom

is defined by solution of the Schroedinger equation with initial condition $U(t_i,t_i)=1$:

$$i\hbar\frac{\partial\hat{U}(t_{i+1},t_i)}{\partial t}=\hat{H}\hat{U}(t_{i+1},t_i),\qquad \hat{U}(t_{i+1},t_i)=\hat{U}^{(0)}(t_{i+1},t_i)\,\hat{U}'(t_{i+1},t_i) \quad (10)$$

$$\hat{U}^{(0)}(t,t_0)=\hat{U}^{(0)}_{mac}(t,t_0)\,\hat{U}^{(0)}_{mic}(t,t_0),$$

$$\hat{U}^{(0)}_{мак}(t,t_0)=\exp\left(-\frac{i}{\hbar}H_{мак}(R(t_0))(t-t_0)\right),\quad \hat{U}^{(0)}_{мак}(t,t_0)=\exp\left(-\frac{i}{\hbar}H_{мак}(R(t_0))(t-t_0)\right)$$

U' is defined by coupling term between collective and microscopic variables

$$\hat{U}'(t_{i+1},t_i)=\exp\left(-\frac{i}{2\hbar}\int_{t_i}^{t_{i+1}}\delta V^{(I)}(R(t))dt\right). \quad (11)$$

A.Messia, "Quantum mechanics" Vol.1

Calculation of the transport coefficients.

The dissipation of kinetic energy of the relative motion occurs due to interaction between macroscopic and microscopic degrees of freedom. An estimation of the averaged values of dynamical variables :

$$< \hat{A}(t) >=< \hat{U}(t,t')\ \hat{A}(t')\ \hat{U}^{-1}(t,t') >, \qquad (12)$$

$$< \delta\hat{V}(t) >= \Re(t) + \delta\tilde{U} + \Delta R(t)[F_R(R_{t_i}) + F_{iner}(R_{t_i})] \qquad (13)$$

allows us to obtain expression for the kinetic coefficients:

$$H = \left[\tilde{H}_1 + \tilde{H}_2\right] \ + \ \left[\frac{P^2}{2\mu} \ + \ U(R) \ + \ \Delta U\right] \ + \ \left[\Delta R\ (F_{mp}(R) \ + \ F_{инер}(R))\right] \qquad (14)$$

The s.p. states of nucleons of dinuclear system

Relative motion of nuclei

Dynamical forces caused by interaction of multinucleon systems

The change of nuclear shape

The change of the nuclear shape was taken into account by solving of equations of motion for the quadrupole (2+) and octupole (3-) collective excitations in nucleus *i* (*i*=1,2):

$$\frac{d^2\beta_\lambda^{(i)}}{dt^2} + \gamma_\lambda^{(i)} \frac{d\beta_\lambda^{(i)}}{dt} + \omega_\lambda^{(i)2} = \sqrt{\frac{2\lambda+1}{4\pi}} \frac{R_0^{(i)}}{D_\lambda^{(i)}} \frac{\partial U(R,\beta)}{\partial R}\bigg|_{\beta_0^{(i)}}$$

where $\omega\lambda$, $\gamma\lambda$ and $D\lambda$ are the frequency, damping and mass coefficients for the surface vibration multipolarity λ, respectively;
R0 is radius of the spherical nucleus. The values of $\omega\lambda$ and reduced electric-multipole transition rate $BE\lambda$ are obtained from the Tables in G. Audi, A.H. Wapstra, Nucl. Phys. A **595**, 509 (1995).
The damping coefficient $\gamma\lambda$ is calculated from the estimation of the coupling term between surface vibrations and nucleon motion in nuclei

Friction coefficients

$$\gamma_\lambda = \frac{2}{i\hbar^2 D_\lambda} \sum_{i,i',j,k} \left(n_j^{(i)} - n_k^{(i')}\right) \left| \frac{\partial V_{jk}(R,\beta_\lambda)}{\partial \beta_\lambda} \right|^2 \int_{t_0}^{t} dt'(t-t') \exp\left(\frac{t-t'}{\tau_{jk}}\right) \sin\left[(\varepsilon_j - \varepsilon_k)(t-t')/\hbar\right]$$

$$\frac{1}{\tau_i^{(\alpha)}} = \frac{\sqrt{2}\pi}{32\hbar\varepsilon_{F_K}^{(\alpha)}} \left[(f_K - g)^2 + \frac{1}{2}(f_K + g)^2 \right] \left[(\pi T_K)^2 + (\varepsilon_i - \lambda_K^{(\alpha)})^2 \right] \left[1 + \exp\left(\frac{\lambda_K^{(\alpha)} - \varepsilon_i}{T_K}\right) \right]^{-1}$$

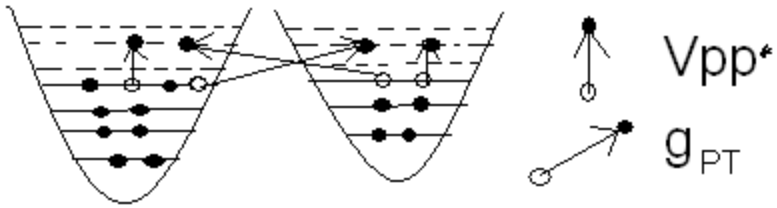

ε_j and ε_k are single particle energies of components of dinuclear system;

$$\Gamma_j = \hbar / \tau_j$$

is a width of the excited single-particle states due to residual interaction between nucleons.

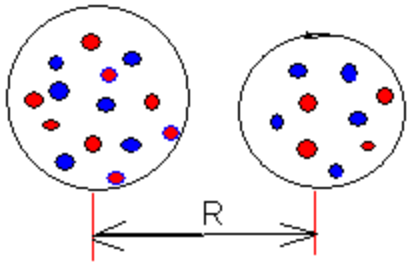

G.G. Adamian, et al. Phys. Rev. C**56** No.2, (1997) p.373-380

Comparison of the friction coefficients calculated by the different methods

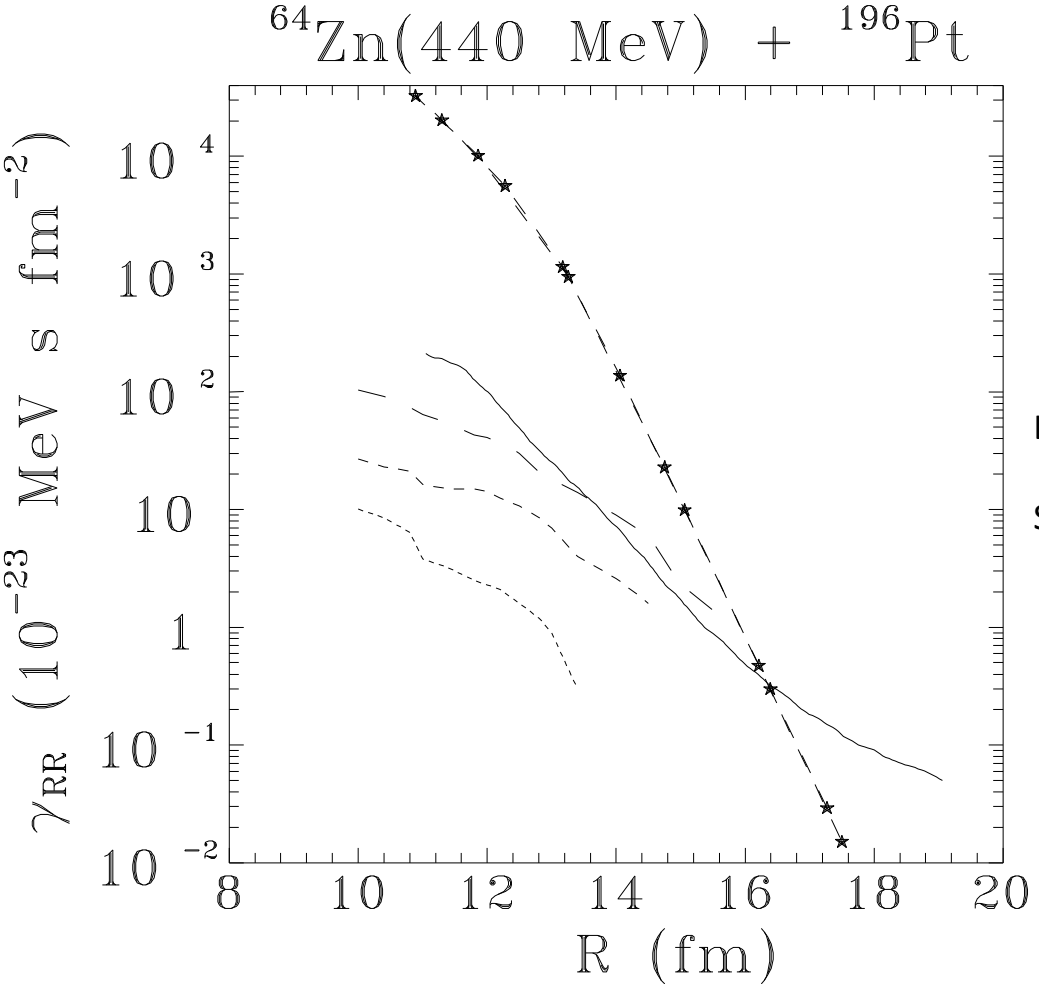

★ -- Gross-Kalinovski

Solid line – semi-microscopic method

Linear response theory by Yamaji

Long dashed __ Temperature= 2 МэВ

Short dashed.- - Temperature = 1 МэВ

Dotted …. Temperature = 0.5 МэВ

Phys. Rev. C**56** No.2, (1997) p.373-380

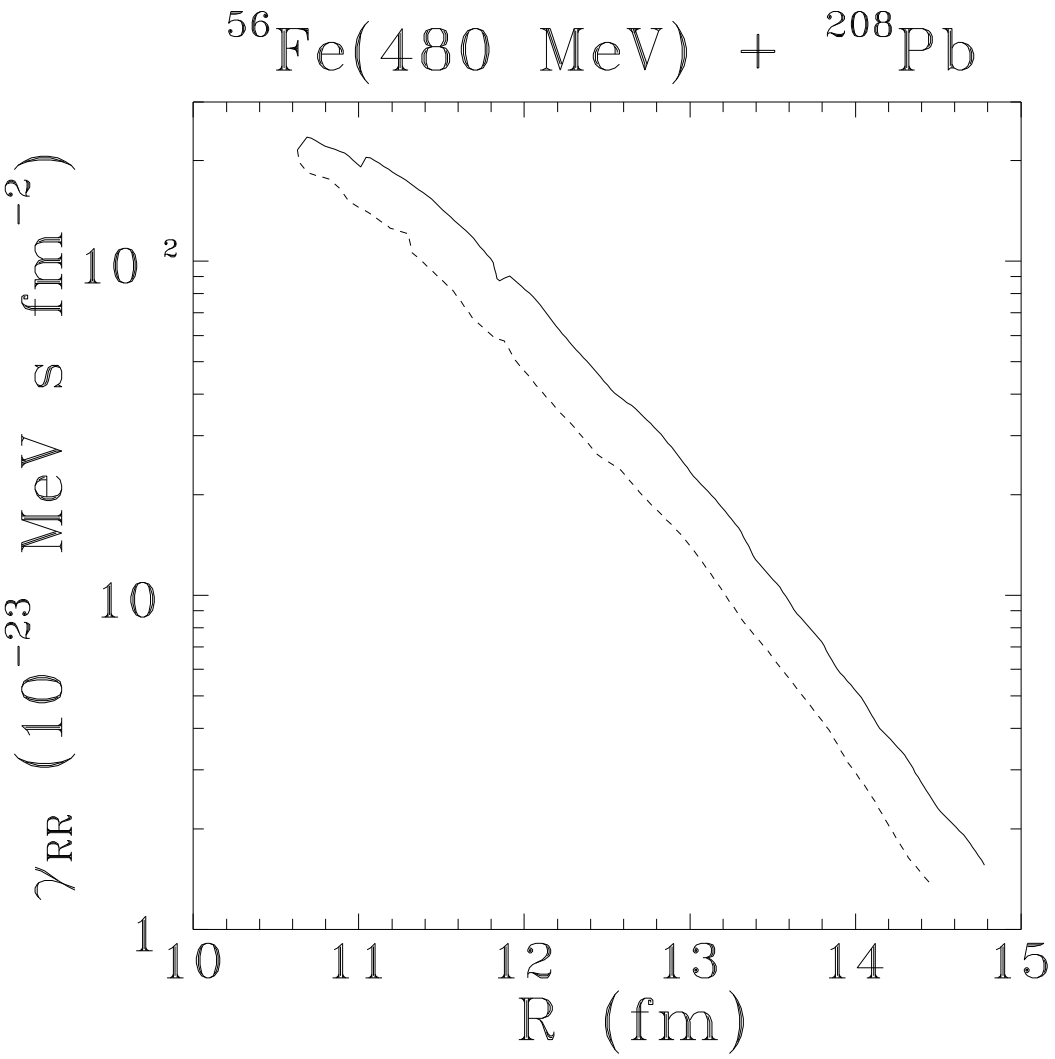

The friction coefficient depends on the relative distance between centers of nuclei and increases by temperature of nuclei.

Dotted curve ····· Incoming path

Solid curve —— Outgoing path

Angular distribution of the nucleon transfer products in reaction ^{103}Rh (^{16}O,^{15}O)^{104}Rh at different beam energies.

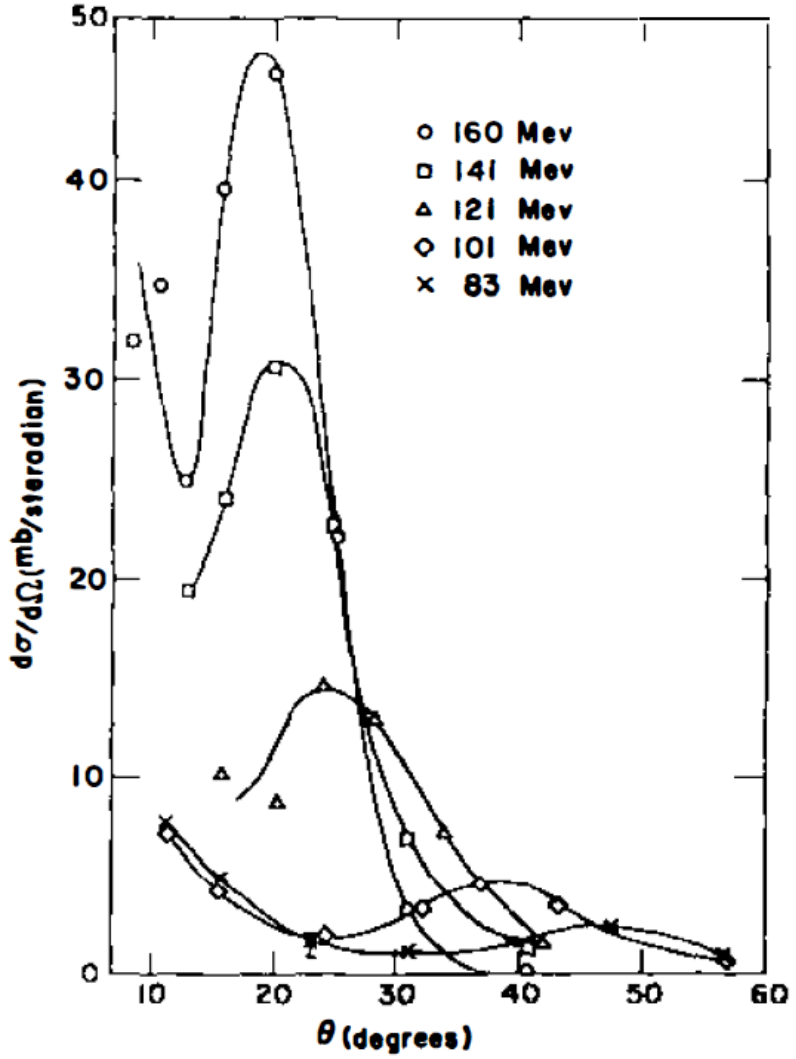

Figure 12 Differential cross section for the reaction $^{103}Rh(^{16}O, ^{15}O)^{104}Rh$ at various bombarding energies [from (1)].

W.U. Schröder, J.R. Huizenga, Ann. Rev. Nucl. Sci. 1977. 27: 465-547

Deeply Inelastic Collisions & Quasifission

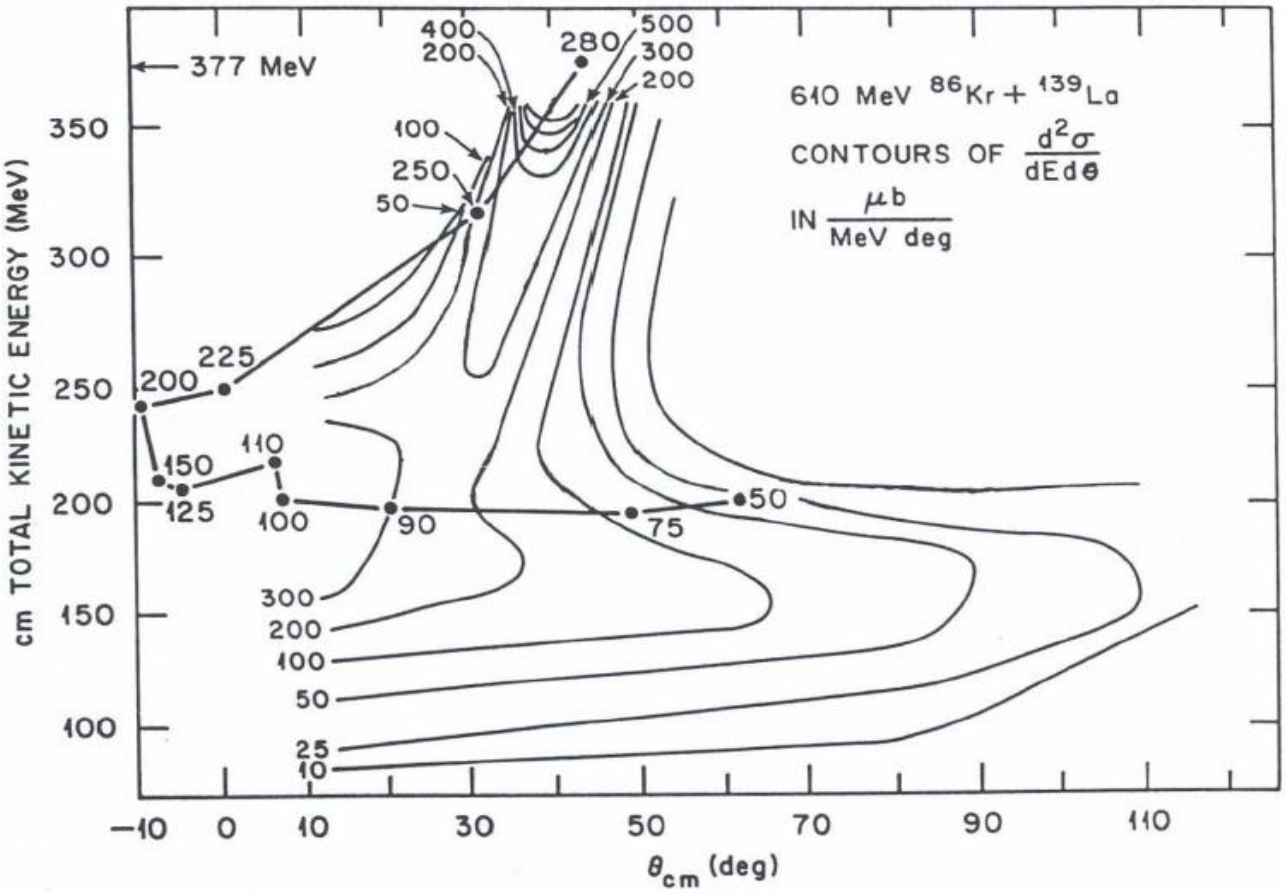

Figure 11.5 Correlation of energy loss and angular deflection for heavy ion collisions near the Coulomb barrier. Above: interpretation in terms of classical trajectories for various angular momenta. Below: Wilczynski plot gives contours of equal $d^2\sigma/d\theta dE$ for the reaction of ^{86}Kr on ^{139}La at 610 MeV laboratory energy. Broken line connects theoretical energy losses and deflection angles for various angular momentum values (solid points), for Time-Dependent Mean Field computation of fig. 11.8. [*data R. Vandenbosch, M. Webb, P. Dyer, R. Pugh, R. Weisfield, T. Thomas, and M. Zisman, Phys. Rev.* **C17** *(1978) 1672*].

For angular momenta somewhat less than ℓ_{gr}, a part of the energy of relative motion is turned into internal excitation. The most striking experimental evidence for this is seen in the Wilczynski plot which displays the doubly-differential cross section $d^2\sigma/ d\vartheta dE$.

Dependence of the collision trajectory on the orbital angular momentum.

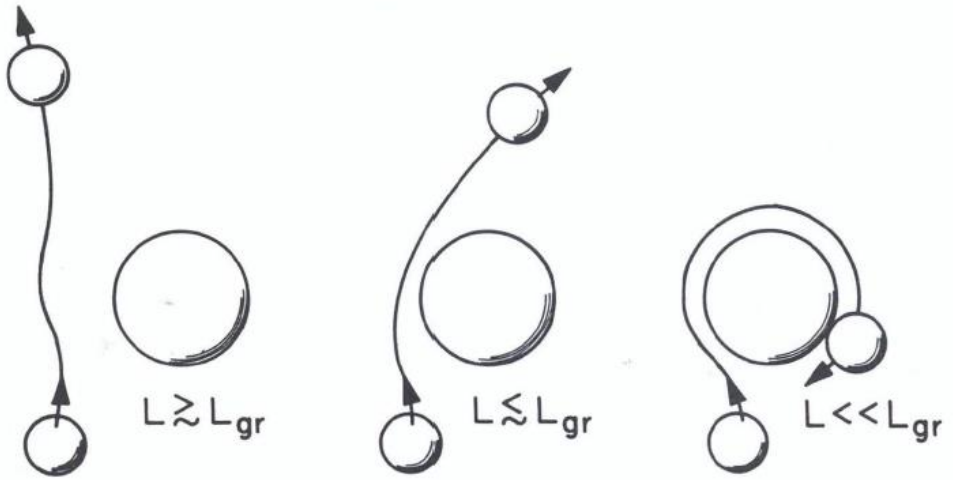

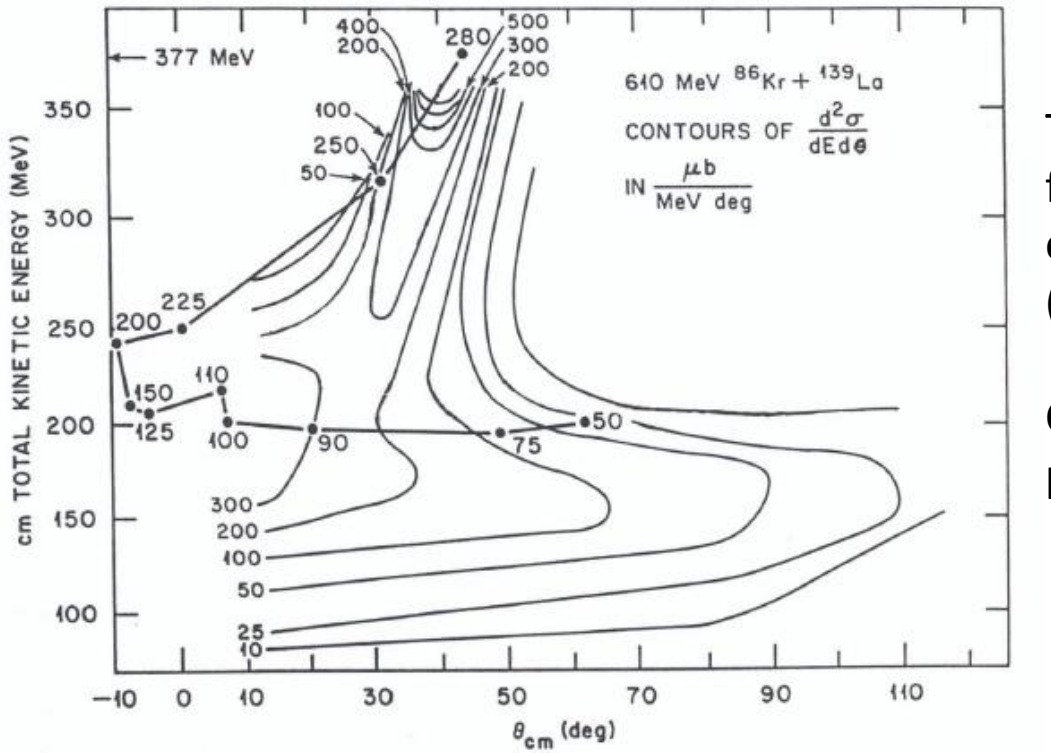

The yield of a particular projectile-like fragment is a function of the beam energy $E_{c.m.}$, impact parameter b (or orbital angular momentum $\vec{L} = \left[\vec{b} \times \vec{P}\right]$) and deflection angle ϑ.
Contours of equal cross section are plotted in the (E, ϑ) plane.

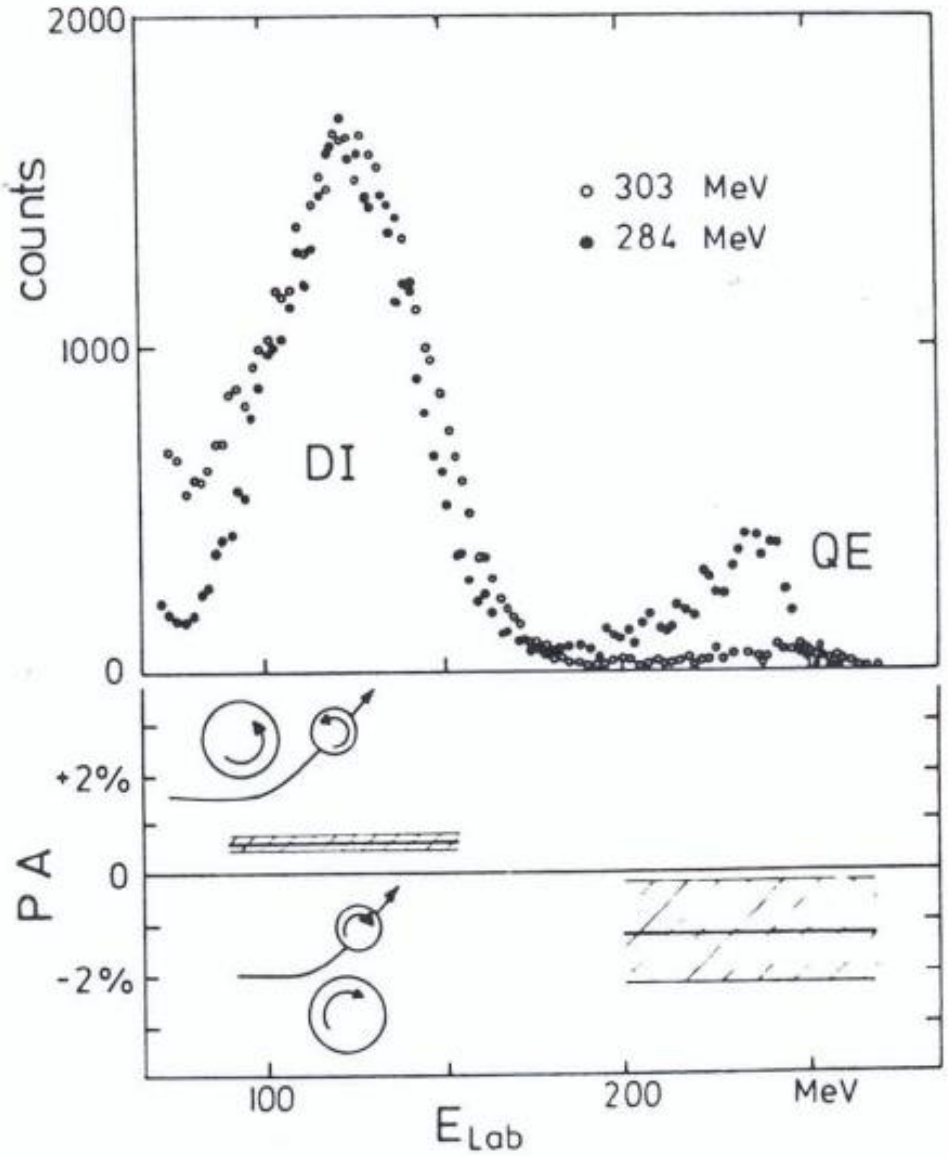

Polarization of photons from target remnants in the reaction of 284 MeV (dots) and 303 MeV (circles) ^{40}Ar on Ag. The count-rate asymmetry measures the circular polarization of the photons, shown as a function of the laboratory energy of the ejectiles. The ejectiles, whose charges range from Z = 11 to 21, are detected at 35° in the laboratory, about 10° outside the grazing angle. Their spectrum is shown in the upper part of the figure.
[from W. Trautman, J. de *Boer, W. Dunn weber, G. Graw, R. Kopp, C. Lauterbach, H. Puchta, and U. Lynen, Phys. Rev. Lett.* 39 *{1977} 1062].*